Investigation of the innate immune response to circulating tumor cells in preclinical animal models of cancer metastasis

A Dissertation

Presented to the Faculty of the Graduate School

of Cornell University

In Partial Fulfillment of the Requirements for the Degree of

Doctor of Philosophy

by

Elizabeth Celeste Wayne

February 2016

INVESTIGATION OF THE INNATE IMMUNE RESPONSE TO CIRCULATING TUMOR CELLS IN PRECLINICAL ANIMAL MODELS OF CANCER METASTASIS

Elizabeth Celeste Wayne, Ph.D.

Cornell University 2016

Metastasis is the leading cause of death in cancer patients because of the difficulty to treat the secondary tumors and the latency period between dissemination of metastatic cells from the primary tumor to other sites and clinical detection. As such, metastasis accounts for a considerable bulk of the $100 billion yearly cost of cancer medical treatment. Understanding the mechanisms underlying metastasis events could have an enormous impact on patient survival rates and how clinicians and scientists target drugs to reduce metastasis. Targeting CTCs has garnered much attention as a therapeutic target in recent years. They are a bottleneck in the progressive stages of metastasis. My thesis explores how circulating tumor cells interact with the host environment and the host innate immune response that ensues. There are two host environments that I investigate 1) blood circulation where circulating tumor cells come in contact with white blood cells and 2) the inflammatory cells in a secondary organ, in this case the brain. My methods include extensive use of transgenic animal models, two-photon microscopy, bioluminescence imaging and imaging analysis. The work presented in this dissertation contributes information about how the innate immune system can be used as a therapeutic drug carrier to target CTCs.

BIOGRAPHICAL SKETCH

Elizabeth Celeste Wayne was born in a small town in Louisiana in 1987. Elizabeth proclaimed she wanted to be a high-energy physicist at the age of 11. However, her first internship was in biophysics and she hasn't looked back since. Elizabeth earned her Bachelors of Arts degree in Physics from the University of Pennsylvania in 2009. There, she was actively involved in the Music & Composition Performance Floor, New Spirit of Penn Gospel Choir, was a Ronald E. McNair Scholar, a Moelis Access Science Fellow, and managed a student run café with an 11-person staff called the *High Rise N' Shine Café*. She did some research too.

In 2010, Elizabeth started her PhD journey in Biomedical Engineering at Cornell University. She joined Prof. Chris Schaffer's laboratory where she studied cancer metastasis in the brain microenvironment. In total, Elizabeth authored 3 peer-reviewed publications, 1 patent submission, and assisted in a technical consultation role in numerous projects with colleagues within her department and beyond. Elizabeth became very active in the NCI Physical Sciences in Oncology (PSOC) initiative and founded the Cancer Brainstorming Club, a student led group to nurture collaboration amongst young scientists and perhaps inspire the next big advancement in cancer therapy. Through her efforts, Elizabeth fostered numerous educational trips amongst 3 large cancer research institutions and helped start the local Cancer Patient and Scientist conversations at the Fingerlakes Cancer Resource Center in downtown Ithaca that still occur monthly to this day.

During her PhD, Elizabeth organized the Northeast Conference for Undergraduate Women in Physics, bringing over 100 women from 61 institutions and 2 countries to Cornell (the most impressive part was that it was in the middle of a brutal Ithaca winter). Elizabeth went on to receive the renowned Alice and Constance Cook Award, a university-wide recognition for work to improve the climate for women on campus.

Elizabeth also served as a Graduate Resident Fellow in Hans Bethe House, a part of the West Campus Housing System. For two years, Elizabeth nurtured Cornell undergraduates as they found their identity, their true passions, and occasionally their room keys. She became a true Cornell community member, serving as an interlocutor between Cornell faculty and students. When she was being awesome in the lab, she was hanging out with her friends and living life large.

To Bobby
This is everything times the space-time continuum

To all the women in my life
You tell me that I am their dreams made flesh, that I've accomplished things you have only dreamed of. I hope that's still true.

ACKNOWLEDGMENTS

I would like to thank my friends for supporting me throughout my educational journey. You didn't always understand what I was doing but you always supported it.

Special thanks to the POB crew: Sara, Natalie, Stephanie, Karin, and Young-hye. We have been friends since the first day of Cornell orientation. It has been fun and I am grateful for your light-heartedness, patience, occasional protectiveness, and love of food and any movie involving minions. Thanks for enduring me and my sometimes questionable behavior. You are one of the few constants I've had while at Cornell and I feel blessed that you guys still want to be friends with me.

To Nizeet, Kirk, and Mingchee, the most awkward four-some I have ever been a member of. You saved me, each in your own ways. Nizeet, you are super kind. We poke fun at your youthful enthusiasm but I have always been amazed and appreciative of your capacity to love and withhold judgment. I would have become such a hardened bitter person if you hadn't been around to soften me out. Mingchee, you are super chill. We have had over a million conversations since our first friendship-defining one. You make me laugh even when you aren't trying to be funny. Your presence is calming, which you must find hilarious since you dislike being around people so much and hearing all their secrets. Kirk, you are just super. You have helped me probably just as much as you have also aggravated me over the last few years. I have found that if I listen to your actions and not your words that I understand you better. I hope you

eventually find all the things you are looking for. Also, hopefully we were all right and Putnam never overheard through the thin walls of Weill Hall any of the raunchy conversations we ever had in your office.

Bethe House. I could not have survived Cornell without you. Jose, I remember thinking that I would never get a GRF job if I had to compete with you! So I'm glad we got to do it together. Xine and Nadia: #PhDivas #bethebump #notpregnant. I couldn't have found better peers and friends to talk about life, fashion, academics, hashtags, sushi, and cats. Erica and Scott, if you ever read this I already know you're secretly taking credit for making all these friendships happen. You should. Thank you for being such great possibility models. I really can't thank you enough. I feel so much more empowered because of your mentorship and friendship. To my Bethe residents, I didn't realize I would like my job so much, and yes, a little flattery for occasionally being mistaken for being 20 years old. But mostly, I'm grateful to have been helpful to you in your time of need.

My labmates. We've been through a lot together. I think we're bonded forever. A few drunken all-nighters followed by passing each other in the hallways as we attempt to do work the next morning will do that to you. Remember those times when we would end up in drunken group huddles promising we'd have each other backs? The long conversations about life and academia? Singing karaoke when it was clear that I was the only one who wanted to do so? Thank you. Jason, thank you for the mountains and the "farts" conversations. JC, thank you for saying you loved me; I promise I was

listening. Yu-ting, thanks for letting me teach you English. Catharine, Steve Tilley, Matt, Flor, John, Poornima aka "Big P", Amanda, Morgan, Yiming, Mitch, Sung Ji, Jiahn. You all kept me laughing and/or ranting. Can't remember which sometimes. You listened to me when I complained, saved me my dignity when I randomly started crying. Nate and Puifai, thank you for your extended friendship, even after you left lab. You're so wise and insightful. It was great for me to have someone a few years ahead to tell me what was to come. David Infanger, you are my Ron Swanson.

My undergrads. Danielle, Rahul, Esther, Rachel, Camille, and Laura. You guys are all so unique. I wish you could see what I see. You are strong, funny, adventurous, hard-working, creative, busy. Rahul excluded, you were all my strong-independent Asian women. You kept me going. I learned a lot from each of you. It was quite a challenge to figure out how to be a mentor to all of you. There was a point when I realized research itself was only about 70% of what I could really teach you. I'm sure some students in the future will forever be in your debt. Danielle, you single-handedly created the "Quotes from Undergrads" wall. I still have the pictures of you falling asleep on the lab couch (courtesy of Steve Tilley). Sandy Chan, you single-handedly finished the quote wall. I could have renamed it, "The Rise and Fall of Sandy Chan: A Lab story." I appreciate your valiant attempts to procure postdocs for me who look like Matthew McConaughey on my behalf. Shiva, you've got spunk and attitude and class. Saif, you are now the King of the Undergrads as you prophesied two years ago.

My UNC family. I thought we would graduate together. So much happened. For years I kept your letters on my desk. I was then and continue to be grateful for your friendship. Stephani, you're still the sister I never had. Weston, Vinal, Ankunda, Laura, Kauilani, and the Albritton Lab, thank you so much for your continued support.

My advisors. Prof Chris Schaffer and Prof. Nozomi Nishimura, thank you for your mentorship throughout my PhD. You took a chance on me and I am grateful that you did. I am also sure there are plenty of things you have done for me over the past few years that I was wholly unaware of. Thank you. There were many initiatives that I wanted to perform during my PhD and I am appreciative that you were actively supportive of those goals. Finally, because of you guys I have a greater appreciation for scotch, bourbon, whiskey, and a lot of other really expensive pleasures in life. May I never be poor. Prof. Peter Doerschuk. I am so glad that you talk so loudly because now I can hope to hear your voice even after I leave Ithaca. I can't thank you enough for your support and your open door policy.

My committee members. I'd like to thank Prof. Frank Wise and Prof John Schimenti for supporting my PhD and giving guidance throughout the entire process. You have always been reliable and great people to bounce ideas off of. A special thanks to Prof. Michael King for allowing me to work on such a special project that the ES/TRAIL liposome study turned out to be. I remember in 2011 when it was only supposed to take 2 months! This work became a much larger part of my thesis than any of us could have anticipated. Nonetheless, I learned how impactful and actually how much fun

research is when people from different backgrounds/experience come together. I will carry those lessons throughout my career.

UPenn. Prof. Larry Gladney, your calm confidence inspired me. You helped me so much. I'm still amazed when you answer my emails sometimes. Prof. Arjun Yodh, you gave me an opportunity to do research. You had so much faith in me and I was so intimidated by you. It's a funny combination really. Thank you for your encouragement and support.

Therapists. God bless them.

Bobby. Back in the day, I liked to read the acknowledgements section of people's dissertations. I thought it was the most interesting part of the dissertation (I mean who cares about that research stuff, right?). I would read them aloud to you. Some people get all mushy about it. Once I told you that I would write paragraphs about you in my own acknowledgements and cite all the ways you helped me finish my thesis. You just rolled your eyes and gave me the most exasperated, uninterested look, which you often did when you thought I said something comical. Of course that meant I teased you about writing it even more. I had no idea I would be writing about you like this. From the outside looking inward, this is a tragedy. Boy loves girl. Girl loves boy. Girl moves for boy. Boy dies in the most epic manner possible without saying goodbye. Girl continues PhD in boy's large shadow and attempts to carve her own path, hiding her pain behind large amounts of success. And yes, it is a tragedy, all the more so

because it is real and it is my reality. I get asked about this a lot. People are very fascinated with fate and whether I would do it all over again. I'm not sure about fate, or being able to avoid pain. I do know that it was worth the risk. Even though I know so much more now than I did at age 18, I am not sure I would have chosen to not love. I can't say that I wouldn't have moved to Cornell. This isn't quite a "thank you" as the rest of my comments have been. Grief/anger is too complicated for a simple statement such as that. But rather, it is a true acknowledgement of the impact you had on my life.

TABLE OF CONTENTS

LIST OF FIGURES

LIST OF TABLES

LIST OF ABBREVIATIONS

2PEF	two photon excited fluorescence
CTCs	circulating tumor cells
ES	E-selectin
TRAIL	TNF-related apoptosis-inducing ligand
TNF	tumor necrosis factor
WBCs	white blood cells (or leukocytes)
BM	brain metastasis
PCa	prostate cancer

CHAPTER 1

INTRODUCTION AND ORGANIZATION OF DISSERTATION

Introduction

Metastasis is the leading cause of death in cancer patients because of the difficulty to treat the secondary tumors and the latency period between dissemination of metastatic cells from the primary tumor to other sites and clinical detection. As such, metastasis accounts for a considerable bulk of the $100 billion yearly cost of cancer medical treatment (1). Understanding the mechanisms underlying metastasis events could have an enormous impact on patient survival rates and how clinicians and scientists target drugs to reduce metastasis.

One way to achieve this is by understanding the impact of circulating tumor cells, which are a bottleneck in the progressive stages of metastasis. Circulating tumor cells (CTCs) represent a rare but volatile population of cells that are shed from the primary tumor into the bloodstream. CTCs have garnered much attention as a diagnostic target in recent years because increased amounts of CTCs found in a patient correlates with a poor prognosis. My thesis explores how circulating tumor cells can be used a therapeutic target to reduce metastasis. We find that CTCs are a highly effective therapeutic target and use of a E-selectin and Tumor necrosis factor (TNF)-related apoptosis-inducing ligand (TRAIL) nanoparticle drug delivery vehicle effectively reduced CTC load within a single dose and in long-term administration results in a reduction of metastatic lesions (2, 3).

Despite the promise of our therapeutic approach, the circulating tumor cell population was dramatically diminished but not eradicated. Minimal residual disease (MRD) as this leftover population is often referred can acquire resistance to and re-populate with a vengeance. This is an issue not only for the therapy presented in my

thesis but for all therapies. The latter part of my thesis creates an *in vivo* platform to explore how host organ microenvironment responds to an invading CTC, particularly in the brain which is a tightly regulated environment and often most complicated metastatic site to treat.

The methods in this thesis include extensive use of transgenic animal models, advanced surgical preparations to mimic hematogenous spread of cancer, two-photon microscopy to allow for time-lapse imaging and deeper visibility into highly scattering tissue such as lung and lymphnode, bioluminescence imaging and imaging analysis.

The work presented in this dissertation contributes information on the value of CTCs as a therapeutic target and demonstrate the use of the innate immune system as a carrier for therapeutic agents. Secondly, the preliminary work on identifying key changes in the host organ microenvironment to invading CTCs could aid future investigators in how to target therapies. The ultimate goal is to identify cells in the microenvironment are that are the most crucial in either killing CTCs and/or maintaining a dormant state. This work spans the pre-clinical realm and also tries to understand basic principles behind metastasis.

Organization of Dissertation

The work in this dissertation centers on the use of circulating tumors cells (CTCs) and their role as a bottleneck for metastasis. In this text, we take advantage of CTCs using them as a therapeutic target and secondly to gain insight into how the host metastatic environment supports and/or undermines CTC completion of metastasis.

Chapter 2: This chapter provides a general introduction to two-photon excited fluorescence microscopy and its superior value in in vivo imaging of dynamic processes such as cancer metastasis. Enclosed is a brief description of the process, history of its development, and a discussion of *in vivo* cellular labeling strategies.

Chapter 3: This chapter outlines the prevalence and significance of studying cancer metastasis. The stages of metastasis are discussed with an emphasis on the role of circulating tumor cell population as a rate-limiting stage of this process.

Chapter 4: This chapter introduces a nanomedicine formulation that can selectively target and kill cancer cells within the bloodstream. This therapy displays TNF-related apoptosis inducing ligand (Apo2L/TRAIL) and E-selectin adhesion receptor liposomes on the surface of circulating leukocytes where it will have increased contact opportunities with circulating tumor cells (CTCs). The therapy was exciting in that at least 75% of CTCs had been killed within 3 hours of drug circulation. These results were published in PNAS where I am a co-author.

Chapter 5: In this chapter, we demonstrate an approach using nanoscale liposomes conjugated with E-selectin adhesion protein and Apo2L/TRAIL (TNF-related apoptosis-inducing ligand) apoptosis ligand that attach to the surface of leukocytes and rapidly clear viable cancer cells from circulating blood, both in human blood samples and in the living mouse. For the first time, it is shown that such an approach can be used to prevent the spontaneous formation and growth of metastatic

tumors in an orthotopic xenograft model of prostate cancer, by greatly reducing the number of circulating tumor cells. We conclude that the use of circulating leukocytes as a carrier for the anti-cancer protein TRAIL could be an effective tool to directly target circulating tumor cells for the prevention of prostate cancer metastasis, and potentially other cancers that spread through the bloodstream. These results are currently in the submission pipeline where I am a co-first author.

Chapter 6: This chapter outlines the study of circulating tumor cell metastasis into the brain microenvironment using 2PEF microscopy. Herein discussed are previous animal models used for studying circulating tumor cell extravasation into brain, and background on microglia activation in cancer. Finally, we discuss the preliminary results of the study on the role of microglia to circulating tumor cell metastasis into the brain microenvironment and future directions.

Chapter 7: This chapter concludes the findings from the previous chapters and posits future directions pertaining to the work on CTC metastasis into the brain and the potential of CTC targeting for treating metastasis in a clinical setting.

References

1. Siegel R, Naishadham D, Jemal A (2012) Cancer statistics, 2012. *CA: A Cancer Journal for Clinicians* 62(1):10–29.

2. Mitchell MJ, King MR (2015) Leukocytes as carriers for targeted cancer drug delivery. *Expert Opinion on Drug Delivery* 12(3):000–000.

3. Mitchell MJ, Wayne E, Rana K, Schaffer CB, King MR (2014) TRAIL-coated leukocytes that kill cancer cells in the circulation. *Proceedings of the National Academy of Sciences* 111(3):930–935.

CHAPTER 2

TWO PHOTON EXCITED FLUORESCENCE MICROSCOPY

2.1 Power of the In Vivo approach

In situ histology studies have generated essential information about cancer metastasis. However, this method only provides a single timepoint to explore the intended pathology in a single animal. This results in the use of large numbers of animals and inconsistency in data due to animal variability. Furthermore, with only a single timepoint, it is impossible to conclude the fate of the circulating tumor cell and vital spatial and temporal information is lost. The real allure of *in vivo* experiments is the ability to observe phenomena as it occurs within an intact organism. Two photon excited fluorescence (2PEF) microscopy provides the optical best platform to conduct *in vivo* imaging at the subcellular level. In this chapter we give an overview of the history of 2PEF, a description of two-photon excitation processes, and the use of 2PEF microscopy for *in vivo* imaging of cancer metastasis processes. The imaging techniques discussed in this chapter are used primarily in Chapters 3 and 6.

2.2 What is 2PEF?

2PEF microscopy is a nonlinear optical technique that relies on the near simultaneous interaction of two photons with a single fluorophore. Two photons combine energies to excite a fluorophore to a higher energy state, much the same way a one-photon excitation process occurs. The excited fluorophore electron spontaneously relaxes, releasing a signal photon. Because this nonlinear interaction demands the near simultaneous interaction of two photons ($\sim 10^{-16}$s) with the same fluorophore, the process only occurs where the photon density is highest within the focal volume of a pulsed femtosecond laser beam. This provides intrinsic optical

sectioning, as fluorescent labels outside the focus are not excited. Any photon emitted can be attributed to the location of the laser focus. Therefore, an image volume may be generated voxel-by-voxel simply by scanning a sample in a raster fashion in three dimensions.

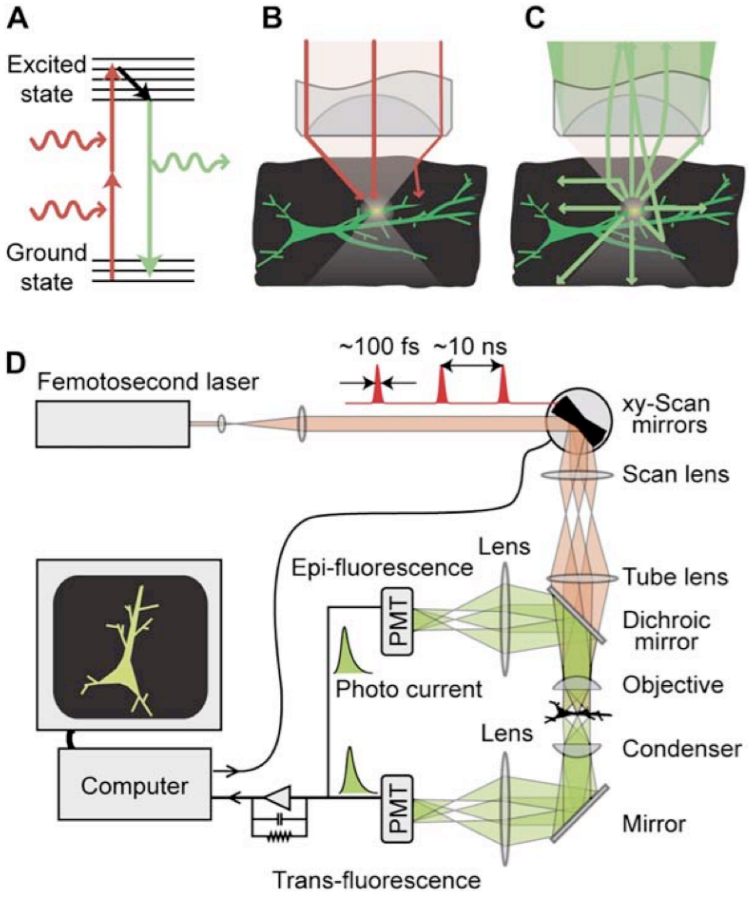

Figure 2.1. Two-Photon Excitation Microscopy

(A) Simplified Jablonski diagram of the 2PE process.(B) Localization of excitation in a scattering medium (black). The ex- citation beam (red) is focused to a diffraction-limited spot by an ob- jective where it excites green fluorescence in a dendritic branch, but not in a nearby branch. The paths of two ballistic photons and one scattered photon are shown (red lines). Scattered photons are too dilute to cause off-focus excitation. The intensity of the beam de- creases with depth as an increasing number of excitation photons are scattered.(C) Fluorescence collection in a scattering medium. Fluorescence photons are emitted isotropically from the excitation volume (red lines). Even scattered fluorescence photons contribute to the signal if they are collected by the objective. Since the field of view for de- tection is larger than for excitation, the fluorescence light exiting the objective back-aperture will diverge substantially (green).(D) Schematic of a 2PE microscope with epifluorescence and trans-fluorescence detection.

Two-photon excited fluorescence was first theorized by Maria Göppert-Mayer in the 1930s and the first designs for manipulating this process for a microscope was published in 1978 by Sheppard and R Kompfner(1). Despite the formulation of theory and designs, the power required to achieve sufficient photon densities for excitation would burn biological tissue. It wasn't until the arrival of the femtosecond laser that 2PEF in living tissue became a reality, with the first demonstration paper published in 1990 by Winfried Denk, James Strickler, and Watt W. Webb (2) at Cornell University. Femtosecond lasers, though providing the high-energy flux needed, were still custom built, incredibly expensive, and challenging to operate and maintain. The first commercial 2PEF system wasn't available until 1996 and was produced by Biorad Microsciences (3). The advancements in laser technology combined with the increased user-friendliness of commercial systems, has steadily made 2PEF an niche imaging tool for subcellular resolution imaging that had long been a obstacle for intravital imaging.

2.3 Advantages of 2PEF

2PEF has three distinct advantages for imaging within scattering media, the primary limitation for imaging tissue through optical methods. First, 2PEF excitation requires longer wavelengths that possess a longer scattering length, when compared with the short wavelengths used in one-photon imaging. Longer scattering length leads to higher penetration depth, as signal photons can travel further out of the tissue before their path is disrupted. The requirement for high photon density to generate signal in 2PEF provides optical sectioning without the need for spatial filters (such as in

confocal microscopy) and increases detection efficiency (4). Furthermore, the low average power of the femtosecond excitation pulses reduces the amount of damage to cell structure and destruction of fluorescent molecules due to phototoxicity and photobleaching respectively. Differences in imaging capability between 2PEF and other optical imaging technique have been experimental demonstrated in numerous studies (5-8). Altogether, these advantages make it possible to chronically image individual cell populations deep within an intact, living organism which has breathed new life into our understanding of the progression of cancer metastasis.

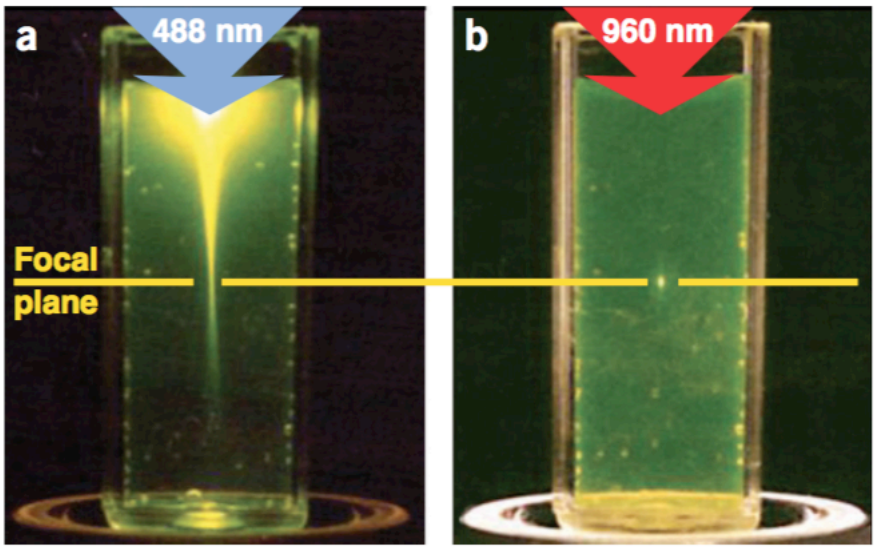

Figure 2.2 Loca**lization of excitation by two-photon excitation.**
(**a**) Single-photon excitation of fluorescein by focused 488-nm light (0.16 NA). (**b**) Two-photon excitation using focused (0.16 NA) femtosecond pulses of 960-nm light.

2.4 2PEF Imaging of Cancer Metastasis

In the past, studies of metastasis relied on histological methods and end-point studies that only satisfy binary questions (did a metastasis form or did it not form) and does not yield insight into the process of cancer metastasis progression. Bioluminescence imaging provides whole animal long-term imaging, but has very low resolution (> 1mm) Video and confocal microscopy offer some intravital imaging capability but lack the resolution and imaging depth. 2PEF microscopy, combined with advanced surgical techniques and fluorescent dye capabilities, sheds light on the spatial and temporal dynamics of cancer progression and in particular, the role of the tumor microenvironment in the stages of metastasis (9-11). The use of surgically implanted organ windows provide long-term optical access while protecting tissue from the external environment, permitting observation in real-time of tumor cell intravasation, circulation, extravasation (12), and proliferation (13). We can observe tumor cell interactions with individual components of the microenvironment such as interaction with leukocytes, platelets, endothelial cells, and other stromal cells. Moreover, we can perturb these systems and use 2PEF to understand how genetic expression and cytokine signaling effect tumor cell involvement in the microenvironment (14, 15). Using 2PEF, we can begin to answer the question of how cancer cells metastasize in real-time. The impact of 2PEF microscopy on intravital imaging of cancer metastasis is unparalleled.

In the metastasis model presented in Chapter 6, fluorescently labeled cancer cells were injected into the intracarotid artery on C57Bl6 transgenic mice expressing

GFP labeled microglia. With the aid of a previously implanted cranial window(16, 17), We use a custom built 2PEF microscope to image the transit of circulating tumor cells through brain parenchyma and correlate their ability to metastasize with the microglia activation response.

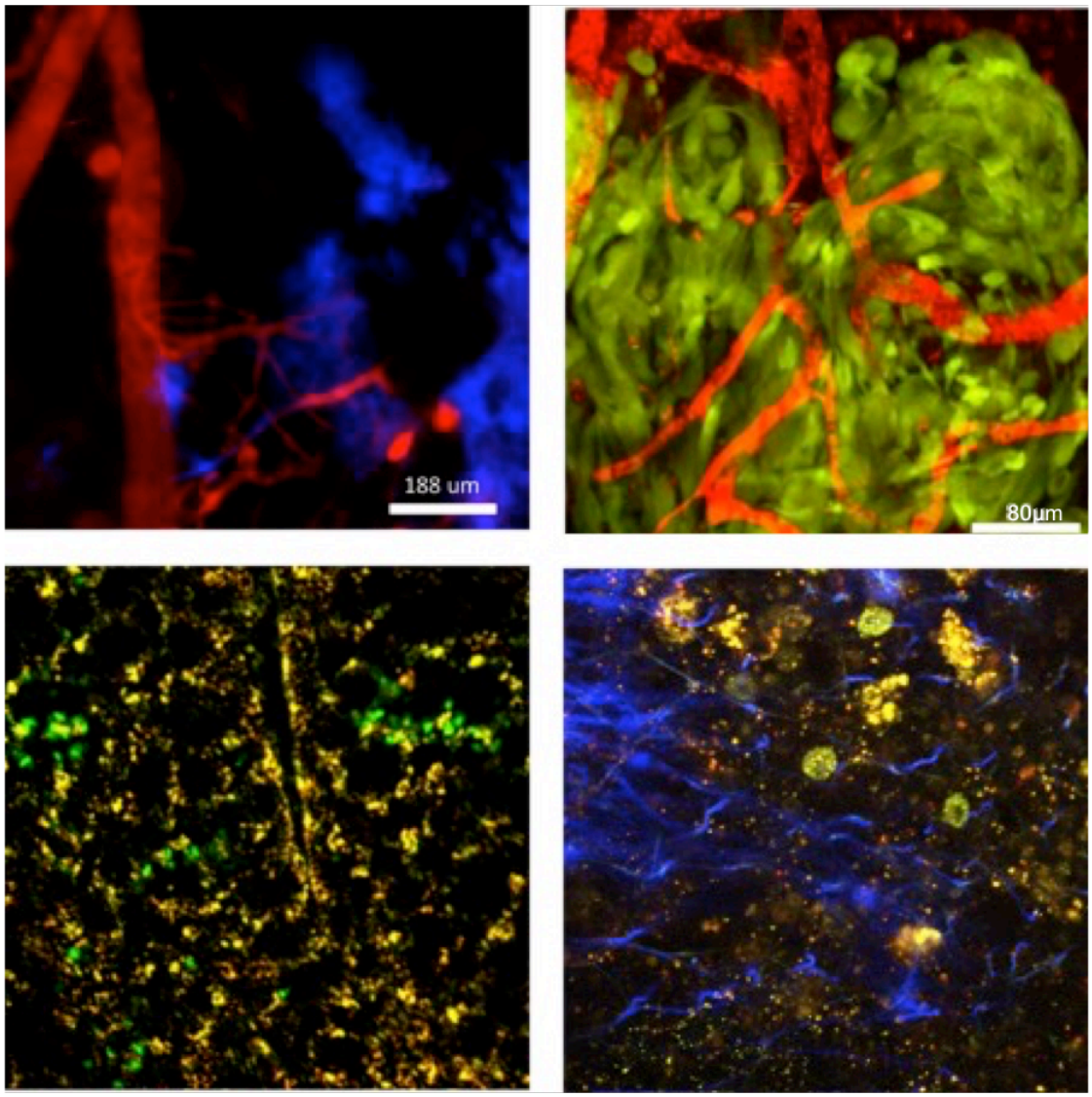

Figure 2.3 Examples of 2PEF microscopy in highly scattering tissue. A) *in vivo* human endothelial cells (HCMEC, blue) interacting with brain vasculature (red). B) *in viv*o image of advanced glioblastoma (GBM-TSC, green) and newly developed vasculature (red). C) *ex vivo* image of COLO 205 cells (green) lodged into lung tissue (yellow). D) *ex vivo* image of dendritic cells (green) containing nanoparticles (red), in an intact lymph node. Collagen fibers (blue) in lymph node revealed from SHG signal.

2.5 Cell Labeling Strategies for in vivo Imaging

Labeling strategies become very important for imaging multiple cells populations involved in the study of cancer metastasis. With most microscope detection arrangements, a maximum of four colors can be separated into detection channels. In an optimal situation, each label appears in only one channel, clearly differentiating between cellular structures that may not be separable by visual inspection of the image. However, many dyes have broad emission spectra and as such, signal from one dye may appear in more than one channel. Although post imaging un-mixing algorithms can correct for this, if the morphology of the cells in question are visually similar, it may be difficult to distinguish cell populations *in vivo*. To overcome this challenge, use of multiple excitation wavelengths where the selected dyes have disparate absorption spectra can remove ambiguity.

Prior to imaging, cells can be labeled endogenously or exogenously. Endogenous labeling includes insertion of fluorescent proteins (FP) into the cell genome. This method is typically very stable and allows visualization of cells after division since the FP is stably passed on to progeny. Exogenous labeling involves dye incorporation via cell uptake from its outside surroundings and is usually done 1 hour to 3 days prior to imaging. Dyes are mixed in with cell media and after an allotted amount of time are endocytosed into the cell cytosol. This method is ideal for short-term *in vivo* experiments or when using freshly isolated cells not suited for long-term cell culture. Often these dyes are using as tracking for quantitative analysis of cellular activity and compartmentalization. Label choice depends greatly on the experimental

setup. Table 1 lists dyes used in studies throughout my thesis along with optimal emission, excitation wavelengths and comments on usage.

	Peak 2PE Absorption (nm)	Peak 2PE Emission (nm)	Common Use/Notes
CMTMR	800	590	Cell labeling (cytosol)
BCECF (Invitrogen)	800	526	Cell labeling (cytosol) Not ideal label for ex vivo imaging. Cells lost fluorescence post-injection
DiD/DiO/DiI (Invitrogen)	810 - 830	670/500/571	Cell labeling (cytosol) Ideal for adoptive transfer studies
Fluorescent Nanospheres Crimson red	800 - 900	641-680	Cell labeling; can be injected directly into vasculature for use as phagocytosis indicator
Hoechst 33258	780nm-830nm	455nm	Labels nuclei. Can be injected directly into vasculature to label all nuclei in bloodstream

Table 2.1 Common fluorescent labeling strategies for 2PEF cellular imaging

2.6 Conclusion

Since the inception of the femtosecond laser and the first published demonstration of two-photon microscopy (2, 3, 18) over 25 years ago, we have witnessed amazing discoveries within the field of cancer metastasis. Two photon excited fluorescence (2PEF) microscopy provides a large imaging depth, sub-cellular resolution, and a longer-term imaging capacity compared to other imaging modalities. Furthermore, it provides a unique capability to visualize processes occurring within intact tissue.

A number of technological advancements within the imaging field have further enhanced imaging capability. The development of laser systems with longer infrared wavelengths allow us to image deeper and excite higher order nonlinear processes (19-21). Using the same optical configuration, we can simultaneously excite multiple nonlinear optical processes, such as harmonic generation (22), in addition to multiphoton processes. This is of particular significance when considering the fluorescence of collagen under second harmonic generation (SHG) (23-26) and myelin under third harmonic generation (THG) (27). More sophisticated detection systems collect and separate sample fluorescence to provide greater spectral resolution, facilitating the practical observation of more fluorescent dyes.

What was once a highly specialized imaging technique has become more accessible, making it possible for more non-optical scientists to use. There are now many popular commercial 2PEF microscopes, including the Ultima series (Bruker),

LSM780 (Zeiss), and FluoView FV1000-MPE (Olympus). While commercial sources provide easy access they are often constructed in a standardized way that provides little room for adjustments. Individual laboratories are also making completely customizable microscopes such as the Parker Lab (UC Irvine) and the microscopes built and used in the Schaffer-Nishimura Labs. 2PEF microscopy has become a key visualization tool. Combined with the increasing development of transgenic mouse models, an ever-expanding catalog of fluorescent dyes and proteins (28), and sophisticated detection systems, we are now able to answer questions that were never possible before in the physiologically relevant *in vivo* system.

2.7 References

1. Sheppard CJ, Kompfner R (1978) Resonant scanning optical microscope. *Appl Opt* 17(18):2879–2882.

2. Denk W, Strickler JH, Webb WW (1990) Two-photon laser scanning fluorescence microscopy. *Science* 248(4951):73–76.

3. Zipfel WR, Williams RM, Webb WW (2003) Nonlinear magic: multiphoton microscopy in the biosciences. *Nat Biotechnol* 21(11):1369–1377.

4. Centonze VE, White JG (1998) Multiphoton Excitation Provides Optical Sections from Deeper within Scattering Specimens than Confocal Imaging. *Biophysical Journal* 75(4):2015–2024.

5. Masters B, So P (2001) Confocal microscopy and multi-photon excitation microscopy of human skin in vivo. *Opt Express* 8(1):2–10.

6. Schwille P, Haupts U, Maiti S, Webb WW (1999) Molecular Dynamics in Living Cells Observed by Fluorescence Correlation Spectroscopy with One- and Two-Photon Excitation. *Biophysical Journal* 77(4):2251–2265.

7. Gu M, Gan X, Kisteman A, Xu MG (2000) Comparison of penetration depth between two-photon excitation and single-photon excitation in imaging through turbid tissue media. *Appl Phys Lett* 77(10):1551.

8. Tsai T-H, et al. (2006) Optical signal degradation study in fixed human skin using confocal microscopy and higher-harmonic optical microscopy. *Opt Express* 14(2):749–758.

9. Condeelis J, Segall JE (2003) Intravital imaging of cell movement in tumours. *Nat Rev Cancer* 3(12):921–930.

10. Tanaka K, et al. (2014) In vivo optical imaging of cancer metastasis using multiphoton microscopy: a short review. *Am J Transl Res* 6(3):179–187.

11. Fein MR, Egeblad M (2013) Caught in the act: revealing the metastatic process by live imaging. *Disease Models & Mechanisms* 6(3):580–593.

12. Kienast Y, et al. (2009) technical reports. *Nature Medicine* 16(1):116–122.

13. Winkler F, et al. (2009) Imaging glioma cell invasion in vivoreveals mechanisms of dissemination and peritumoral angiogenesis. *Glia* 57(12):1306–1315.

14. Brown EB, et al. (2001) In vivo measurement of gene expression, angiogenesis

and physiological function in tumors using multiphoton laser scanning microscopy. *Nature Medicine* 7(7):864–868.

15. Wang W, et al. (2002) Single cell behavior in metastatic primary mammary tumors correlated with gene expression patterns revealed by molecular profiling. *Cancer Research* 62(21):6278–6288.

16. Holtmaat A, et al. (2009) Long-term, high-resolution imaging in the mouse neocortex through a chronic cranial window. *Nature Protocols* 4(8):1128–1144.

17. Mostany R, Portera-Cailliau C (2008) A Craniotomy Surgery Procedure for Chronic Brain Imaging. *JoVE* (12). doi:10.3791/680.

18. Xu C, Zipfel W, Shear JB, Williams RM, Webb WW (1996) Multiphoton fluorescence excitation: new spectral windows for biological nonlinear microscopy. *Proc Natl Acad Sci USA* 93(20):10763–10768.

19. Kobat D, et al. (2009) Deep tissue multiphoton microscopy using longer wavelength excitation. *Opt Express* 17(16):13354–13364.

20. Kobat D, Horton NG, Xu C (2011) In vivo two-photon microscopy to 1.6-mm depth in mouse cortex. *J Biomed Opt* 16(10):106014.

21. Theer P, Hasan MT, Denk W (2003) Optics InfoBase: Optics Letters - Two-photon imaging to a depth of 1000 μm in living brains by use of a Ti:Al2O3 regenerative amplifier. *Opt Lett*.

22. Balu M, et al. (2009) Effect of excitation wavelength on penetration depth in nonlinear optical microscopy of turbid media. *J Biomed Opt* 14(1):010508.

23. Zipfel WR, et al. (2003) Live tissue intrinsic emission microscopy using multiphoton-excited native fluorescence and second harmonic generation. *Proceedings of the National Academy of Sciences* 100(12):7075–7080.

24. Roth S, Freund I (1979) Second harmonic generation in collagen. *J Chem Phys* 70(4):1637–1643.

25. Zoumi A, Yeh A, Tromberg BJ (2002) Imaging cells and extracellular matrix in vivo by using second-harmonic generation and two-photon excited fluorescence. *Proceedings of the National Academy of Sciences* 99(17):11014–11019.

26. Cicchi R, et al. (2014) In vivo non-invasive monitoring of collagen remodelling by two-photon microscopy after micro-ablative fractional laser resurfacing. *J Biophotonics* 7(11-12):914–925.

27. Farrar MJ, et al. (2012) Chronic in vivo imaging in the mouse spinal cord using

an implanted chamber. *Nat Meth* 9(3):297–302.

28. Bestvater F, et al. (2002) Two-photon fluorescence absorption and emission spectra of dyes relevant for cell imaging. *J Microsc* 208(2):108–115.

CHAPTER 3
CIRCULATING TUMOR CELLS

Permission to reproduce **Table 3.1** was granted by American Cancer Society. *Cancer Facts & Figures 2015*. Atlanta: American Cancer Society; 2015.

3.1 Prevalence and Clinical Significance

Metastasis is the state of disease when a primary tumor has disseminated to other organs to form secondary tumors. Metastatic cancers are more difficult to treat than primary tumors due to vast genetic differences and their ability to remain dormant for years before becoming clinically apparent. Moreover, the majority of cancer treatments only target cancer growth rather than cancer spread. As such, metastasis is a major problem, accounting for over 90% of cancer-related deaths (1). In addition, the 5-year survival rate **(Table 1)** decreases dramatically for tumors that are detected distantly. In the case of prostate cancer, 99% of patients reach the 5-year survival landmark if detected locally whereas the prognosis decreases to 23% (2). Much research has been devoted to understanding the metastatic process in an effort to gain insight into the best therapeutic targets to contain and prevent its spread.

Five-Year Relative Survival Rates		
	Local	**Disseminated**
Breast	99	25
Colon & Rectum	90	13
Pancreas	26	2
Prostate	99	28
Stomach	64	4
Ovary	92	27
Melanoma	98	16
Kidney	92	12
Oral Cavity	83	37

Table 3.1 Five-year Relative Survival Rates by Stage at Diagnosis, US, 2004-2010.

Adapted from American Cancer Society. Cancer Facts & Figures 2015. Atlanta: American Cancer Society; 2015.

3.2 Stages of Metastasis

Metastasis is a highly complex and inefficient process that can be characterized in five stages, invasion, intravasation, circulation, extravasation, and proliferation (Figure 1). First, tumor cells undergo *invasion*; the migration of cells from the primary tumor mass in response to a chemical and/or oxygen gradient. Next, migrating cells *intravasate* into the blood circulation where they are commonly referred to as circulating tumor cells (CTCs). Lymphatic intravasation also occurs, however to a lesser extent. Many CTCs can be shed from a primary tumor but most are unable to withstand the force of circulation and die. Small numbers of CTCs are able to *extravasate*, exiting the blood and/or lymphatic circulation to enter a secondary organ. Upon extravasation, cells can die, enter a dormant non-proliferative state, or continue to *proliferate* into what finally becomes a metastatic lesion. Although these steps are described as a progression, it is likely that metastasis occurs as a loop. A new batch of CTCs can be shed, just as older ones extravasate into a secondary organ. This reality is all the more relevant since current imaging technologies may not reveal the presence of a micrometastasis at the time of diagnosis.

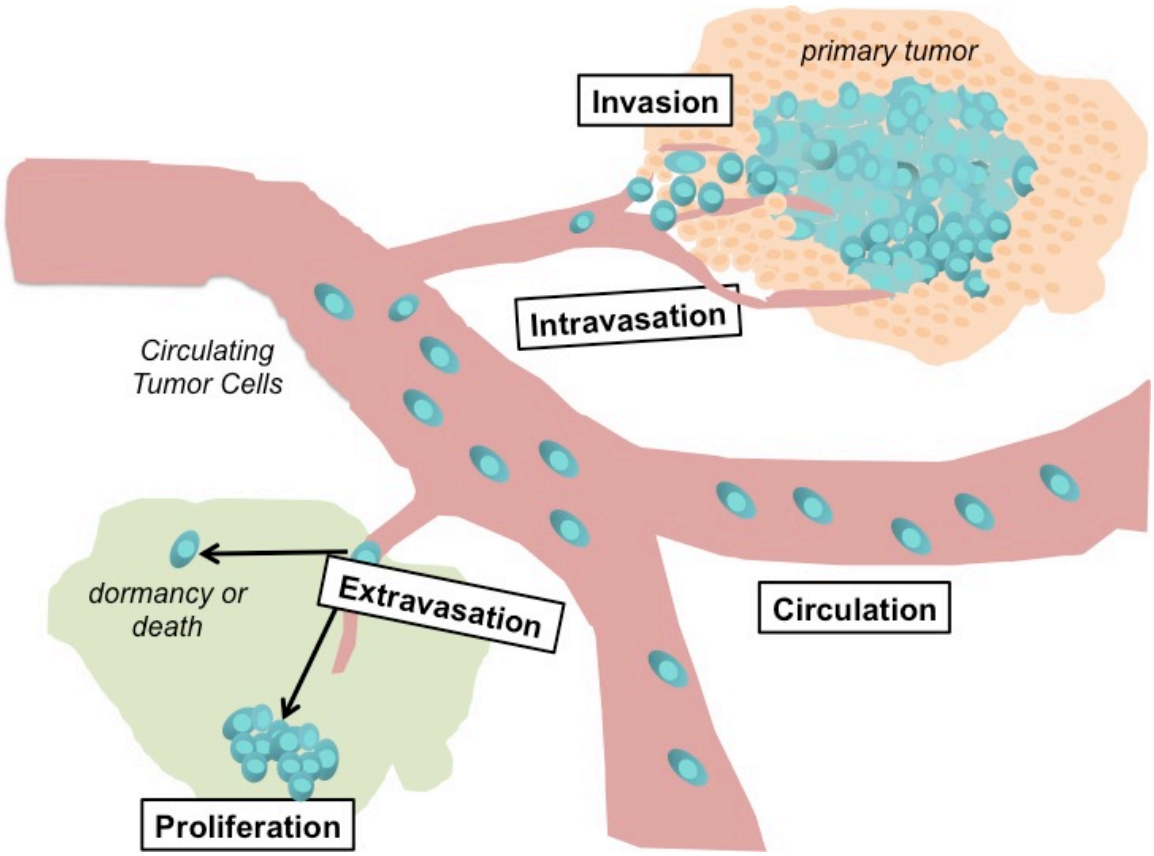

Figure 3.1 Diagram of the Stages of Metastasis

Therapeutically, each stage can be seen as a target to limit and prevent metastasis process. Eliminating metastatic cells at any step in the process, has the ability to prevent proliferation at a secondary site and associated poorest clinical outcome. Many drugs that attempt to do just that. Bevacizumab targets intravasation by inhibiting angiogenesis (3). MMP inhibitors like Prinomastat and Metastat, prevent cancer cells from being able to degrade extracellular matrix, a process that is known to promote both intravasation and extravasation in preclinical animal models (4). Disappointingly, MMP inhibitors have not shown efficacy in human clinical trials (5) and drugs that target angiogenesis are effective in limiting tumor growth but only lead to dormancy rather than a real cure (6). The remainder of this chapter explores how targeting CTCs while in the circulation environment can eliminate metastasis.

3.3 Circulating Tumor Cells

CTCs are a rare cell population with monumental consequences for cancer progression and treatment. CTCs are secreted from a primary tumor, travel through the circulation, and ultimately extravasate into a second organ. Depending on the origin of cancer and the disease stage, up to 1 million cells can be shed per gram of tumor per day (7). This cell shedding also can occur in a temporally inconsistent pattern (8). CTCs are a bottleneck form metastasis, since cells must breakaway from the primary tumor and travel through the blood or lymphatic circulation to form a successful metastasis in another organ. This poses great possibilities to manipulate and monitor CTCs for cancer treatment.

3.4 Circulating Tumor Cells as Clinical Prognosis Marker

CTCs are a useful prognosis marker because they can be used as an indicator of cancer disease progression. CTCs can be found within the bloodstream before the primary tumor is detectable, after primary tumor resection and can appear before tumor recurrence (9, 10). Still, the significance of these circulating cells is still debated due to the inhomogeneity of CTC enumeration results not only amongst patients, but amongst measurement technologies.

Great efforts have been made to isolate and characterize circulate tumor cells from patient samples; Finding CTCs is a needle in a haystack problem. In half liter of blood there are approximately 6 billion white blood cells (leukocytes), over 3 trillion red blood cells (11), whilst only 1-8 CTCs. Multiple attempts have been made to isolate CTC by using physical or labeling procedures (8, 12-14). However, variability in the sensitivity and specificity of each capturing device to employ different criteria, makes the isolation of CTCs extremely difficult (15). In addition, a trained observer often verifies isolated CTCs which introduces another element for variability. One of the most trusted sources for CTC isolation is CellSearch, which has the first and only FDA-approved CTC testing kit. The CellSearch CTC strategy uses immunomagnetic assays to fluorescently select for cells that contain a nuclei, cytokeratin labeling (marker for cells of epithelial origin) and are negative for CD45 (a global marker for leukocytes) (16).

Caution should however be given to the interpretation of CTC counts. CTC shedding can occur sporadically, increasing the possibility of a false reading. Every assay has a limitation, also leading to the possibility labeling normal cells as CTC and vice versa. Questions remain about the significance of analyzing isolated CTCs. The answer is complicated because captured CTCs do not necessarily represent successful metastasis. This is corroborated by studies that show a significant proportion of isolated and detected CTCs to be apoptotic (17). CTCs can undergo cell death at any stage of metastasis. Therefore, the few that persist acquire survival mutations and to contain a genetically different profile in comparison to the primary tumor. Bypassing the variability amongst isolation methods, enumerating CTCs has allowed clinicians to determine patient prognosis and therapy efficacy (18). The number of detected CTCs, is consistently correlated with a shortened lifespan (19-21).

3.5 Circulating Tumor Cells as a Therapeutic Target

CTC research has centered on their utility as a diagnostic, yet CTCs maybe be equally if not more valuable as a therapeutic target. The circulation stage is an ideal period to target metastasis because CTCs are highly sensitive due to a lack of anchorage proteins and the high stress environment of the bloodstream. This is supported by studies demonstrating that CTCs are more sensitive to apoptosis inducing drugs whilst unanchored (22, 23). Manipulating CTCs for therapeutic benefit remains in its infancy, however the advancement in strategies for targeting and eliminating CTCs are elaborate and promising (7, 24). This includes *in vivo* implantable devices that detect CTCs in patients including the use of thin stainless

steel wire (25), vein indwelling needle system (26) and cell capture tubes (27). Most of these devices are limited by the risk of infection, clots, and anatomical design. To eliminate some of these risks, some devices function *ex vivo* similar to dialysis machines where externally filtered blood is returned to the patient in a closed system. While these systems show efficacy in detecting and filtering CTCs, the devices have to be removed periodically and do not provide continuous control of CTC populations.

While the previously mentioned therapies employ implantation of medical devices, improvements in our understanding of metastasis biology and advancements in nanomedicine, have enabled greater specificity to target CTCs. Nanoparticles synthesized from polymers, liposome, or heavy metals, can be loaded with therapeutic drugs and used as nanocarriers (28). Wide selection of nanoparticle materials available allow design of particles that can control the duration of drug release and match particle size to tumor pore size(29). Nanoparticles can be tagged with ligands to confer binding specificity to target cells. The challenge of nanoparticle therapy is that these particles are distributed passively and may not accumulate in desired areas. Targeting nanoparticles to immune cells evades this problem tumor infiltration and cell-based nanoparticle therapies are increasing in use (30-34). In this dissertation, CTCs are targeted via nanoparticles delivered on the surface of circulating immune cells (33, 35). As these new techniques come to fruition, CTC therapeutics could very well halt the nature of metastatic disease progression and ultimately how clinicians provide cancer treatment.

3.6 References

1. Marx V (2013) Tracking metastasis and tricking cancer. *Nature* 494(7435):133–136.

2. Jemal A, Siegel R, Xu J, Ward E (2010) Cancer statistics, 2010. *CA: A Cancer Journal for Clinicians* 60(5):277–300.

3. Jain RK, et al. (2007) Angiogenesis in brain tumours. *Nat Rev Neurosci* 8(8):610–622.

4. Reymond N, d'Água BB, Ridley AJ (2013) Crossing the endothelial barrier during metastasis. *Nature Publishing Group* 13(12):858–870.

5. Bissett D (2005) Phase III Study of Matrix Metalloproteinase Inhibitor Prinomastat in Non-Small-Cell Lung Cancer. *Journal of Clinical Oncology* 23(4):842–849.

6. Weber GF (2013) Cancer Letters. *Cancer Lett* 328(2):207–211.

7. Hughes AD, King MR (2011) Nanobiotechnology for the capture and manipulation of circulating tumor cells. *WIREs Nanomed Nanobiotechnol* 4(3):291–309.

8. Paterlini-Brechot P, Benali NL (2007) Circulating tumor cells (CTC) detection: Clinical impact and future directions. *Cancer Lett*.

9. Pantel K, Brakenhoff RH, Brandt B (2008) Detection, clinical relevance and specific biological properties of disseminating tumour cells. *Nature Publishing Group* 8(5):329–340.

10. Lin H, Balic M, Zheng S, Datar R, Cote RJ (2011) Disseminated and circulating tumor cells: Role in effective cancer management. *Crit Rev Oncol Hematol* 77(1):1–11.

11. Dean L (2005) Blood and the cells it contains. 1–1.

12. Stott SL, et al. (2010) Isolation and Characterization of Circulating Tumor Cells from Patients with Localized and Metastatic Prostate Cancer. *Science Translational Medicine* 2(25):25ra23–25ra23.

13. Galletti G, et al. (2014) Circulating Tumor Cells in Prostate Cancer Diagnosis and Monitoring: An Appraisal of Clinical Potential. *Mol Diagn Ther* 18(4):389–402.

14. Li J, Sharkey CC, Huang D, King MR (2015) Nanobiotechnology for the Therapeutic Targeting of Cancer Cells in Blood. *Cel Mol Bioeng* 8(1):137–150.

15. Barradas A, Terstappen L (2013) Towards the Biological Understanding of CTC: Capture Technologies, Definitions and Potential to Create Metastasis. *Cancers* 5(4):1619–1642.

16. Allard WJ, et al. (2004) Tumor cells circulate in the peripheral blood of all major carcinomas but not in healthy subjects or patients with nonmalignant diseases. *Clinical Cancer Research* 10(20):6897–6904.

17. Méhes G, Witt A, Kubista E, Ambros PF (2001) Circulating breast cancer cells are frequently apoptotic. *The American Journal of Pathology* 159(1):17–20.

18. Ma X, et al. (2014) Prognostic role of circulating tumor cells and disseminated tumor cells in patients with prostate cancer: a systematic review and meta-analysis. *Tumour Biol* 35(6):5551–5560.

19. Danila DC, et al. (2007) Circulating Tumor Cell Number and Prognosis in Progressive Castration-Resistant Prostate Cancer. *Clinical Cancer Research* 13(23):7053–7058.

20. Budd GT, Cristofanilli M, Ellis MJ, Stopeck A (2006) Circulating Tumor Cells versus Imaging—Predicting Overall Survival in Metastatic Breast Cancer. *Clinical cancer ….*

21. Cristofanilli M (2006) Circulating tumor cells, disease progression, and survival in metastatic breast cancer. *Semin Oncol* 33(3 Suppl 9):S9–14.

22. Goldberg GS, et al. (2001) Global effects of anchorage on gene expression during mammary carcinoma cell growth reveal role of tumor necrosis factor-related apoptosis-inducing ligand in anoikis. *Cancer Research* 61(4):1334–1337.

23. Lane D, Cartier A, Rancourt C, Piché A (2008) Cell detachment modulates TRAIL resistance in ovarian cancer cells by downregulating the phosphatidylinositol 3-kinase/Akt pathway. *Int J Gynecol Cancer* 18(4):670–676.

24. King MR (2012) Rolling in the deep: therapeutic targeting of circulating tumor cells. *Front Oncol* 2. doi:10.3389/fonc.2012.00184.

25. Saucedo-Zeni N, et al. (2012) A novel method for the in vivo isolation of circulating tumor cells from peripheral blood of cancer patients using a functionalized and structured medical wire. *Int J Oncol* 41(4):1241–1250.

26. Zhang H, et al. (2015) In Vivo Capture of Circulating Tumor Cells based on Transfusion with a Vein Indwelling Needle. *ACS Appl Mater Interfaces*. doi:10.1021/acsami.5b06874.

27. Wojciechowski JC, et al. (2008) Capture and enrichment of CD34-positive haematopoietic stem and progenitor cells from blood circulation using P-selectin in an implantable device. *Br J Haematol* 140(6):673–681.

28. Ang CY, Tan SY, Zhao Y (2014) Recent advances in biocompatible nanocarriers for delivery of chemotherapeutic cargoes towards cancer therapy. *Org Biomol Chem* 12(27):4776–4806.

29. Chauhan VP, Jain RK (2013) Strategies for advancing cancer nanomedicine. *Nature Materials* 12(11):958–962.

30. Stephan MT, Moon JJ, Um SH, Bershteyn A, Irvine DJ (2010) Therapeutic cell engineering with surface-conjugated synthetic nanoparticles. *Nature Medicine* 16(9):1035–1041.

31. Stephan SB, et al. (2015) Biopolymer implants enhance the efficacy of adoptive T-cell therapy. *Nat Biotechnol* 33(1):97–101.

32. Huang B, et al. (2015) Active targeting of chemotherapy to disseminated tumors using nanoparticle-carrying T cells. *Science Translational Medicine* 7(291):291ra94.

33. Mitchell MJ, Wayne E, Rana K, Schaffer CB, King MR (2014) TRAIL-coated leukocytes that kill cancer cells in the circulation. *Proceedings of the National Academy of Sciences* 111(3):930–935.

34. Batrakova EV, Gendelman HE, Kabanov AV (2011) Cell-mediated drug delivery. *Expert Opinion on Drug Delivery* 8(4):415–433.

35. Mitchell MJ, King MR (2015) Leukocytes as carriers for targeted cancer drug delivery. *Expert Opinion on Drug Delivery* 12(3):000–000.

CHAPTER 4
TRAIL-COATED LEUKOCYTES THAT KILL CANCER CELLS IN THE CIRCULATION

In this chapter, we present a study that investigates a unique approach to target and kill colon and prostate cancer cells in the blood that causes circulating leukocytes to present the cancer-specific TNF-related apoptosis inducing ligand (TRAIL) on their surface along with E-selectin adhesion receptor. This approach demonstrated in vitro with human blood and also in mice, mimics the cytotoxic activity of natural killer cells and increases the surface area available for delivery of the receptor-mediated signal. The resulting "unnatural killer cells" hold promise as an effective means to neutralize circulating tumor cells that enter blood with the potential to form new metastases.

The following text contains the entire study as I thought it would put my contribution in better context. My specific contribution to the study was using two-photon excited fluorescence (2PEF) microscopy to enumerate live and dead circulating tumor cells lodged in lung tissue, and performed all of the animal experiment data, shown in Figures 2, 5, and 6.

This work is published in *Proceedings of the National Academy of the Sciences*. The manuscript can be found with the following citation:

Mitchell MJ, Wayne E, Rana K, Schaffer CB, King MR (2014) TRAIL-coated leukocytes that kill cancer cells in the circulation. *Proceedings of the National Academy of Sciences* 111(3):930–935.

4.1 Introduction

Over 90% of cancer-related deaths are due to cancer metastasis, the spread of cancer cells from a primary tumor to anatomically distant organs (1). In many types of cancer, cancer cells from the primary tumor can intravasate into the peripheral circulation as circulating tumor cells (CTCs) (2, 3). These CTCs can then interact with the receptor-bearing endothelial cell wall under flow in other organs, in a manner similar to leukocyte extravasation during inflammation and lymphocyte homing to lymphatic tissues (4). Recent studies have shown that CTCs from many types of primary tumors express sialylated carbohydrate ligands similar to leukocytes, which mediate interactions with selectins on the endothelium (5, 6). Selectins possess rapid, force-dependent binding kinetics, which can trigger the rolling adhesion of CTCs along the blood vessel wall (7, 8). CTCs can subsequently transition from rolling to firm adhesion, allowing for transendothelial migration into tissues and eventual formation of micrometastases (9). Surgery and radiation have proven effective at treating primary tumors that do not invade the basement membrane; however, the difficulty of detecting distant micrometastases has made the majority of metastatic cancer treatments unsuccessful.

The development of technologies to directly target CTCs in vivo holds promise in reducing both the metastatic load and the formation of new tumors. Although studies have reported that as many as 1×10^6 cancer cells detach from the primary tumor (per gram) of patients per day (10, 11), CTCs are difficult to detect due to their

sparse concentrations in the bloodstream, as low as 1–100 cells per mL (3, 12). Additionally, there are ~1×10^6 leukocytes or 1×10^9 erythrocytes per single CTC in blood (13). Despite the difference in numbers, both leukocytes and CTCs share similar characteristics in terms of their migration within the bloodstream. Highly deformable erythrocytes experience a drift velocity away from the vessel wall and collect in the center region, displacing less deformable leukocytes and CTCs to the near-wall region in a mechanism termed margination (14). Such margination phenomena can effectively surround CTCs within the circulating leukocyte population, thus making leukocytes a potentially attractive carrier of treatments to CTCs by exploiting

The utilization of leukocytes to treat CTCs directly within the bloodstream has not previously been explored. Here, we describe a therapeutic approach to target and kill circulating cancer cells in the bloodstream by functionalizing leukocytes with the apopto- sis-inducing ligand TRAIL, and the adhesion receptor E-selectin directly within blood under shear flow. The functionalization of leukocytes under flow, effectively creating a form of "unnatural killer cells" within the bloodstream, is shown to be highly effective at treating circulating cancer cells in flowing human blood in vitro, and in the peripheral circulation of mice in vivo.

4.2.1 E-Selectin /TRAIL Liposomes Adhesively Interact and Induce Apoptotic Cancer-Cell Death Under Shear Flow.

Many types of circulating tumor cells (CTCs) and cancer cell lines derived from colon, breast, prostate, and pancreas are known to display glycosylated ligands that allow them to adhesively interact with E-selectin (ES) under physiological shear

flow (15). This interaction has been proposed to explain why some cancers home to tissue-specific capillary beds such as the bone marrow and liver (16, 17). In an attempt to target and kill cancer cells of this form, nanoscale liposomes conjugated with a mixture of recombinant human ES protein and tumor necrosis factor (TNF)-related apoptosis-inducing ligand (TRAIL) were developed **(Fig. 1A, Fig. S1, and Table S1).** TRAIL binds to death receptors 4 and 5 on the surface of cancer cells to induce apoptosis through the intrinsic and extrinsic pathways (18, 19). ES/TRAIL liposomes consisting of a 10% weight ratio of (1,2-dioleoyl-sn-glycero-3-{[N-(5-amino-1-carboxy-pentyl) iminodiacetic acid] succinyl}(nickel salt) (DOGS-Ni-NTA), used to conjugate ES and TRAIL to the liposome surface, were found to be most effective at inducing apoptotic cell death in a colorectal adenocarcinoma (COLO 205) cell line under static conditions **(Fig. S2**), as determined using an Annexin-V apoptosis assay.

In the postcapillary venules where selectin-mediated adhesion and cell extravasation into tissues typically occur, moderate shear rates can initiate flowing cell interactions with the endothelial cell wall (20, 21). To recreate these physical forces in vitro, a cone-and-plate shear assay was developed to probe the inter- actions of cancer cells and ES/TRAIL liposomes under venular shear rates. After exposure to shear flow (shear rate: 188 s^{-1}) for 2 h, COLO 205 cells exposed to ES liposomes displayed their normal morphology whereas substantial membrane blebbing was observed in samples exposed to ES/TRAIL liposomes, characteristic of cells undergoing apoptosis **(Fig. 1B)**. Annexin-V assay revealed that exposure to shear flow for 2 h induced minimal COLO 205 cell apoptosis in untreated controls **(Fig. 1C)**, in addition to treatment with

liposomes in the absence of conjugated protein **(Fig. 1D)** or conjugated solely with ES **(Fig. 1E)** or TRAIL **(Fig. 1F)**. However, a combination of ES/TRAIL conjugated to the liposome surface induced a significant decrease in COLO 205 vi- ability following exposure to shear flow **(Fig. 1 G and H)**.

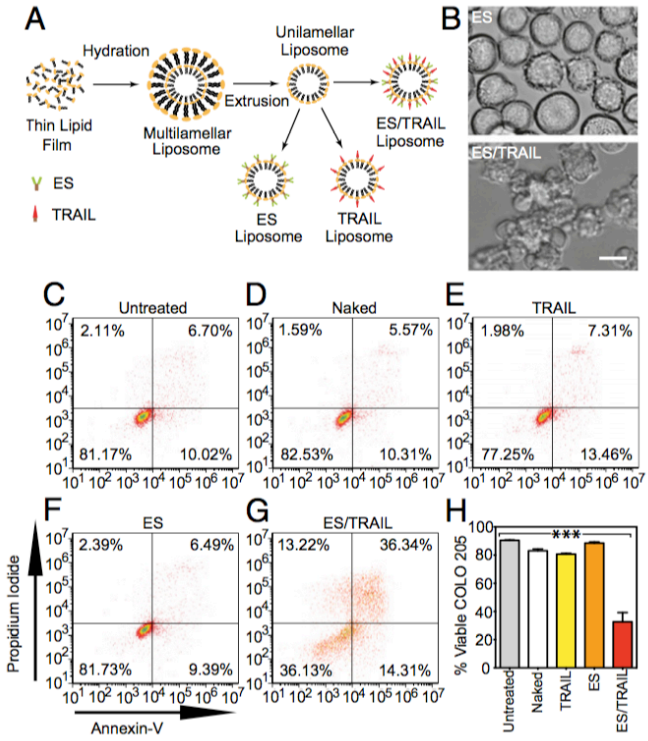

Figure 4.1 ES/TRAIL liposomes adhesively interact with and kill cancer cells under uniform shear flow.

(A) Synthesis of ES, TRAIL, and ES/TRAIL uni- lamellar liposomes using a thin film hydration method. Briefly, lipids in chloroform were dried overnight to form a thin lipid film. Lipids were then hydrated and subjected to freeze–thaw cycles to form multilamellar liposomes, which were extruded through membranes to form unilamellar liposomes. ES, TRAIL, or a combination of ES and TRAIL was then conjugated to Ni-NTA on the liposome surface. To assess the ability of ES/TRAIL liposomes to target and kill cancer cells under flow, ES/TRAIL liposomes were added to a suspension of COLO 205 cancer cells and exposed to shear flow in a cone-and-plate viscometer at a shear rate of 188 s^{-1} for 2 h. Cells were then removed, washed, placed into culture for 24 h, and assessed for cell viability. (B) COLO 205 morphology after treatment with ES (Upper) and ES/TRAIL (Lower) liposomes under shear flow. (Scale bar, 20 μm.) (C–G) Representative propidium iodide/Annexin-V flow cytometry plots of unsheared cancer cells (C) and cells sheared with naked (D), TRAIL-bound (E), ES-bound (F), and ES/TRAIL-bound liposomes (G) under shear flow. Cells were classified into four categories based on dye uptake: viable cells [negative for Annexin-V and propidium iodide (PI)], early apoptotic cells (posi- tive for Annexin-V only), late apoptotic cells (positive for Annexin-V and PI), and necrotic cells (positive for PI only). (H) Percent of viable cells after treatment for each group. n = 3 for all samples. Bars represent the mean ± SD in each treatment group. ***P < 0.0001 (one-way ANOVA with Tukey posttest).

To investigate the adhesive characteristics of ES/TRAIL liposomes to cancer cells under flow, COLO 205 cells were ex- posed to ES/TRAIL liposomes consisting of fluorescent cholesterol and exposed to shear flow as in previous in vitro shear assays. Flow cytometry revealed that >99.9% of the COLO 205 cell population was adhered to ES/TRAIL liposomes after exposure to shear flow **(Fig. S3 A and B)**. Fluorescent micrographs and brightfield overlay images clearly displayed ES/TRAIL liposomes adhered to the surface of COLO 205 cells **(Fig. S3 C and D)**. These data suggest that the presence of the ES adhesion receptor enhances the effect of TRAIL by promoting tighter contacts with the cancer-cell membrane.

4.2.2 ES/TRAIL Liposomes Functionalize Leukocytes in Whole Blood Under Shear Flow in Vitro.

In addition to CTCs, circulating leukocytes also possess ligands for ES, which are necessary in the inflammatory response and lymphocyte homing to lymphatic tissues (1, 22). To assess the potential to functionalize leukocytes with ES/TRAIL to target and kill CTCs, we treated human blood with fluorescent ES/TRAIL liposomes under shear flow in a cone- and-plate viscometer. Upon exposure to shear (shear rate: 188 s^{-1}), ES/TRAIL liposomes readily bind to leukocytes via selectin ligands on the leukocyte surface **(Fig. 2A)**.

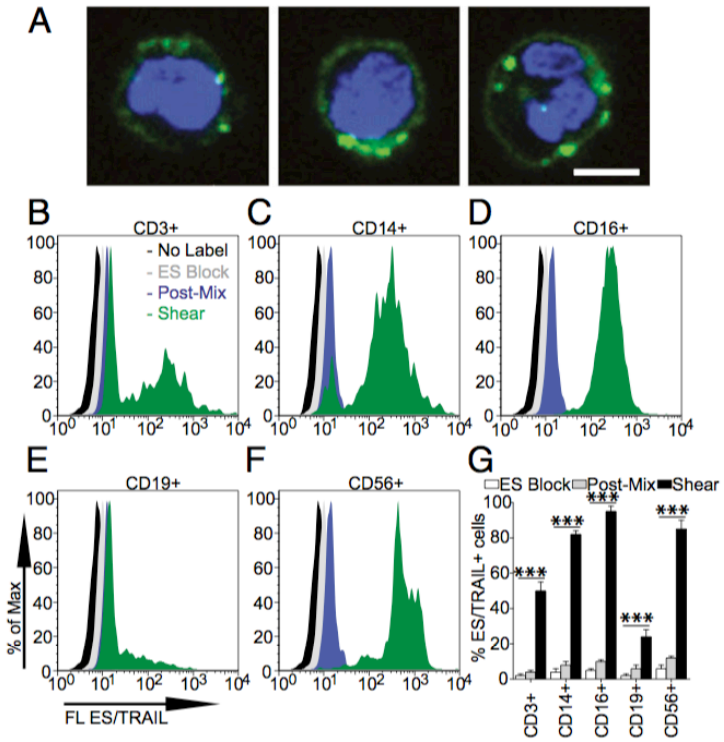

Figure 4.2 ES/TRAIL liposomes adhere to multiple leukocyte subpopulations after exposure to shear flow in whole blood.

(A) Confocal images of ES/TRAIL liposomes (green) bound to human leukocytes (blue, cell nuclei) after ex- posure to shear flow in whole blood in a cone-and-plate viscometer at 188 s^{-1} for 30 min. Leukocytes have nuclear morphology characteristic of monocytes (Left), lymphocytes (Center), and neutrophils (Right). (Scale bar, 5 μm.) (B–G) To assess the adhesion of ES/TRAIL liposomes to leukocyte subpopulations, fluorescent ES/TRAIL liposomes were added to human blood and exposed to shear flow in a cone-and-plate viscometer at a shear rate of 188 s^{-1} for 30 min. Leukocytes were isolated from blood using a Polymorphs density gradient and labeled with CD3, CD14, CD16, CD19, and CD56, which is typically expressed on T lymphocytes, monocytes, neutrophils, B-lympho- cytes, and natural killer cells, respectively. Expression of fluorescent ES/TRAIL (FL ES/TRAIL) liposomes on the surface of leukocytes that are CD3+ (B), CD14+ (C), CD16+ (D), CD19+ (E), and CD56+ (F), determined using flow cytometry. Expression of CD3, CD14, CD16, CD19, and CD56 on the leu- kocyte surface was determined using isotype controls. No label, unsheared cells that were not treated with fluorescent ES/TRAIL liposomes; ES Block, cells treated with fluorescent ES/TRAIL liposomes that were pretreated with an ES functional blocking antibody; Post-Mix, cells labeled with fluorescent ES/TRAIL liposomes immediately after mixing liposomes in whole blood. (G) Percent of CD3+, CD14+, CD16+, CD19+, and CD56+ leukocytes adhered to ES/TRAIL liposomes. n = 3 for all samples. Bars represent the mean ± SD in each treatment group. ***P < 0.0001 (one-way ANOVA with Tukey posttest).

To quantify leukocyte subpopulations that adhere to ES/TRAIL liposomes under flow, leukocytes were separated from whole blood and analyzed for both leukocyte marker expression and adherent ES/TRAIL liposomes using flow cytometry. Functionalized leukocytes were labeled with CD3, CD14, CD16, CD19, and CD56 antibodies, as such markers are commonly expressed on most T lymphocytes, monocytes, neutrophils, B-lymphocytes, and natural killer (NK) cells, respectively (23). Minimal adhesion of ES/TRAIL liposomes to leukocytes in blood was observed in the presence of a functional blocking ES antibody **(Fig. 2 B–G)**. Minimal ES/TRAIL liposome adhesion was also observed immediately after treatment with whole blood. However, after exposure to shear flow, flow cytometry analysis revealed that leukocyte subpopulations positive for CD3 **(Fig. 2B)**, CD14 **(Fig. 2C)**, CD16 **(Fig. 2D)**, CD19 **(Fig. 2E)**, and CD56 **(Fig. 2F)** adhered to ES/TRAIL liposomes to varying degrees **(Fig. 2G)**. Adhesion was also observed on populations of lymphocytes, which suggests that some cytotoxic patrolling of the lymphatic system may also occur in vivo. Leukocyte subpopulations can vary in their E- selectin ligand expression (24) and thus could explain the variations in the number of bound ES/TRAIL liposomes.

4.2.3 ES/TRAIL Functionalization Does Not Induce Significant Leukocyte or Endothelial Cell Death.

To assess the effects of ES/TRAIL functionalization on leukocyte viability, mononuclear leukocytes isolated from human blood were treated with ES/TRAIL liposomes under both static and shear-flow conditions. Annexin-V assays revealed no significant differences in leukocyte viability when leukocytes were incubated with ES

(Fig. S4B) or ES/TRAIL **(Fig. S4C)** liposomes under static conditions for 24 h, compared with untreated leukocyte controls **(Fig. S4 A and D)**. Upon functionalization with liposomes under shear flow for 2 h (shear rate, 188 s^{-1}), no significant decreases were found in ES **(Fig. S4F)** or ES/TRAIL **(Fig. S4G)** functionalized leukocytes, compared with untreated leukocyte controls **(Fig. S4 E and H)**. These data suggest that ES/TRAIL liposomes can functionalize leukocytes under flow to target and kill cancer cells, while exerting negligible cytotoxic effects on leukocytes. It is important to note that individual subpopulations of leukocytes have shown apoptotic effects in the presence of TRAIL (25); however, this study focused on the overall effects of ES/TRAIL liposomes on blood- borne leukocytes.

To assess the effects of ES/TRAIL functionalization on endothelial cell viability, human umbilical vein endothelial cells (HUVECs) were treated with ES/TRAIL liposomes in human blood under shear-flow conditions in vitro. Treatment with ES/ TRAIL liposomes or an equivalent concentration of soluble TRAIL in human blood under shear flow for 4 h induced no significant differences in HUVEC viability, compared with un- treated HUVECs exposed to shear in human blood **(Fig. S5)**. These data suggest that ES/TRAIL-functionalized leukocytes exert negligible toxic effects on human endothelial cells under blood-flow conditions.

4.2.4 Apoptotic Effects of ES/TRAIL Therapy Are Enhanced in Human Blood Under Flow

Clinically, CTCs are sparsely distributed in the complex milieu of whole blood, at concentrations as low as 1–100 cells per mL (3, 12). To examine whether

ES/TRAIL liposomes would effectively target cancer cells in the presence of blood cells and serum under flow conditions, we fluorescently labeled colorectal COLO 205 and prostate PC-3 cancer-cell lines and spiked them into human peripheral blood. Surprisingly, under identical shear-flow conditions, ES/TRAIL therapy was even more effective at killing cancer cells in the presence of human blood **(Fig. 3 A–D)**, compared with shearing COLO 205 or PC-3 cells alone in buffer **(Fig. 3E),** with <5% of the fluorescent, viable cancer-cell populations remaining after ES/TRAIL treatment **(Fig. 3E)**. These results suggest that ES/TRAIL therapy is effective at targeting circulating cancer cells derived from multiple organs in human blood.

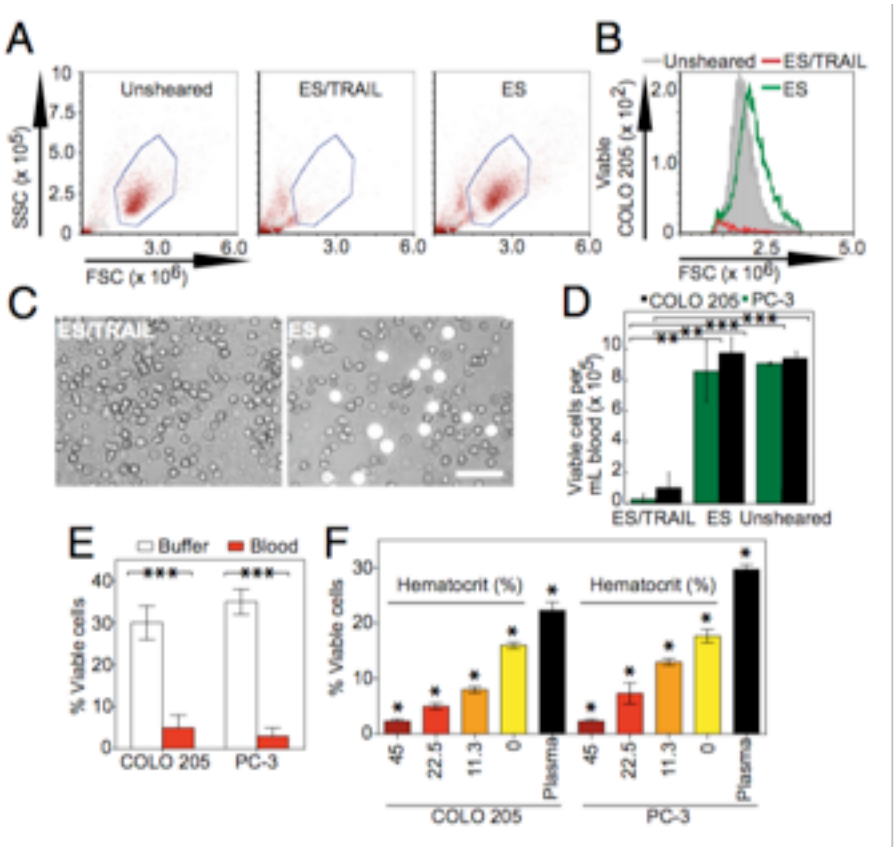

Figure 4.3 ES/TRAIL liposome therapeutic effects are enhanced in human blood under flow in vitro.

(A) Flow cytometry of COLO 205 cancer cells after treatment with ES/TRAIL or ES liposomes in blood under shear flow in a cone-and-plate viscometer at 188 s^{-1} for 2 h. Unsheared, viable untreated cancer cell control. (B) Representative flow cytometry histogram showing the number of viable cancer cells collected. (C) Representative micrographs of COLO 205 cells (white) in blood when treated with ES/TRAIL (Left) and ES only (Right) liposomes in blood under shear flow. (Scale bar, 50 μm.) (D) Number of viable COLO 205 and PC-3 cells per volume of blood after treatment with ES/TRAIL or ES liposomes in blood under shear flow. n = 3 for all samples. Bars represent the mean ± SD in each treatment group. **P < 0.001, ***P < 0.0001 (unpaired t test). (E) Comparison of fraction of COLO 205 and PC-3 cells that remained viable after treatment with ES/TRAIL liposomes in buffer versus blood. n = 3 for all samples. Bars represent the mean ± SD in each treatment group. ***P < 0.0001 (unpaired t test). (F) Fraction of COLO 205 and PC-3 cells that remained viable after treatment with ES/TRAIL lip- osomes in blood with varying percentages of normal hematocrit. Hematocrit was varied whereas other blood components remained constant, based on a normal hematocrit of 45%. Plasma indicates removal of all blood cells. n = 3 for all samples. Bars represent the mean ± SD in each treatment group. *P < 0.05 (one-way ANOVA with Tukey posttest).

To evaluate the impact of blood cells on the efficacy of ES/ TRAIL treatment, fluorescent COLO 205 and PC-3 cells were spiked in human blood of varying hematocrit percentages. All additional blood-cell components were maintained whereas the volume of removed erythrocytes was replaced with plasma from the same blood donor. Interestingly, the apoptotic effects were hematocrit-dependent, as higher hematocrit significantly de- creased the number of viable COLO 205 and PC-3 cells after ES/ TRAIL treatment **(Fig. 3F)**. The enhanced apoptotic effect suggests that blood-cell collisions under flow can promote the apoptotic effects of ES/TRAIL liposomes and agrees with our intuitive understanding of blood rheology, as the presence of erythrocytes is known to create erratic cell paths with frequent cross-streamline displacements (26) and increase the lifetime of colliding doublets to promote aggregate formation (27).

To assess the mechanism by which leukocytes act as a pervading carrier surface for functional TRAIL, blood was pretreated with ES/TRAIL liposomes under shear flow, with blood cells subsequently separated from unbound ES/TRAIL via centrifugation and replaced with fresh blood plasma. ES/TRAIL therapeutic effects under shear flow remained nearly identical, as COLO 205 and PC-3 cells, spiked into a suspension of blood with washed, pretreated blood cells, were killed at roughly the same rate as unwashed blood **(Fig. 4 A–C)**. Thus, upon addition of the ES/ TRAIL liposomes to cancer cell-spiked blood, liposomes attach to the surface of leukocytes and are available for inducing apoptosis in cancer cells that they come into contact with **(Fig. 4 D and E)**. As an indicator of unbound ES/TRAIL liposomes and/or liposome fragments remaining in human blood after shearing pretreatment, the toxicity

of supernatant collected from pretreated blood was tested in COLO 205 culture. An Annexin-V assay showed min- imal COLO 205 cell death after treatment with a supernatant of human plasma and unbound ES/TRAIL, compared with cells treated with plasma supernatant alone **(Fig. S6)**. These data suggest that ES/TRAIL liposomes readily bind to the surface of leukocytes, with minimal unbound liposomes remaining to target and kill cancer cells under flow.

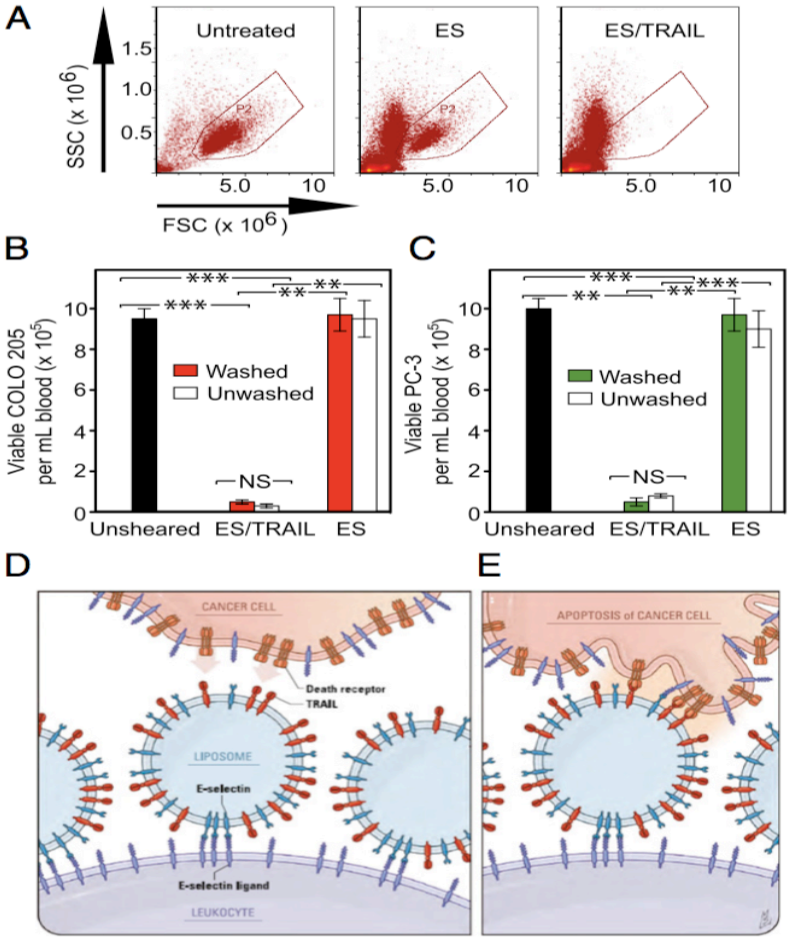

Figure 4.4 ES/TRAIL liposomes functionalize leukocytes under shear flow in vitro to target and kill cancer cells. (A) Flow cytometry plots of COLO 205 cells in untreated samples (Left) and when treated in human blood with ES (Center) or ES/TRAIL (Right) functionalized leukocytes (but no unbound liposomes) under shear flow. (B and C) Number of viable COLO 205 (B) and PC-3 (C) cells per volume of blood after treatment with leukocytes func- tionalized with ES/TRAIL or ES liposomes, but with no unbound liposomes, in human blood (Washed), or after treatment with ES or ES/TRAIL liposomes in blood (Unwashed). n = 3 for all samples. Bars represent the mean ± SD in each treatment group. **P < 0.001, ***P < 0.0001 (unpaired t test). (D and E) Schematic of the two-step mechanism involving decoration of leuko- cytes with liposomes (D), which then contact circulating cancer cells and activate the death receptor (E).

4.2.5 ES/TRAIL Functionalized Leukocytes Reduce Number of Viable Cancer Cells in Mouse Circulation in Vivo.

To assess and compare the cytotoxic effects in vivo with our previous results in vitro, ES/ TRAIL liposomes were also tested for their ability to kill cancer cells flowing in the peripheral circulation of mice. Two million fluorescently labeled COLO 205 cells were injected into the tail vein of immunocompetent C57BL/6J mice, 30 min after injection of 120 μL of either ES/TRAIL liposomes, ES liposomes, or soluble TRAIL **(Fig. 5A)**. Tail-vein injection was used to model leukocyte/CTC interactions in mouse circulation, as this technique has been an accepted and widely used model of lung metastasis (28–31) since the pioneering work of Fidler et al. (32– 34). For these studies, the use of recombinant human E-selectin was continued because of its ability to bind both human COLO 205 cancer cells and mouse neutrophils, which were previously shown to have cross-reactivity and roll on E-selectin (35). Mice were killed 2.5 h after the initial injection, and cancer cells were recovered from the circulation via cardiac puncture. Cancer cells were placed back into culture for 2–3 h before the number of viable cells was quantified.

Using flow cytometry, we measured ~130,000 cancer cells per mL of blood for mice injected with control ES liposomes, compared with <2,000 cancer cells per mL of blood surviving from ES/TRAIL-treated mice **(Fig. 5 B and C)**. Mice injected with buffer or soluble TRAIL had intermediate numbers of cells **(Fig. 5C)** compared with ES and ES/TRAIL-treated samples, likely indicating that ES functionalized liposomes help to retain cancer cells in the circulation by blocking selectin-mediated interaction of the COLO 205 cells with the endothelium. Brightfield micrographs of COLO 205

cells exposed to buffer and soluble TRAIL showed characteristic cancer-cell morphology **(Fig. 5D)**. Micrographs of COLO 205 cells exposed to ES revealed adherent leukocytes on the COLO 205 cell surface without significant morphological change whereas the cancer cells from ES/TRAIL- treated mice showed notable membrane blebbing of COLO 205 cells in the proximity of leukocytes **(Fig. 5D)**. To assess the adhesion of ES/TRAIL liposomes to leukocytes in mouse circulation, mice were injected with ES/TRAIL liposomes containing fluorescent cholesterol and were allowed to circulate for 2.5 h. Brightfield overlay micrographs showed that leukocytes recovered from the mouse circulation were functionalized with ES/ TRAIL liposomes **(Fig. 5E)**, suggesting that ES/TRAIL remains functionalized to leukocytes, which can exert cytotoxic effects onto cancer cells in mouse circulation.

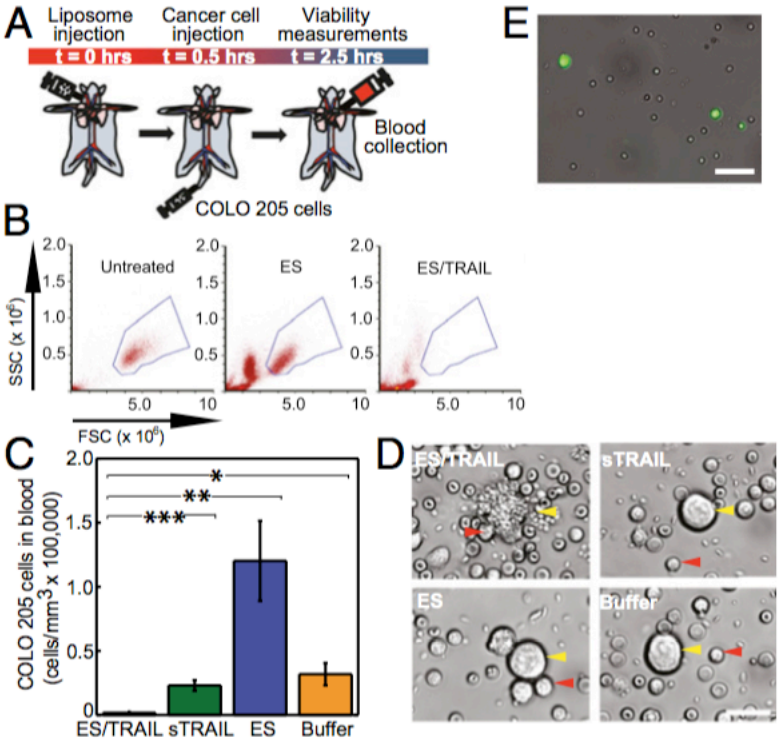

Figure 4.5 ES/TRAIL functionalized leukocytes target and kill cancer cells in the circulation of mice in vivo.

(A) Schematic of in vivo mouse experiment. (B) Flow cytometry of untreated COLO 205 cancer cells (Left) and those re- covered from cardiac puncture from mice treated with ES (Center) and ES/ TRAIL liposomes (Right). (C) Number of viable cancer cells recovered per volume of mouse blood for mice treated with ES/TRAIL liposomes, soluble TRAIL (sTRAIL), ES liposomes, and buffer injections. n = 3 for all samples. Bars represent the mean ± SD in each treatment group. *P < 0.01, **P < 0.001, ***P < 0.0001 (one-way ANOVA with Tukey posttest). (D) Representative micrographs of COLO 205 cells removed from circulation in mice treated with ES/TRAIL liposomes (Upper Left), sTRAIL (Upper Right), ES liposomes (Lower Left), and buffer (Lower Right) injections. (Scale bar, 20 μm.) (E) Leukocytes functionalized with fluorescent ES/TRAIL liposomes (green) upon removal from mouse circulation 2.5 h after injection. (Scale bar, 50 μm.)

4.2.7 ES/TRAIL Treatment Reduces Number and Increases Apoptosis of Remaining Circulating COLO 205 Cells Lodged in Vivo in Mouse Lung.

Previous studies have shown that tumor cells that enter the vasculature via tail-vein injection can lodge into lung vasculature within the first two hours (36). To assess the viability of the remaining circulating cancer cells lodged within mice, fluorescent COLO 205 cells lodged within the lungs of mice were identified using two-photon excited fluorescence microscopy **(Fig. 6 A and B)**. Immediately following euthanasia, the lungs were resected, and two-photon images were acquired in three regions of the lung that were identical for each animal, to obtain an accurate estimate of cell counts **(Fig. 6A)**. Roughly twice as many cells were found in the ES-, soluble TRAIL (sTRAIL), and buffer-treated animals as the ES/TRAIL-treated animals **(Fig. 6C)**, suggesting that many COLO 205 cells had already died and degenerated. The cancer-cell density found in lung suggests that about 1.4 million cancer cells were lodged in the lung for buffer-treated animals (assuming a lung volume of ~0.4 mL), representing the bulk of the two million COLO 205 cells injected.

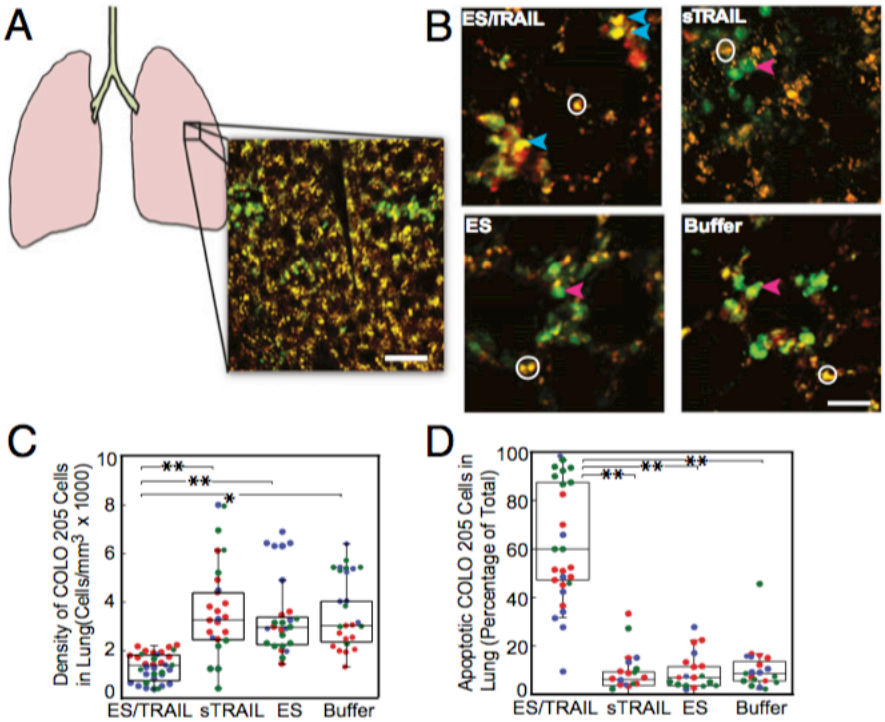

Figure 4.6 Decreased number and increased apoptosis in COLO 205 cells lodged in mouse lung after treatment with ES/TRAIL liposomes. (A) Schematic of mouse lung and example two-photon excited fluorescence (2PEF) image stack from mouse lung where Hoechst-labeled COLO 205 cells (green) are arrested in lung tissue (visible by autofluorescence, yellow). (Scale bar, 80 μm.) (B) The 2PEF images of Hoescht-labeled COLO 205 cells (green) with Alexa Flour 568-labeled Annexin-V apoptosis probe (red) for each experimental group. Red arrows point to apoptotic COLO 205 cells (red and green colocalized), and blue arrows indicate nonapoptotic COLO 205 cells (green only). White circles indicate regions of autofluorescence from lung tissue. (Scale bar, 30 μm.) (C) Density of COLO 205 cells lodged in the lung for each experimental group. (D) Percentage of lodged COLO 205 cells positive for Annexin-V probe for each experimental group. Individual data points represent data from one image stack, with points shown in the same color representing image stacks from the same animal. Superimposed box plots bound the 25th to 75th percentage of all data points and the whiskers extend 1.5 times the interquartile range beyond the boxes. The horizontal lines within the boxplot represent the median. n = 3 animals for each experimental group. *P < 0.01, **P < 0.0001 (one-way ANOVA with Tukey posttest).

We then evaluated the apoptotic effects of ES/TRAIL liposomes on cancer cells that have already lodged into the lungs of mice. After the injections of liposomes and COLO 205 at previously used time points **(Fig. 5A)**, we injected a solution of Annexin-V tagged with a fluorescent Alexa 594 dye to assess for phosphatidylserine flipping on the COLO 205 cell membrane, characteristic of apoptosis. Mouse lungs were imaged using two-photon microscopy to determine whether Hoescht-labeled COLO 205 cells were also positive for Annexin-V labeling. In addition to the de- creased density of cancer cells lodged in mouse lung **(Fig. 6C)**, we also found a dramatic increase in apoptosis of the cancer cells **(Fig. 6 B and D)** in the ES/TRAIL liposome-treated mice com- pared with other groups. Soluble TRAIL protein injected into mice following the same protocol displayed minimal cytotoxic activity comparable with control, as expected due to its short circulation half-life (37). Mice injected with ES/TRAIL liposomes survived for over 2 wk with no loss in body weight (n = 3). These data suggest that ES/TRAIL treatment serves to decrease the number of remaining circulating COLO 205 cells lodged in mouse lung, while increasing the fraction of them that are apoptotic.

4.3 Discussion

Natural killer cells, activated by interleukin-2 or other factors, are induced to present TRAIL protein on their surface. These cells participate in immunosurveillance against micrometastases in the body and comprise 10–20% of peripheral blood mono- nuclear cells (38, 39). Although the liposome-coated leukocytes described here are not specifically programmed to actively in- vade tissues and seek out solid tumors, they do

have frequent opportunities for incidental contact with CTCs in the blood- stream. Interestingly, infiltration of neutrophils and macro- phages throughout the interior of solid tumor masses has been found in dynamic, self-seeding tumors, suggesting that some degree of homing of normally functioning leukocytes to solid tumors could be expected (40, 41). We find that TRAIL is most potent when in its natural state—tethered to the surface of leukocytes in shear flow—rather than freely soluble or on untethered liposomes in the absence of blood. Tethering nanoscale liposomes to the surface of peripheral blood leukocytes is also beneficial for increasing liposome circulation time, by avoiding renal clearance mechanisms.

So why do leukocytes coated with ES/TRAIL liposomes have much higher cytotoxic activity in shear flow, compared with isolated ES/TRAIL liposomes or soluble TRAIL protein? The answer may lie in the compressive force between surfaces. Two spherical particles colliding in linear shear flow will experience a compressive force between them, which scales as $F_c \sim \mu*G*a*b$, where μ is the fluid viscosity, G is the shear rate, and a and b are the radii of the smaller and larger sphere, respectively (42). Thus, a 10-μm-diameter leukocyte colliding with a cancer cell will experience 100 times the compressive force of a 100-nm liposome colliding with a cancer cell. Compressive forces act to flatten down any cell-surface glycocalyx composed of biologically inert macro- molecules, thus allowing TRAIL to come within a reactive distance to the cancer cell death receptors and form bonds. The physics of force-induced flattening and penetration of cell glycocalyx to facilitate surface receptor binding to ligands on an op- posing cell surface has been analyzed in

the context of leukocyte adhesion to the vascular endothelium (43, 44).

Recombinant human TRAIL/Apo2L, also known as PRO1762 developed by Amgen/Genentech, has been the subject of numerous Phase 1, 1a, 2, and 3 clinical trials over the past decade, with minimal adverse effects reported (45, 46). There are many intracellular proteins, such as the inhibitors of apoptosis protein (IAPs) family members, that also confer TRAIL resistance to normal cells (47). Additionally, the dosages of TRAIL used in this current study ranged from 0.06–0.08 mg/kg, two orders of magnitude lower than the clinical dosages of 1–30 mg/kg used in human clinical trials. Although different types of cancer cells show different levels of sensitivity to TRAIL-induced apoptosis, it has been well documented that there is a wide range of agents known to sensitize cancer cells to TRAIL-mediated apoptosis, including conventional chemotherapeutics (camptothecin, cisplatin, doxorubicin, 5-fluorouracil, irinotecan, paclitaxel, gemcitabine), proteasome inhibitors, Bcl-2 inhibitors, IAP antagonists, histone deacetylase inhibitors, CD20 antibodies, irradiation, synthetic triterpenolds, Sorafenib, aspirin, and natural products such as curcumin and piperlongumine (48).

What remains to be seen is whether ES/TRAIL liposomes can successfully prevent the formation of metastatic tumors; future work should focus on addressing this question. Additionally, human hepatocytes have shown sensitivity to TRAIL (49) although ES/TRAIL liposome adhesion to the leukocyte surface could reduce TRAIL uptake by the reticulo-endothelial system in the liver. The present study, however, represents an important first step toward the targeting of CTCs in the bloodstream as a

means to prevent cancer metastasis. Clinically, for instance, one could envision using these liposomes as a preventive mea- sure upon diagnosis of highly metastatic hematogenous cancers such as those originating in breast, prostate, and lung.

4.4 Acknowledgements

The authors thank Dr. Razelle Kurzrock for discussion on TRAIL toxicity, Julie Kohn and Brooke Mason of the Reinhart-King Lab for endothelial cell protocols, and Jeff Mattison for blood work. The work described was supported by the Cornell Center on the Microenvironment and Metastasis through Award U54CA143876 from the National Cancer Institute.

4.5 References

1. Chaffer CL, Weinberg RA (2011) A perspective on cancer cell metastasis. Science 331(6024):1559–1564.
2. Riethdorf S, Wikman H, Pantel K (2008) Review: Biological relevance of disseminated tumor cells in cancer patients. Int J Cancer 123(9):1991–2006.
3. Maheswaran S, Haber DA (2010) Circulating tumor cells: A window into cancer bi- ology and metastasis. Curr Opin Genet Dev 20(1):96–99.
4. Coussens LM, Werb Z (2002) Inflammation and cancer. Nature 420(6917):860–867.
5. McDonald B, et al. (2009) Systemic inflammation increases cancer cell adhesion to hepatic sinusoids by neutrophil mediated mechanisms. Int J Cancer 125(6):1298–1305.
6. van Ginhoven TM, van den Berg JW, Dik WA, Ijzermans JNM, de Bruin RWF (2010) Preoperative dietary restriction reduces hepatic tumor load by reduced E-selectin- mediated adhesion in mice. J Surg Oncol 102(4):348–353.
7. Gassmann P, Kang ML, Mees ST, Haier J (2010) In vivo tumor cell adhesion in the pulmonary microvasculature is exclusively mediated by tumor cell—

endothelial cell interaction. BMC Cancer 10:177.

8. Köhler S, Ullrich S, Richter U, Schumacher U (2010) E-/P-selectins and colon carcinoma metastasis: First in vivo evidence for their crucial role in a clinically relevant model of spontaneous metastasis formation in the lung. Br J Cancer 102(3):602–609.

9. Rahn JJ, et al. (2005) MUC1 mediates transendothelial migration in vitro by ligating endothelial cell ICAM-1. Clin Exp Metastasis 22(6):475–483.

10. Chang YS, et al. (2000) Mosaic blood vessels in tumors: Frequency of cancer cells in contact with flowing blood. Proc Natl Acad Sci USA 97(26):14608–14613.

11. Butler TP, Gullino PM (1975) Quantitation of cell shedding into efferent blood of mammary adenocarcinoma. Cancer Res 35(3):512–516.

12. Allard WJ, et al. (2004) Tumor cells circulate in the peripheral blood of all major carcinomas but not in healthy subjects or patients with nonmalignant diseases. Clin Cancer Res 10(20):6897–6904.

13. Yu M, Stott S, Toner M, Maheswaran S, Haber DA (2011) Circulating tumor cells: Approaches to isolation and characterization. J Cell Biol 192(3):373–382.

14. Firrell JC, Lipowsky HH (1989) Leukocyte margination and deformation in mesenteric venules of rat. Am J Physiol 256(6 Pt 2):H1667–H1674.

15. Läubli H, Borsig L (2010) Selectins promote tumor metastasis. Semin Cancer Biol 20(3): 169–177.

16. Gout S, Tremblay PL, Huot J (2008) Selectins and selectin ligands in extravasation of cancer cells and organ selectivity of metastasis. Clin Exp Metastasis 25(4):335–344.

17. Barthel SR, et al. (2009) Alpha 1,3 fucosyltransferases are master regulators of prostate cancer cell trafficking. Proc Natl Acad Sci USA 106(46):19491–19496.

18. Ashkenazi A, Holland P, Eckhardt SG (2008) Ligand-based targeting of apoptosis in cancer: the potential of recombinant human apoptosis ligand 2/Tumor necrosis factor-related apoptosis-inducing ligand (rhApo2L/TRAIL). J Clin Oncol 26(21):3621–3630.

19. Walczak H, et al. (1999) Tumoricidal activity of tumor necrosis factor-related apo- ptosis-inducing ligand in vivo. Nat Med 5(2):157–163.

20. Kim MB, Sarelius IH (2003) Distributions of wall shear stress in venular convergences of mouse cremaster muscle. Microcirculation 10(2):167–178.

21. Mitchell MJ, King MR (2013) Computational and experimental models of

cancer cell response to fluid shear stress. Front Oncol 3:44.

22. Springer TA (1994) Traffic signals for lymphocyte recirculation and leukocyte emigration: the multistep paradigm. Cell 76(2):301–314.

23. Doherty TA, et al. (2012) STAT6 regulates natural helper cell proliferation during lung inflammation initiated by Alternaria. Am J Physiol Lung Cell Mol Physiol 303(7):L577–L588.

24. Malý P, et al. (1996) The alpha(1,3)fucosyltransferase Fuc-TVII controls leukocyte trafficking through an essential role in L-, E-, and P-selectin ligand biosynthesis. Cell 86(4):643–653.

25. Janssen EM, et al. (2005) CD4+ T-cell help controls CD8+ T-cell memory via TRAIL- mediated activation-induced cell death. Nature 434(7029):88–93.

26. Goldsmith HL (1968) The microrheology of red blood cell suspensions. J Gen Physiol 52(1):5–28.

27. Goldsmith HL, Bell DN, Braovac S, Steinberg A, McIntosh F (1995) Physical and chemical effects of red cells in the shear-induced aggregation of human platelets. Biophys J 69(4):1584–1595.

28. Yan L, Cai Q, Xu Y (2013) The ubiquitin-CXCR4 axis plays an important role in acute lung infection-enhanced lung tumor metastasis. Clin Cancer Res 19(17):4706–4716.

29. Tucci P, et al. (2012) Loss of p63 and its microRNA-205 target results in enhanced cell migration and metastasis in prostate cancer. Proc Natl Acad Sci USA 109(38):15312–15317.

30. Chang C-Y, Lin S-C, Su W-H, Ho C-M, Jou Y-S (2012) Somatic LMCD1 mutations pro- moted cell migration and tumor metastasis in hepatocellular carcinoma. Oncogene 31(21):2640–2652.

31. Kim S, et al. (2009) Carcinoma-produced factors activate myeloid cells through TLR2 to stimulate metastasis. Nature 457(7225):102–106.

32. Fidler IJ (1975) Biological behavior of malignant melanoma cells correlated to their survival in vivo. Cancer Res 35(1):218–224. 33.

33. Fidler IJ (1974) Inhibition of pulmonary metastasis by intravenous injection of specifically activated macrophages. Cancer Res 34(5):1074–1078.

34. Fidler IJ, Nicolson GL (1976) Organ selectivity for implantation survival and growth of B16 melanoma variant tumor lines. J Natl Cancer Inst 57(5):1199–1202.

35. Kato N, et al. (2009) The E-selectin ligand basigin/CD147 is responsible for neutrophil recruitment in renal ischemia/reperfusion. J Am Soc Nephrol 20(7):1565–1576.

36. Fidler IJ, Nicolson GL (1977) Fate of recirculating B16 melanoma metastatic variant cells in parabiotic syngeneic recipients. J Natl Cancer Inst 58(6):1867–1872.

37. Xiang H, Nguyen CB, Kelley SK, Dybdal N, Escandón E (2004) Tissue distribution, stability, and pharmacokinetics of Apo2 ligand/tumor necrosis factor-related apoptosis-inducing ligand in human colon carcinoma COLO205

tumor-bearing nude mice.
38. Drug Metab Dispos 32(11):1230–1238. 38. Takeda K, et al. (2005) TRAIL identifies immature natural killer cells in newborn mice and adult mouse liver. Blood 105(5):2082–2089.
39. Waldhauer I, Steinle A (2008) NK cells and cancer immunosurveillance. Oncogene 27(45):5932–5943.
40. Kim MY, et al. (2009) Tumor self-seeding by circulating cancer cells. Cell 139(7):1315–1326.
41. Bernal M, et al. (2011) Leukocyte infiltrate in gastrointestinal adenocarcinomas is strongly associated with tumor microsatellite instability but not with tumor immunogenicity. Cancer Immunol Immunother 60(6):869–882.
42. Shankaran H, Neelamgham S (2004) Hydrodynamic forces applied on intercellular bonds, soluble molecules, and cell-surface receptors. Biophys J 86(1 Pt 1):576–588.
43. Zhao Y, Chien S, Weinbaum S (2001) Dynamic contact forces on leukocyte microvilli and their penetration of the endothelial glycocalyx. Biophys J 80(3):1124–1140.
44. Sabri S, et al. (2000) Glycocalyx modulation is a physiological means of regulating cell adhesion. J Cell Sci 113(Pt 9):1589–1600.
45. Subbiah V, et al. (2012) Targeting the apoptotic pathway in chondrosarcoma using recombinant human Apo2L/TRAIL (dulanermin), a dual proapoptotic receptor (DR4/ DR5) agonist. Mol Cancer Ther 11(11):2541–2546.
46. Herbst RS, et al. (2010) Phase I dose-escalation study of recombinant human Apo2L/ TRAIL, a dual proapoptotic receptor agonist, in patients with advanced cancer. J Clin Oncol 28(17):2839–2846.
47. Zhang XD, Nguyen T, Thomas WD, Sanders JE, Hersey P (2000) Mechanisms of resistance of normal cells to TRAIL induced apoptosis vary between different cell types. FEBS Lett 482(3):193–199.
48. Ashkenazi A, Herbst RS (2008) To kill a tumor cell: The potential of proapoptotic
49. receptor agonists. J Clin Invest 118(6):1979–1990.
50. Jo M, et al. (2000) Apoptosis induced in normal human hepatocytes by tumor necrosis factor-related apoptosis-inducing ligand. Nat Med 6(5):564–567.

4.6 Supplemental Information Materials and Methods

Reagents and Antibodies

Human serum albumin (HSA), BSA, Accutase, Hepes, DMSO, NaCl, $MgCl_2$, $CaCO_3$ and chloroform (ACS grade with 0.5–1% ethanol added as stabilizer) were all obtained from Sigma-Aldrich. RPMI 1640 cell culture media, FBS, HBSS, penicillin-streptomycin (PenStrep), and Dulbecco's PBS (DPBS) were all obtained from Invitrogen. His-tagged re- combinant human tumor necrosis factor-related apoptosis-inducing ligand (TRAIL), his-tagged recombinant human E-selectin-IgG chimera (ES), and Annexin-V FITC Apoptosis Detection Kit were purchased from R&D Systems. 2′,7′-bis-(2-carboxyethyl)- 5-(and-6)-carboxyfluorescein, acetoxymethyl ester solution and trypsin-EDTA solution were obtained from Invitrogen. PBS- based enzyme-free cell dissociation media was purchased from Millipore. L-α-lysophosphatidylcholine from egg (Egg PC), sphin- gomyelin from egg (Egg SM), ovine wool cholesterol (Chol), 1,2-dioleoyl-sn-glycero-3-[(N-(5-amino-1-carboxypentyl) imino- diacetic acid) succinyl] (nickel salt) (DOGS-Ni-NTA), and 23-(dipyrrometheneboron difluoride)-24-norcholesterol (Bdp-Chol, Ex/Em 490 nm/504 nm) either dissolved in chloroform (Egg PC, Egg SM, Chol, DOGS NTA-Ni) or in powder form (Bdp-Chol) were purchased from Avanti Polar Lipids. Rat anti-human CD62E (E-selectin) antibody was purchased from Abcam. Anti- human CD3, CD14, CD16, CD19, and CD56 conjugated with Pacific Blue, APC Cy7, PERCP-Cy5.5, APC, and PE, respectively, along with corresponding isotypes were all purchased from BD Biosciences.

Cell Lines and Cell Culture

Colon cancer cell line COLO 205 (ATCC number CCL-222) was obtained from ATCC and cul- tured in RPMI 1640 supplemented with 2 mM L-Glutamine, 25 mM Hepes, 10% (vol/vol) FBS and 100 U/mL PenStrep (com- plete media) under humidified conditions at 37 °C and 5% CO_2. Prostate cancer cell line PC-3 (ATCC number CRL-1435) was obtained from ATCC and cultured in F-12K medium supple- mented with 10% (vol/vol) FBS and 100 U/mL PenStrep. Hu- man umbilical vein endothelial cells (HUVECs) were purchased from Cascade Biologics and maintained in Medium 200 (Cas- cade Biologics) supplemented with low-serum growth supple- ment (Cascade Biologics) and 5% FBS (Invitrogen). HUVECs from passages 2–5 were used for experiments. For all experi- ments, >95% viability was assessed by trypan blue exclusion dye.

Preparation of Liposomes

Multilamellar liposomes, composed of egg L-α-lysophosphatidylcholine (Egg PC), egg sphingomyelin (Egg SM), ovine wool cholesterol (Chol), and 1,2-dioleoyl-sn-glyc- ero-3-[(N-(5-amino-1-carboxypentyl) iminodiacetic acid) succinyl] (nickel salt) (DOGS NTA-Ni) at weight ratios 60–50%:30%:10%:0– 10% (Egg PC/Egg SM/Chol/DOGS NTA-Ni), were prepared using a thin lipid film method. DOGS-NTA-Ni is a lipid conjugated to nickel-nitrilotriacetic acid (Ni-NTA) that allows for attachment to his-tagged proteins. Briefly, stock solutions of all lipids were pre- pared by dissolving powdered lipids in chloroform to produce a final concentration of 5 mg/mL Egg PC, 20 mg/mL Egg SM, 5 mg/mL Chol, and 20 mg/mL DOGS-NTA-Ni

in glass containers and stored at −20 °C. Appropriate volumes of the lipids were taken from the stock solution to make lipids with varying concentrations of DOGS NTA-Ni in a glass tube and gently dried under nitrogen. To ensure complete removal of chloroform, the lipids were left under vacuum for an additional 12 h. With increasing amounts of DOGS NTA-Ni, the corresponding amount of Egg PC was decreased (Table S1). The lipid film was hydrated with a liposome buffer composed of 150 mM

NaCl, 10 mM Hepes, and 1 mM $MgCl_2$ dissolved in nuclease-free water to create multilamellar liposomes. The resulting multi- lamellar liposomes were sized by repeated thawing and freezing, and then subjected to 15 extrusion cycles at 60 °C through two different pore size (200 and 100 nm) polycarbonate membranes (Nucleopore; Whatman) to produce unilamellar nanoscale lip- osomes. Recombinant human ES and TRAIL were dissolved in nuclease-free sterile water to a final concentration of 1 mg/mL, and 100 μg/mL aliquots of stock solutions were stored at – 20 °C and used as needed within 60 d. Freshly prepared nanoscale liposomes were then incubated with ES (final concentration 71.43 nM) and TRAIL (250 nM final concentration) for 30 min at 37 °C and then overnight at 4 °C, to ensure maximum protein binding via the interaction between his-tag and Ni-NTA. Based on approximations for ligand density on liposomes suggested in previous work by Huang and Mason (1), there were ~65 TRAIL and 19 E-selectin proteins present on the surface of each li- posome, assuming a unilamellar liposome diameter of 100 nm. To remove unbound TRAIL and ES, liposomes were diluted 1:6 with liposome buffer and subjected to ultracentrifugation at 100,000 × g for 3 h at 4 °C. The supernatant with unbound TRAIL and ES was carefully removed and collected for further evaluation,

and the remaining liposomes were gently resuspended in buffer. A similar procedure was used to create fluorescent conjugated liposomes by replacing ovine wool cholesterol with 23- (dipyrromethe neboron difluoride)-24-norcholesterol. Freshly pre- pared nanoscale liposomes were diluted in buffer, and the mean particle diameter and surface charge (zeta potential) were mea- sured by dynamic light scattering using a Malvern Zetasizer nano ZS (Malvern Instruments Ltd.), according to the manufacturer's protocols. Conjugated liposomes were measured to be 117.8 ± 10.3 nm in diameter, with a zeta potential of −5.7 ± 4.6 mV.

Static Experiments

COLO 205 cells were seeded in multiwell plates at a seeding density of 300,000 cells per mL, 1 d before experimentation to ensure that the cells were in the linear phase of the growth cycle. Media was changed before experimentation. Cells were incubated with either the supernatant from ultra- centrifugation or 10 μL of conjugated and purified liposomes. The cells were maintained in culture conditions with the super- natant or nanoscale lipids for 24 h and later analyzed by an Annexin-V assay to quantify the proportion of viable cells.

Uniform Shear-Flow Experiments

To simulate the shear-stress conditions of blood flow, cancer cells were subjected to uniform shear in a cone-and-plate viscometer (2, 3). Cancer cells seeded 1 d before the experiment were gently detached from the surface using PBS-based enzyme-free cell-detachment solution or accutase. Cells were then washed twice in 1×

DPBS and resuspended in buffer at a concentration of 1×10^6 cells per mL. Then, 10 μL of lipids was added to 490 μL of cell suspension (at 10^6 cells per mL) and immediately added to the cone-and-plate viscometer. Cell suspensions were exposed to shear flow at a shear rate of 188 s^{-1} for 2 h. All samples were exposed to shear flow at room temperature to prevent potential sample evaporation and/or drying in the cone-and-plate viscometer over prolonged periods of shear. After 2 h, the cells were removed and washed twice in resuspension buffer at 200 × g for 5 min. Cells were resuspended in complete media and cultured for 24 h. In the case of fluo- rescent lipids, an aliquot was taken for visual inspection on an inverted microscope (Olympus America Inc.) equipped with fluorescence and an intensified CCD digital camera (Cooke Corporation) to record images. For spiking experiments, periph- eral blood was collected into Vacutainer tubes containing heparin and allowed to equilibrate to room temperature before use. Then, 1×10^6 COLO 205 or PC-3 cells were tagged fluorescently with 3 μM BCECF AM solution for 15 min at 37 °C, washed twice, and collected via centrifugation at 200 × g for 5 min. The supernatant was discarded, and the collected cells were re- suspended in 1 mL of whole blood. Then, 10 μL of lipid was then added to 490 μL of spiked blood and immediately added to a cone-and-plate viscometer previously coated with 5% BSA. Spiked blood was subjected to a uniform shear rate of 188 s^{-1} for 2 h. As an additional comparison for spiking experiments, identical experiments were performed in buffer instead of whole blood. In leukocyte functionalization experiments, 10 μL of lipid was added to 490 μL of human blood, sheared in a cone-and-plate viscometer at a uniform shear rate of 188 s^{-1} for 2 h, and

sub- sequently centrifuged to remove the plasma containing unbound liposomes. The removed plasma was replaced with freshly isolated plasma, and the blood samples were used for identical spiking experiments mentioned above. After shearing, the blood sample was collected from the device and carefully layered over 1.5 mL of Ficoll and centrifuged at 480 × g for 50 min at room temperature. The buffy coat containing mononuclear cells (MNCs) and cancer cells was recovered and washed twice in resuspension buffer, col- lected, cultured for 24 h, and analyzed for viable fluorescent cancer cells using flow cytometry. To evaluate the effect of hematocrit, the number of RBCs was varied by removal via centrifugation. Vol- umes of RBCs were replaced with excess plasma from the same blood donor. Cancer cells were spiked into blood samples as mentioned earlier, at a concentration of 1×10^6 cells per mL. Then, 10 μL of liposome solution was added to 490 μL of blood and sheared for 2 h at 188 s^{-1}. Samples were collected, incubated, and analyzed for viability on a flow cytometer as described in Flow Cytometry. In some experiments, 490 μL of whole blood was sheared with 10 μL of liposome solution, and the plasma and any remaining unbound liposomes and/or liposome fragments were separated by centrifugation. To determine the effects of remaining unbound liposomes and/or liposome fragments on cancer-cell vi- ability, the recovered plasma was incubated with 500,000 COLO 205 cells for 24 h at 37 °C and analyzed for cell viability using flow cytometry.

Polymorphonuclear and Mononuclear Cell Isolation

All human subject protocols were approved by the Institutional Review Board for Human Participants of Cornell University. Peripheral blood was collected from

healthy donors after informed consent into Vacutainer tubes containing heparin and allowed to equil- ibrate at room temperature before use (2, 4). Then, 3 mL of blood diluted with resuspension buffer was carefully layered over 3 mL of 1-Step Polymorphs (Accurate Chemical & Scientific Corporation) and centrifuged at 480 × g for 50 min at room temperature. Two separate layers of MNCs and polymorpho- nuclear cells (PMNs) were collected and washed twice with re- suspension buffer.

Leukocyte Functionalization with ES/TRAIL Liposomes in Whole Blood.

To assess the adhesion of ES/TRAIL liposomes to leukocytes in whole blood under flow, 490 μL of whole blood was sheared with 10 μL of fluorescent ES/TRAIL liposome solution for 30 min in a cone-and-plate viscometer at a shear rate of 188 s^{-1}. Leuko- cytes were then separated using 1-Step Polymorphs and assessed for adherent ES/TRAIL liposomes using confocal microscopy. To assess the fraction of leukocyte subpopulations that adhere to ES/TRAIL liposomes, leukocytes were labeled with anti-human CD3, CD14, CD16, CD19, and CD56, along with corresponding isotype controls, and analyzed for adherent ES/TRAIL liposomes using flow cytometry. To assess the specificity of the ES interaction with leukocytes, liposomes were incubated with a functional blocking anti-human E-selectin antibody before shearing in whole blood. To assess the fraction of leukocytes in blood ad- hered to ES/TRAIL liposomes before shear, fluorescent ES/ TRAIL liposomes were added to whole blood and then sepa- rated using 1-Step Polymorphs.

Endothelial-Cell Viability Assay

Forty-millimeter-diameter circular glass coverslips (Thermo Scientific) were plasma-treated (Harrick Plasma Cleaner) for 2 min and subsequently incubated in 1% polyethylenemine (PEI) at room temperature for 10 min. Cov- erslips were then washed in water three times and treated with 0.1% glutaraldehyde (Sigma-Aldrich) in PBS at room tempera- ture for 30 min. Coverslips were washed in water three times, dried, and treated with 0.1 mg/mL type I rat-tail collagen (Becton Dickinson) in Hepes (pH 8.0; Sigma-Aldrich) for 2 h at 4 °C. Coverslips were placed in Petri dishes (60 mm × 15 mm; Sigma- Aldrich), washed three times in PBS, and briefly sterilized via UV exposure for 15 min. HUVECs were plated on coverslips, at a density of 500,000 cells per coverslip, in Medium 200 supple- mented with low-serum growth supplement (Cascade Biologics), 5% FBS (Invitrogen), and 100 U/mL PenStrep. HUVECs were cultured for 4 d on coverslips before experiments and then ad- hered to the plate of a cone-and-plate viscometer using vacuum grease. HUVECs were then treated with 2.94 mL of human blood and 60 μL of PBS, ES/TRAIL (TRAIL final concentra- tion: 0.3 μg/mL), or soluble TRAIL in PBS (TRAIL final con- centration: 0.3 μg/mL) for 4 h at 37 °C in a humidified cone-and- plate viscometer at a shear rate of 188 s^{-1}. As a positive control, HUVECs were treated with a high concentration of soluble TRAIL (15 μg/mL). Coverslips were removed from the viscom- eter, gently washed in PBS, and placed in Medium 200 supple- mented with low-serum growth supplement, 5% FBS (Invitrogen), and 100 U/mL PenStrep. HUVEC morphology was assessed using brightfield and phase-contrast microscopy. HUVECs were im- mediately placed into culture for 8 h, maintained at 37 °C and 5% CO_2. HUVECs were then treated with 0.25% Trypsin-EDTA solution (Gibco) for 2 min at 37 °C,

followed by treatment with an equal volume of trypsin neutralizer solution (Gibco). HUVECs were collected from coverslips, washed twice in PBS, and assessed for viability using an Annexin-V assay.

Liposome and COLO 205 Cell Injection in Mice

C57BL/6J mice aged 16–20 wk (both sexes), weighing 25–32 g, were obtained from The Jackson Laboratory. Mice were anesthetized using iso- flurane (5%) for all procedures. Either 120 μL of saline, sTRAIL (15 μg/mL; TRAIL plasma concentration ~1.0 μg/mL), ES/ TRAIL (TRAIL injection concentration 15 μg/mL; TRAIL plasma concentration ~1.0 μg/mL) liposomes, or ES liposomes suspended in saline were injected retro-orbitally using a 30-G needle, and animals were removed from anesthesia. Three mice were used in each group. Thirty minutes later, animals were reanesthetized, and ~2 × 10^6 COLO 205 cells, labeled by 2 μg/ mL Hoescht (H1399; Invitrogen) or 3 μM BCECF AM sus- pended in saline were injected into the tail vein. Animals were removed from anesthesia, and the cancer cells were allowed to circulate for 2 h. All animal procedures were approved by the Cornell University Institutional Animal Care and Use Committee.

Analysis of Circulating COLO 205 Cells

Animals were euthanized with a lethal dose of pentobarbital. Blood was removed from the heart via cardiac puncture and collected into sodium heparin- coated tubes. Leukocytes and circulating COLO 205 cells were separated using Ficoll-Paque PLUS. After centrifugation, the MNC buffy coat was collected, washed in buffer

containing Ca^{2+} and cultured for 2–3 h in multiwell plates. Cell viability was assessed using flow cytometry.

Two-Photon Imaging of Lung Tissue

Animals were anesthetized and received injections of saline, sTRAIL, ES/TRAIL liposomes, or ES liposomes, followed by an injection of Hoescht-labeled cancer cells, as described in Liposome and COLO 205 Cell Injection in Mice. After 2 h of cancer-cell circulation, an Alexa Fluor 568- labeled Annexin-V probe (A13202; Invitrogen) was injected retro- orbitally and allowed to circulate for 2 h to ensure maximum detection of apoptotic cells. Animals were then given a lethal dose of pentobarbital. After euthanasia, intact lungs were re- sected and immediately imaged via two-photon excited fluores- cence microscopy. Two-photon imaging was conducted on a locally designed microscope using a train of 800-nm, 87- MHz, 100-fs pulses from a Ti:sapphire laser oscillator (MIRA HP, pumped by a Verdi-V18; Coherent) for excitation. Laser scanning and data acquisition were controlled by ScanImage software. For high-resolution imaging of COLO 205 Hoechst- labeled nuclei and Annexin V labeling, a 20× (numerical ap- erture: 0.95) water-immersion objective (Olympus) was used. Fluorescence was detected using emission filters with 460-nm and 645-nm center wavelength with 65-nm bandwidth to image Hoescht and Alexa Fluor 568 (Invitrogen), respectively. Spec- trally broad autofluorescence from the lung tissue was visible in both channels.

Counting and Viability Scoring of COLO 205 Cells in Lung

Hoechst- labeled COLO 205 cells were manually counted from ~10 representative two-photon image stacks taken from the lung in each mouse using Image J (NIH) cell counting software. The Hoechst signal was of similar magnitude to the background lung auto- fluorescence in the 460-nm channel. To aid in identifying nuclei, the Hoechst channel was compared with the 645-nm channel, where autofluorescence was also visible, but Hoescht was not and Alexa Fluor 568 signal was significantly brighter than au- tofluorescence. In addition, attributes such as size and shape to distinguish the labeled COLO 205 cells were used. Each imaged volume was about 0.022 mm^3. The total number of cells in the lung was estimated by scaling the imaged volumes to the total lung volume, which was measured via a volume-displacement method. Counts were recorded by two different observers, each blinded to the treatment received, and averaged. To determine which COLO 205 cells were apoptotic, we determined whether Alexa Fluor 568 Annexin V labeling was present at each of the COLO 205 cell nuclei we identified.

Flow Cytometry

Mode of cell death was analyzed using an Annexin-V apoptosis assay on an Accuri C6 flow cytometer. Samples were prepared per the manufacturer's instructions. Briefly, cells were classified into four categories based on dye uptake: viable cells [negative for Annexin-V and propidium iodide (PI)], early apo- ptotic cells (positive for Annexin-V only), late apoptotic cells (positive for Annexin-V and PI), and necrotic cells (positive for PI only). For blood spiking experiments, fluorescent untreated cancer cells and liposome-treated samples were assessed for viability us- ing a flow

cytometer. A gate was set based on a viable, untreated cancer-cell control. Equal volumes from all samples were used for analysis. Cell viability was determined by measuring the amount of cells positive for fluorescent BCECF staining. For in vivo animal experiments, 100 μL of each sample was processed. A gate de- noting viable, BCECF AM-labeled cancer cells was established by processing a viable, fluorescent sample of COLO 205 cells in buffer. COLO 205 cells recovered from mouse blood were differentiated based on size and fluorescence using flow cytometry. The number of cancer cells per milliliter of mouse blood was determined based on the amount of mouse blood recovered from each animal.

Statistical Analysis

Where appropriate, Student t test and one-way ANOVA with Tukey posttest comparing all means were used at a significance level of $\alpha = 0.05$. All statistical analyses were performed using GraphPad Prism 5.0c for Mac OS X (GraphPad software) and Kaleidagraph (Synergy) software.

4.7 Supplementary Results

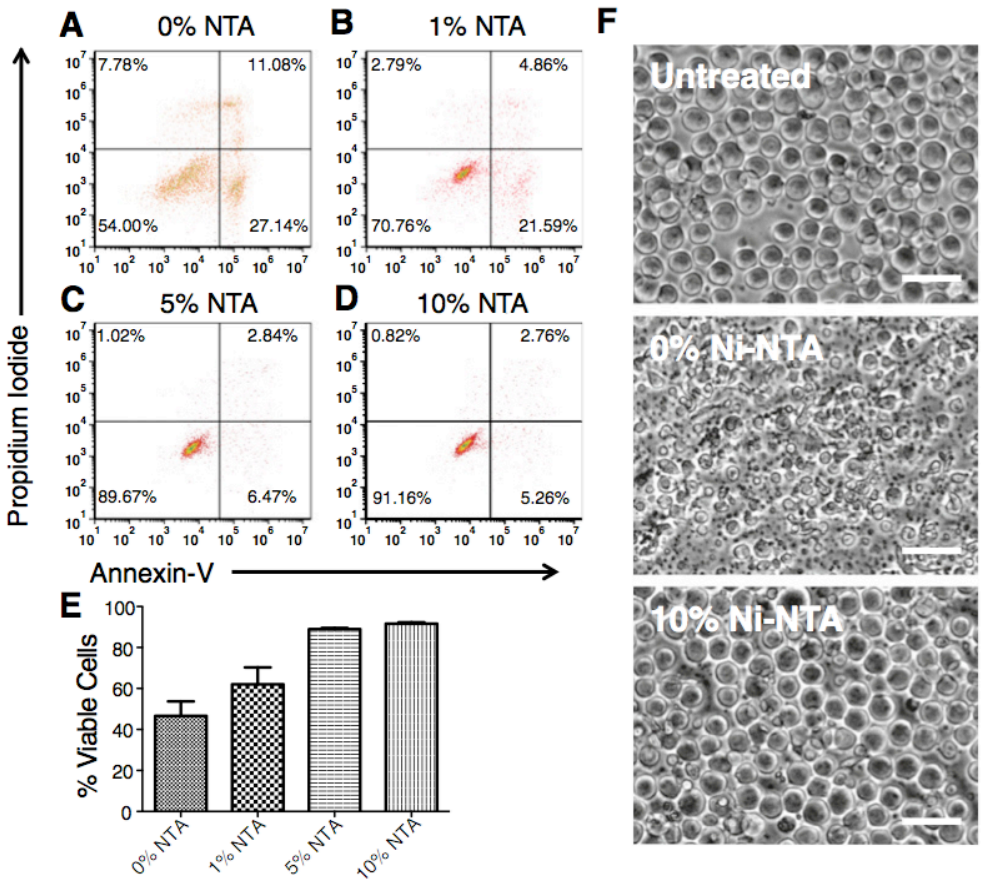

Sup Fig 4.1 Incorporation of Ni-NTA–conjugated lipids on liposomes maximizes protein conjugation to the liposome surface. To determine the optimal amount Ni-NTA-conjugated lipid required to bind TRAIL and ES to the liposome surface, COLO 205 cells were incubated with supernatant left after liposome prep- aration and assayed for cell viability. Increased cell death is indicative of more unbound TRAIL protein in solution. (A–D) Annexin-V apoptosis assay of COLO 205 cell viability after incubation with supernatant of liposomes conjugated to 0% (A), 1% (B), 5% (C), and 10% Ni-NTA (D) postultracentrifugation, with varying amounts of Ni-NTA conjugated to the liposome surface. Cells were classified into four categories based on dye uptake: viable cells (negative for Annexin-V and PI), early apoptotic cells (positive for Annexin-V only), late apoptotic cells (positive for Annexin-V and PI), and necrotic cells (positive for PI only). (E) COLO 205 cell viability after treatment with unbound TRAIL and ES in liposome supernatant. n = 3 for all samples. Bars represent the mean ± SD in each treatment group. (F) Representative micrographs of untreated COLO 205 cells (Top) and those treated with the supernatant of liposomes conjugated to 0% (Middle) and 10% Ni-NTA (Bottom). The 10% Ni-NTA–conjugated lipid on the liposome leads to nearly complete incorporation of TRAIL and ES onto the liposome surface. (Scale bar, 50 μm.)

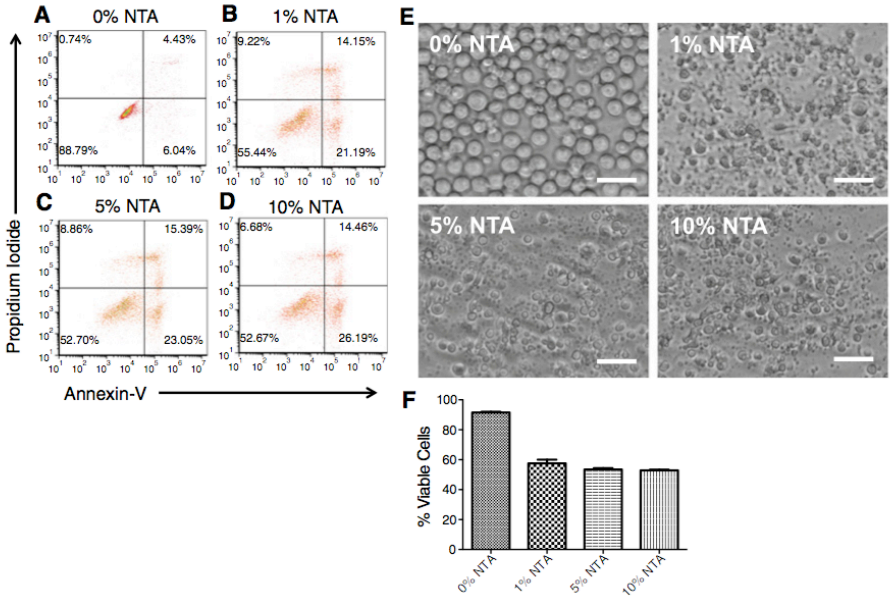

Sup Fig 4.2 ES/TRAIL liposomes are somewhat effective in targeting and killing COLO 205 cells under static conditions. (A–D) Annexin-V apoptosis plots of COLO 205 cells treated with ES/TRAIL liposomes consisting of 0% (A), 1% (B), 5% (C), and 10% Ni-NTA (D) for 24 h. (E) Representative micrographs showing COLO 205 cells after 24 h incubation with liposomes. (Scale bar, 50 μm.) (F) COLO 205 cell viability following incubation with liposomes with varying amounts of Ni-NTA on the liposome surface. n = 3 for all samples. Bars represent the mean ± SEM in each treatment group.

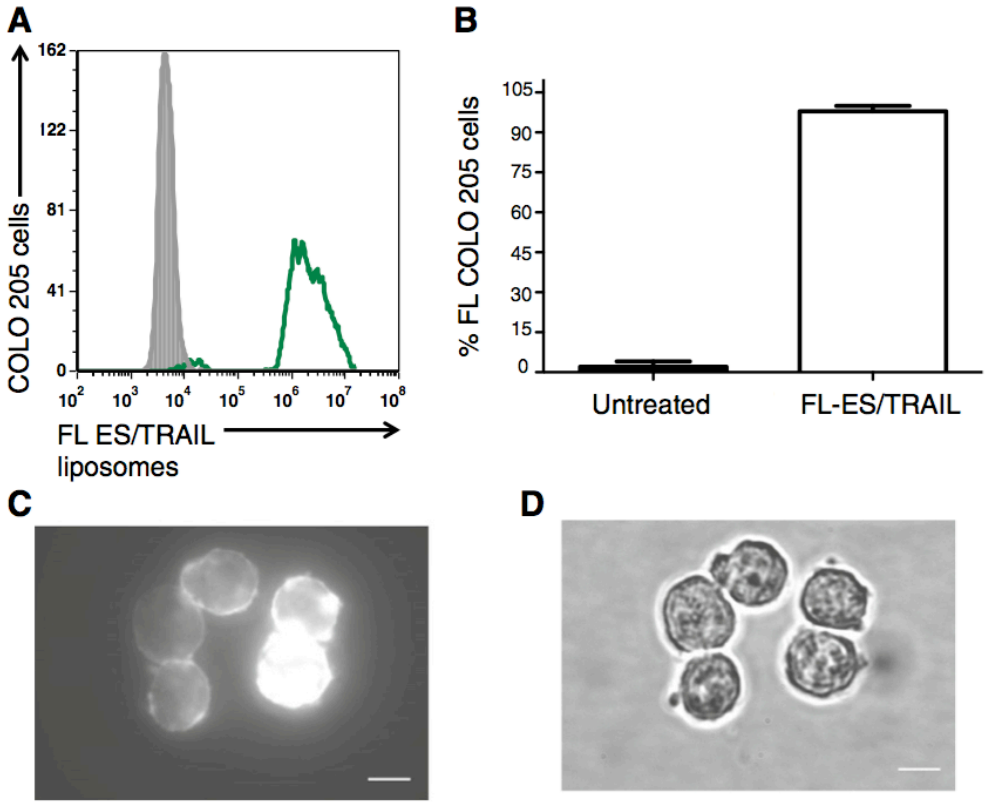

Sup Fig 4.3 ES/TRAIL liposomes adhesively interact with cancer cells. (A) Flow-cytometry plots of cancer cells positive for fluorescently tagged ES/TRAIL liposomes (green). Gray population represents fluorescence of COLO 205 cells in the absence of fluorescent ES/TRAIL liposomes. (B) Percent of COLO 205 cells adhered to liposomes following shear flow at a shear rate of $188s^{-1}$. n = 3 for all samples. Bars represent the mean ± SEM in each treatment group. (C and D) Repre- sentative fluorescent (C) and brightfield (D) micrographs of COLO 205 cells adhered to fluorescently tagged liposomes following shear flow. (Scale bar, 20 μm.)

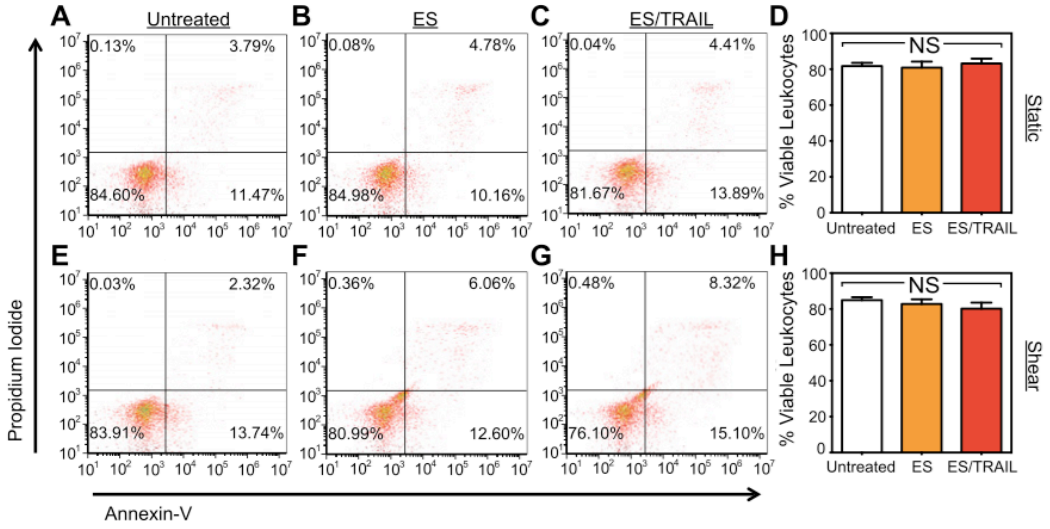

Sup Fig 4.4. Leukocyte functionalization with ES/TRAIL does not induce significant leukocyte death. (A–C) Representative propidium iodide/Annexin-V flow- cytometry plots of untreated mononuclear cells (A) and those treated with ES (B) and ES/TRAIL (C) liposomes under static conditions for 24 h. (D) Viability of mononuclear cells following incubation with liposomes for 24 h. n = 3 for all samples. Bars represent the mean ± SEM in each treatment group. NS, not significant (one-way ANOVA with Tukey posttest). (E–G) Representative propidium iodide/Annexin-V flow-cytometry plots of untreated mononuclear cells (E) and those treated with ES (F) and ES/TRAIL (G) liposomes under shear flow (shear rate: 188 s^{-1}) for 2 h. (H) Viability of MNCs treated with liposomes under shear flow for 2 h. n = 3 for all samples. Bars represent the mean ± SD in each treatment group. NS, not significant (one-way ANOVA with Tukey posttest).

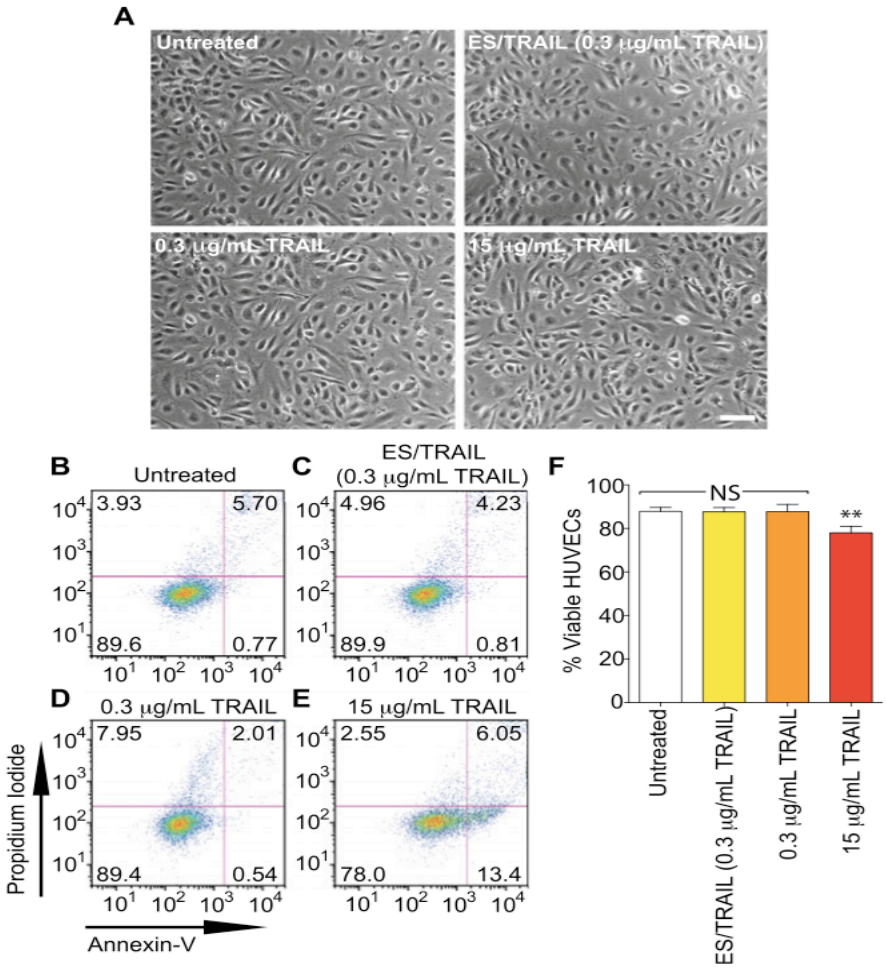

Sup Fig 4.5 Leukocyte functionalization with ES/TRAIL does not induce significant endothelial cell death. (A) Representative images of HUVECs immobilized on coverslips immediately after treatment in human blood, with various drug treatments, under shear flow (shear rate: 188 s^{-1}) for 4 h at 37 °C. (Scale bar, 100 μm.) (B–D) Representative propidium iodide/Annexin-V flow cytometry plots of untreated HUVECs (B) and those treated with ES/TRAIL liposomes (C) (TRAIL concentration 0.3 μg/mL) or soluble TRAIL (D) (TRAIL concentration 0.3 μg/mL) in human blood under shear flow for 4 h at 37 °C. (E) As a positive control, HUVECs were treated with a high dosage of TRAIL (15 μg/mL) in human blood under shear flow for 4 h at 37 °C. HUVECs were classified into four categories based on dye uptake: viable cells (negative for Annexin-V and PI), early apoptotic cells (positive for Annexin-V only), late apoptotic cells (positive for Annexin-V and PI), and necrotic cells (positive for PI only). (F) Percent viability of HUVECs after various drug treatments in human blood under shear flow for 4 h at 37 °C. n = 3 for all samples. Bars represent the mean ± SD in each treatment group. **P <0.001. NS, not significant (one-way ANOVA with Tukey posttest).

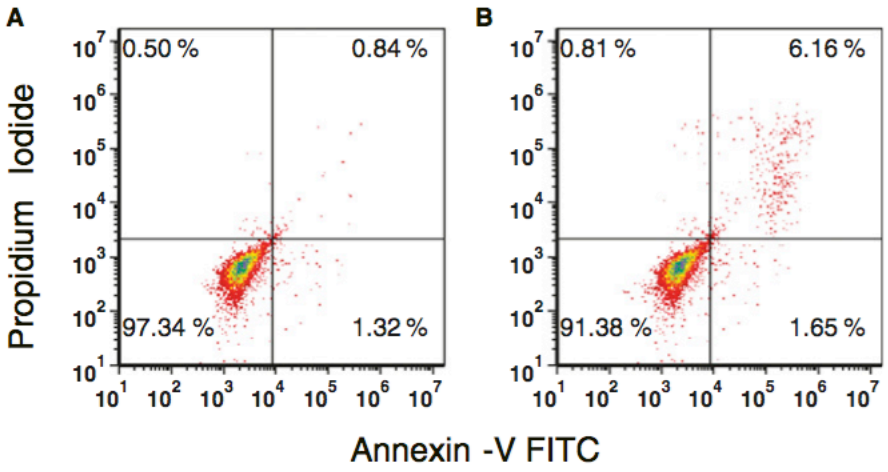

Sup Fig 4.6 Low toxicity of blood plasma after treatment with ES/TRAIL liposomes. (A) Viability of COLO 205 cells after treatment with plasma from normal healthy blood for 24 h. (B) Viability of COLO 205 cells after treatment with plasma extracted from blood that had been sheared with ES/TRAIL liposomes for 30 min. Cells were incubated with plasma, and any remaining unbound ES/TRAIL liposomes and/or liposome fragments in the plasma for 24 h, and analyzed for cell viability.

Table S1. Weight ratios of liposome formulations

DOGS NTA-Ni	Egg PC	Egg SM	Chol/Bdp-Chol
0% NTA	60	30	10
1% NTA	59	30	10
5% NTA	55	30	10
10% NTA	50	30	10

With increasing amounts of Ni-NTA–conjugated lipid, the corresponding amount of Egg PC lipid was decreased.

4.8 References

1. Huang C, Mason JT (1978) Geometric packing constraints in egg phosphatidylcholine vesicles. Proc Natl Acad Sci USA 75(1):308–310.

2. Mitchell MJ, King MR (2012) Shear-induced resistance to neutrophil activation via the formyl peptide receptor. Biophys J 102(8):1804–1814.

3. Mitchell MJ, King MR (2013) Fluid shear stress sensitizes cancer cells to receptor-mediated apoptosis via trimeric death receptors. New J Phys 15:015008.

4. Ball CJ, King MR (2011) Role of c-Abl in L-selectin shedding from the neutrophil surface. Blood Cells Mol Dis 46(3):246–251.

CHAPTER 5

ES/TRAIL COATED LEUKOCYTES ELIMINATE METASTASIS BY TARGETING AND KILLING CIRCULTING TUMOR CELLS IN AN ORTHOTOPIC PROSTATE TUMOR MODEL

In this chapter, we present a study that investigates the use of ES/TRAIL coated leukocytes to kill circulating tumor cells (CTCs) and reduce metastasis in an orthotopic prostate tumor model. For the first time, it is shown that such an approach can be used to prevent the spontaneous formation and growth of metastatic tumors in an orthotopic xenograft model of prostate cancer, by greatly reducing the number of circulating tumor cells. We conclude that the use of circulating leukocytes as a carrier for the anti-cancer protein TRAIL could be an effective tool to directly target circulating tumor cells for the prevention of prostate cancer metastasis, and potentially other cancers that spread through the bloodstream.

At the time of the writing of this dissertation, this work is currently under review in the Proceedings *of the National Academy of the Sciences*. The manuscript cwill eventually have the following citation:

Elizabeth C. Wayne*, Siddarth Chandrasekaran*, Michael J. Mitchell, Maxine F. Chan, Rachel E. Lee, Chris B. Schaffer, and Michael R. King. TRAIL-coated leukocytes that prevent the bloodborne metastasis of prostate cancer.

*These authors contributed equally

5.1 Introduction

Prostate cancer (PCa) is the second most common cancer in men, with an estimated 1.1 million new men diagnosed with prostate cancer and 307,000 deaths worldwide in 2012 [1]. When detected at an early stage, the 5-year survival rate for PCa is close to 100%. In contrast, if diagnosed at a late stage with advanced metastatic disease, the 5-year survival decreases to 33% [1].While effective therapies exist to treat primary tumors of the prostate, metastatic disease is generally considered incurable [2]. The primary tumor sheds tumor cells into the circulation, which can then transit through the bloodstream to form metastases in tissues of the bones, liver, lung, and other organs [1,3]. Clinically, the detection and quantification of circulating tumor cells (CTCs) in PCa patient blood samples before and after treatment is a strong predictor of patient survival – indeed, chemotherapies that cause a net reduction of CTC count from above, to below 5 cells per 7.5 mL of blood (as measured via CellSearch technology) are correlated with improved survival outcomes [4,5]. However, the direct targeting of CTCs as a means to interrupt the metastatic process has gone largely unexplored.

TRAIL is a promising cancer therapeutic because of its ability to induce apoptosis in tumor cells but not normal cells. Since the discovery of TRAIL there have been numerous preclinical trials that showed promising anticancer activity. These results led to the use of TRAIL-receptor agonists (TRAs) in dozens of clinical trials. Unfortunately, the outcomes failed to research their early promise. Primary reasons cited for this failure include the selection of TRAs that were well tolerated but tended

to have lower agonist activity and the realization that many primary cancer cells exhibit resistance to TRAIL therapy. Consequently, there has been a push for developing higher-order configurations of TRAIL to increase potency and for developing chemical sensitizers.

Despite these early disappointing results in treating solid tumors, TRAIL has special potency for treating metastasis and in particular inducing apoptosis to circulating tumor cells within the bloodstream. Previous studies suggest that genetic expression of TRAIL is decreased in anchored tumor cells and further that detachment of tumor cells from the primary tumor sensitizes cells to apoptosis [6-8]. Moreover, blocking integrin-mediated cell adhesion has been found to cause increased sensitivity to TRAIL apoptosis [9]. When considering the physiologic conditions of the blood circulation, tumor cells show increased sensitivity to TRAIL-mediated apoptosis within the shear stress environment of the blood circulation. Tumor cells exhibited greater TRAIL-mediated apoptosis proportional to higher shear stress conditions in a manner that was not recapitulated when treating cells with doxorubicin [10]. Based on this collective evidence, technology that can maximize TRAIL capacity to bind to circulating tumor cells could prove to be quite beneficial.

Immune-based therapies are a promising alternative to radiation and chemotherapy treatment of prostate cancer. Currently, the standard of treatment includes radical prostatectomy, hormone injections, radiation therapy and chemotherapy [2,11]. The success of these therapies is often limited, as many patients become resistant to

conventional therapies once the primary tumor has metastasized [12]. Prostate cancer lends itself to immunotherapies owing to the strong interaction of host immune cells with prostate cancer cells. Nanomedicine combined with immunotherapy approaches is becoming more attractive as formulations offer customizable functionality, improved pharmacokinetics, and targeting specificity. Functionalizing leukocytes to carry therapeutic nanoparticles has gained attention within the last decade. Largely, these have taken the form of *ex vivo* manipulations of immune cells. However, few if any studies have utilized immune cells themselves as a carrier for anti-tumor agents.

Recently, we described a unique nanomedicine approach to target and kill CTCs within the flowing blood [13]. Nanoscale liposomes were conjugated with two proteins: E-selectin (ES), a vascular adhesion molecule important in inflammation that binds to carbohydrate ligands on all leukocytes and many types of CTCs, and TRAIL, a protein produced by immune cells that induces apoptosis in cancer cells but has minimal effect on normal cells. When injected into the bloodstream, ES/TRAIL liposomes attach to the surface of peripheral blood leukocytes, which then become cytotoxic to any cancer cells present in the blood. Under physiological flow conditions, this results in near complete elimination of viable cancer cells within 2 h of shearing human blood samples ex vivo, or following liposome and cancer cell injection into the mouse circulation. The aim of the current study was to determine whether ES/TRAIL liposomes could be effective in preventing new metastatic tumor formation in a more realistic model of metastasis: one in which a primary tumor grows and then begins to shed CTCs into the bloodstream, which subsequently colonize

distant organs. Orthotopic models of prostate cancer have been widely characterized [14-17] and used to investigate the effect of new therapeutics in mice. In this study, we demonstrated the prevention of metastatic tumor development in an orthotopic xenograft model of PCa, through the sustained delivery of ES/TRAIL liposomes designed to induce apoptosis in circulating tumor cells.

5.3 Materials and Methods

Preparation of sterile ES/T liposomes

Multilamellar liposomes, composed of egg L-α-lysophosphatidylcholine (Egg PC), egg sphingomyelin (Egg SM), ovine wool cholesterol (Chol), and 1,2-dioleoyl-sn-glyc- ero-3-[(N-(5-amino-1-carboxypentyl) iminodiacetic acid) succinyl] (nickel salt) (DOGS NTA-Ni) at weight ratios 60–50%:30%:10%:10% (Egg PC/Egg SM/Chol/DOGS NTA-Ni), were prepared using a thin lipid film method. DOGS-NTA-Ni is a lipid conjugated to nickel-nitrilotriacetic acid (Ni-NTA) that allows for attachment to his-tagged proteins. Briefly, stock solutions of all lipids were prepared by dissolving powdered lipids in chloroform to produce a final concentration of 5 mg/mL Egg PC, 20 mg/mL Egg SM, 5 mg/mL Chol, and 20 mg/mL DOGS-NTA-Ni in glass containers and stored at –20°C. Appropriate volumes of the lipids were taken from the stock solution to make lipids in a glass tube and gently dried under nitrogen. To ensure complete removal of chloroform, the lipids were left under vacuum for an additional 12 h. The lipid film was hydrated with a liposome buffer composed of 150 mM NaCl, 10 mM Hepes, and 1 mM $MgCl_2$ dissolved in nuclease-free water to create

multilamellar liposomes. The resulting multi- lamellar liposomes were sized by repeated thawing and freezing, and then subjected to 15 extrusion cycles at 60°C through two different pore size (200 and 100 nm) polycarbonate membranes (Nucleopore; Whatman) to produce unilamellar nanoscale liposomes. A standard autoclaving cycle (15 min, 121°C) was used to sterilize the liposomes after pumping N_2 gas into the liposomes in glass ampules to remove oxygen that can cause liquid oxidation. The ampules were then placed in a vacuum degasser to remove residual air and then transferred to autoclave chambers for sterilization. No change in pH or size of the liposomes was observed after autoclaving. The sterilized liposomes were allowed to cool to 4°C and then conjugated with recombinant human TRAIL and ES as described previously. ELISA was used to determine the final concentration of ES and TRAIL on liposomes (R&D Systems). To remove unbound TRAIL and ES, liposomes were diluted 1:6 with liposome buffer and subjected to ultracentrifugation at 100,000 × g for 6 h at 4°C. The mean particle diameter and surface charge (zeta potential) were measured by dynamic light scattering using a Malvern Zetasizer nano ZS (Malvern Instruments Ltd.), according to the manufacturer's protocols. Unconjugated liposomes were measured to be 103.4 ± 10.3 nm in diameter, with a zeta potential of −3.5 ± 2.3 mV before autoclaving and 104.7 ± 17.2 nm in diameter, with a zeta potential of −5.3 ± 1.1 mV after autoclaving. Conjugated liposomes were measured to be a 120.5 ± 5.7 nm in diameter with a zeta potential of -8.3 ± 4.0 mV. The negative zeta potential upon autoclaving could be attributed to the redistribution of phospholipids within the lipid bilayer [18]. The conjugation of proteins on the liposome surface further reduces the zeta potential, which could minimize their

interaction with negative plasma proteins in circulation [19]. This change was expected, as the liposomes were not PEGylated and protein conjugation on non-PEGylated liposomes have been shown to reduce the surface charge by other groups [20].

ELISA was used to determine the final concentration of ES and TRAIL on liposomes. Unconjugated proteins were removed by ultracentrifugation and liposomes were dissociated using 0.1% Triton X-100. The dissociated liposomes were then diluted at 1:10, 1:100 and 1:1000 with liposome buffer and coated on 96-well ELISA plates, and a protocol supplied by the manufacturer was used to determine the concentration of ES and TRAIL using appropriate calibration curves created with standard ES and TRAIL provided with the ELISA kit.

Pharmacokinetics of ES/T liposomes

Freshly prepared nanoscale liposomes were conjugated with recombinant E-selectin (ES) (16 ng/mL final concentration) and TRAIL (8 ng/mL final concentration) for 30 min at 37°C and then overnight at 4°C, to ensure maximum protein binding via the interaction between his-tag on recombinant proteins and Ni-NTA on liposomes. To determine the circulation half-life of ES/TRAIL liposomes in the peripheral circulation of mouse, male NOD.CB17-Prkdc^{scid}/J mice (6-8 weeks old, Jackson Laboratories) received retro-orbital injections of either ES/TRAIL liposomes or ES liposomes (120 μL per mouse). At t=3, 36 and 72 hr three mice were sacrificed to ensure maximum blood draw by cardiac puncture. Blood from three mice were pooled

for each time point and peripheral polymorphonuclear and mononuclear cells were isolated by density centrifugation on Histopaque-1077 (Sigma Aldrich). About, $1x10^6$ purified leukocytes were incubated for 45 minutes in dark at 4°C with APC conjugated anti-CD45 (eBioscience), a pan-leukocyte maker and its corresponding isotype control (eBioscience). To verify liposome binding to circulating leukocytes, leukocytes were labeled with FITC conjugated anti-human TRAIL (BD Biosciences) and analyzed using a Guava easyCyte™ flow cytometer. At 72 hr, labeled leukocytes were imaged using a Zeiss confocal microscope to verify liposome binding to circulating leukocytes. Appropriate isotype controls were used for all flow cytometry experiment to determine the gating procedure.

Prostate Orthotopic Implantation

Male NOD.CB17-Prkdc^{scid}/J (Jackson Laboratory) mice 6-8 weeks old were used for this study. Animals were placed under anesthesia using 5% isoflurane. Isoflurane was reduced to 2% after the animal was completely anesthetized. Animals were shaved and cleaned using repeated iodine solution and 70% ethanol swabs. Using sterile scalpel, a low midline abdominal incision about 1-3mm wide was created through the skin and muscle layer. The ventral lobes of the prostate were located and 1 million D-luciferase labeled DU145 cells suspended in 50uL PBS were injected into the prostate gland using a 30G needle. Muscles and skin layers from the abdomen wound were closed separately using Vetbond Tissue Adhesive (3M). Animals were monitored every 8 hr and given analgesic medication for 3 days post surgery. Animals

were housed in pathogen free conditions and all procedures are done under sterile conditions in approval from Cornell IACUC.

ES/TRAIL Liposome Treatment

Beginning at three-weeks post tumor implantation, animals received retro-orbital injection of, E-Selectin/TRAIL (ES/T), E-Selectin only (ES), or liposome buffer (Buffer). Treatment was administered once every three days and in alternating eye sockets. Injections were performed under 2% isoflurane anesthesia and the eyes were protected via application of eye ointment.

Circulating Tumor Cell (CTC) Enumeration

After 9 weeks post-implantation, blood was collected from three mice in each treatment group via cardiac puncture using a heparin-coated syringe. Blood samples were carefully layered over 3 mL Histopaque-1077 (Sigma Aldrich) and centrifuged at 480 × g for 50 min at room temperature. The buffy coat containing mononuclear cells and cancer cells was recovered and washed twice in resuspension buffer, collected, and placed into culture at 37°C and 5% CO_2 under humidified conditions for 6 hr in a 24-well plate. The number of CTCs was determined for mCherry positive DU145 cells in culture. Fluorescent micrographs were taken at 100 randomly selected locations within each well, and total DU145 cells were estimated based on the total well area and reported as the number of cells per mL of blood in Figure 3.

Bioluminescence Imaging

Post tumor implantation, animals were monitored weekly for bioluminescent activity. Luciferin was administered at 150mg/kg per animal via intraperitoneal injection using 30G insulin syringe needle. Animals are placed under anesthesia using 2% isoflurane and imaged 5 min post injection for maximum bioluminescence signal. Images were taken at 1 s exposure time using a Xenogen IVIS 200 Imaging System. For the quantitative measurements of average radiance, the area of the primary BLI was constant throughout all time points for each animal.

For the ex vivo organ quantitative measurements of BLI activity, luciferin was injected into the animal 5 minutes before euthanasia. After euthanasia, organs were immediately removed and placed in warm PBS containing luciferin. Once all organs were collected, the organs were arranged on a black sheet and imaged for 120 s for all samples. Each animal was imaged within 5 min post euthanasia for optimal detection of luciferase activity. Luminescence imaging data was acquired using a luminescence-imaging box custom-built by staff at the Cornell University Biotechnology Resource Center.

Individual bioluminescent organ intensities were summed across each image and divided by the number of pixels using a custom Matlab code. Background signal was subtracted from each image. Representative images from each treatment group were displayed.

Liver Enzyme Measurement

Human hepatocytes have shown sensitivity to TRAIL at sufficiently high dosages and we measured the serum levels of alanine aminotransferase (ALT) and aspartate aminotransferase (AST) to assess liver function in treated mice. These proteins, if present in elevated levels in serum, indicate leakage from damaged cells due to inflammation or apoptosis. These enzymes normally reside inside the cells and any damage to the liver cells usually represents hepatocellular damage. Serum levels of ALT and AST were analyzed using a colorimetric assay kit (BioVision).

Hematocrit

Blood was drawn via cardiac puncture using a 28G heparin coated syringe and collected in a heparinized tube. Two drops per animal were placed in hematocrit tubes and spun for 2 minutes using CritSpin Microhematocrit Centrifuge. The ratio of red blood cells to total blood volume was used to calculate the hematocrit.

Weight

Every animal was weighted at least once per week throughout the duration of the experiment. Control animal weight was contributed from Jackson Laboratory website information about this specific strain. There were no significant differences in animal weight between the treatment groups.

Histology

After bioluminescence imaging, samples were transferred to 4% PFA, stored overnight and then transferred to 30% sucrose in PBS. Samples were then submitted to the Cornell Histology Lab for H&E staining and scoring by a veterinary pathologist. For scoring purposes the pathologist had no knowledge of which animals belonged to which treatment groups. Representative images were acquired for presentation.

TUNEL staining was performed on 20-micron thick sections that were incubated in TUNEL-mix (Roche) at 37°C from 60 min. A DAPI counterstain was applied for 3 min to label nuclei. Fluorescent images were acquired immediately after staining and the image exposure time was kept constant for each channel throughout each treatment group.

5.3.1 ES-TRAIL liposome coated leukocytes remain in circulation for greater than 96 hrs

To determine an appropriate timescale for ES-TRAIL treatment, we performed pharmacokinetic studies to determine the half-life of ES-TRAIL in circulation. Blood cells were isolated from mouse blood following injection of liposome treatment groups. Flow analysis was performed to identify the population of cells expressing CD45, a widespread marker for leukocytes, and human TRAIL. It was determined that within 30 min, nearly 100% of leukocytes stained positive for human TRAIL (Fig. 1). Since soluble TRAIL has been widely reported by other scientists as well as in our previous publications to have a half-life <30 minutes and ineffective against circulating tumor cells, a soluble TRAIL treatment group was not included. By 72 hr, only 10% of leukocytes maintained surface TRAIL (Fig. 1). The half-life was thus

estimated to be ~35hrs. Based on the pharmacokinetics presented, animals were treated every 72 hr.

In a separate experiment, confocal imaging was used to confirm that 72 hr post injection ES/TRAIL liposomes remained bound to the leukocyte surface and had not been internalized (Fig. 1). In addition, the confocal images suggest that the exponential decrease in ES/TRAIL coated leukocytes is not due to the shedding or unbinding of ES/TRAIL liposomes from the leukocyte membrane (Fig.1B). Rather, the half-life is likely linked to the lifespan of circulating leukocytes themselves. As an example, neutrophils are the most abundant leukocyte population and have a short half-lifeof 6-8 hours [21]. Thus, we expect that the emergence of new cells and the death of older cells contribute to the decrease in populations of ES/TRAIL liposome labeled leukocytes.

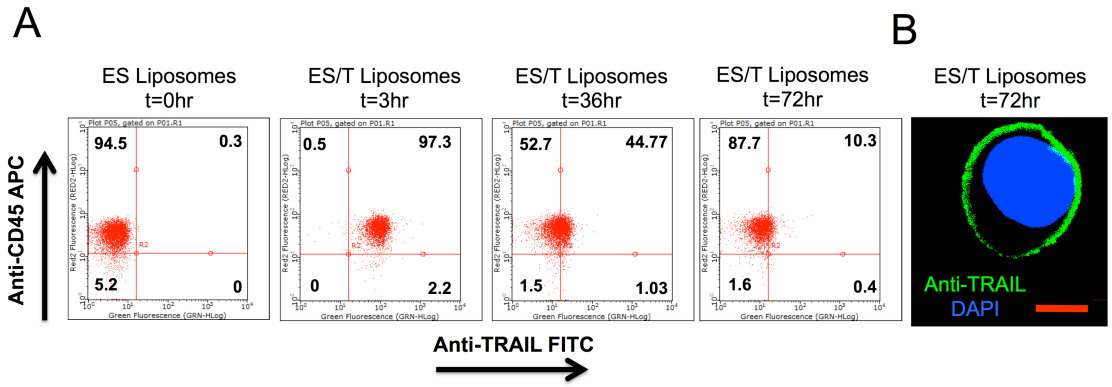

Figure 5.1 Pharmacokinetic dynamics of TRAIL-coated leukocytes. (A) Scatter plots showing percentage of circulating mouse leukocytes staining positive for surface bound human TRAIL protein. (B) Confocal micrograph of a mouse leukocyte presenting human TRAIL protein on its surface at t=72 hours (Scale bar = 10μm).

5.3.2 ES/TRAIL liposome coated leukocytes result in reduction in size of the primary tumor

Dual labeled DU145-luc-mcherry prostate cells were orthotopically injected into the prostate of NOD-SCID animals (Fig. 2A). We observed that CTC populations were detectable after 4 weeks (Fig. 3) and decided to begin treatment in the proceeding week (Fig. 2B). Mice were sorted by primary tumor size at week 2, and three tumor size-matched groups of mice (n=8 each) were formed. The experiment was terminated at week 9 as a humane endpoint, as several of the mice in the two control groups (buffer treatment, ES liposomes without TRAIL) showed visible signs of distress such as skin lesions and lethargy. At week 9, whole animal BLI showed the widespread presence of metastatic tumors throughout the abdominal cavity in the two control groups, with no macroscopic metastases visible in the ES/TRAIL treatment group (Fig. 2C). Remarkably, ES/TRAIL liposomes also caused significant reduction in the growth rate of the primary tumor (Fig. 2D), with no BLI signal detectable in treated mice when imaged from the dorsal side (Fig. 2C). This difference in treatment group is likely due to ES-TRAIL liposome exposure to the cells in the primary tumor due to leukocyte infiltration as is typically associated with cancer inflammation [22]. Our previously published data indicated that ES liposomes may keep CTCs in circulation by blocking the ES-mediated adhesion of CTCs to the endothelium [23]. The difference in the average radiance between the ES-only and Buffer treatment groups, though not significantly different, suggests that leukocytes functionalized with ES liposomes may also be interacting with cells within the primary tumor. In this

light, the stark difference in primary tumor growth between ES and ES/TRAIL treated animals corroborates that ES binding facilitates adhesion to cancer cells and, when combined with the apoptosis inducing TRAIL, leads to efficient cancer cell death.

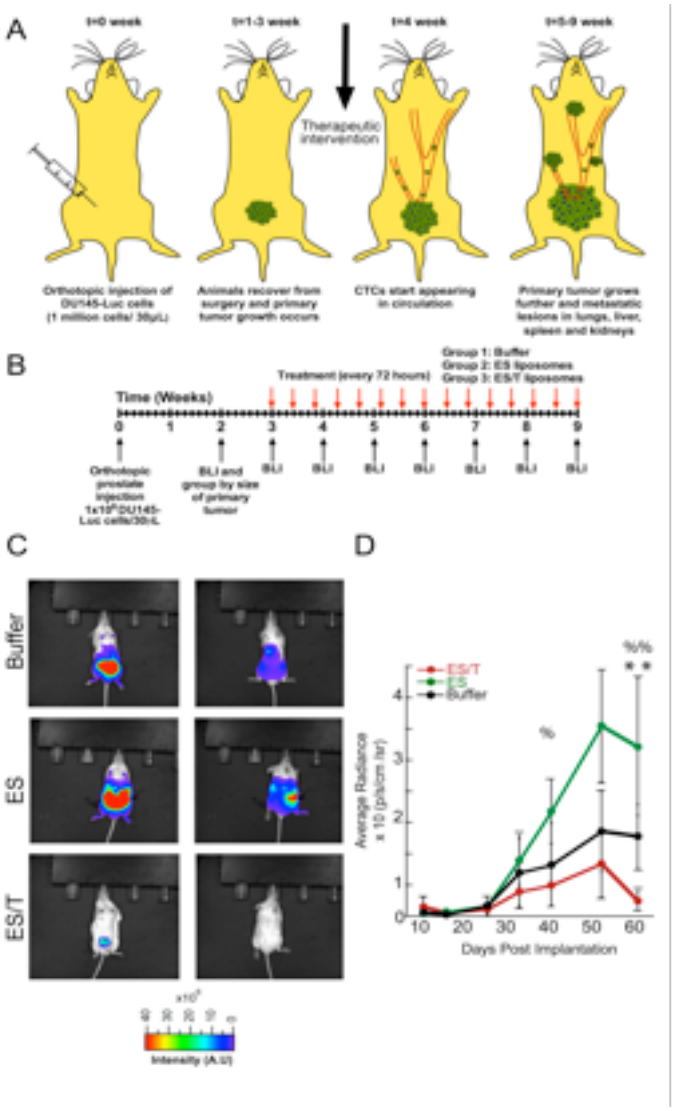

Figure 5.2 Test of ES/TRAIL liposomes to prevent metastasis in an orthotopic model of prostate cancer. (A) Schematic of orthotopic xenograft model for metastatic prostate cancer progression. (B) Timeline for ES/T liposome efficacy trial in tumor-bearing mice. (C) Whole animal BLI of the ventral (left) and dorsal (right) side of representative animals from each treatment group at the end of the trial (week 9) (D) Average radiance from the primary tumor. Comparisons were made via one-way ANOVA with Tukey posttest. Error bars represent the mean ± SD at each timepoint. ES vs ES/TRAIL: %=($p < 0.05$) %%=($p<0.01$). Buffer vs ES/TRAIL: **=($p<0.05$).

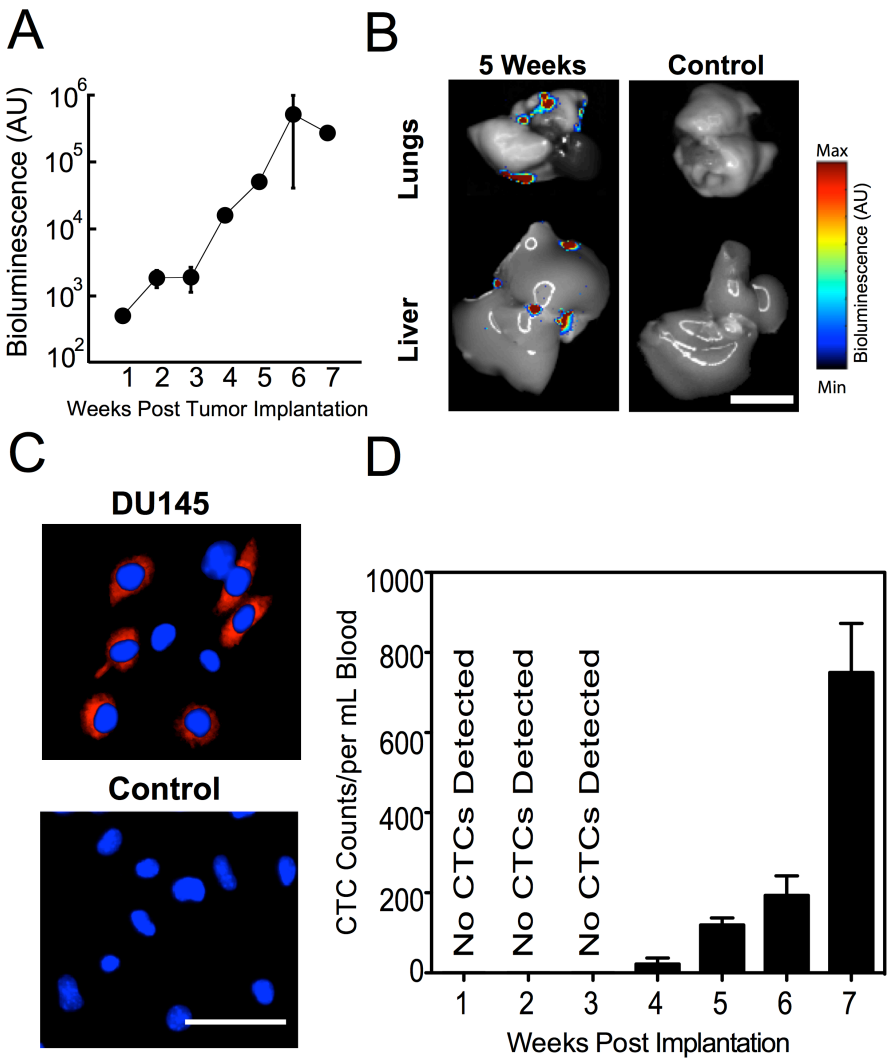

Figure 5.3 Quantification of bioluminescence signal of DU145 cells following orthotopic tumor implantation. (A) Increased bioluminescence signal from tumor growth over time. (B) Bioluminescent signal from excised organs 5 weeks after tumor implantation (left) and age-matched control (right). (Scale bar = 1cm) (C) Confocal micrographs of buffy coat isolated from control mice (age-matched non-tumor bearing SCID mice) and mice bearing orthotopic DU145 tumor six weeks after implantation (blue, cell nuclei and red, mCherry expressing DU145 cells). (Scale bar = 100μm) (D) Number of CTCs per volume of blood, measured weekly after orthotopic implantation of tumor. n=3 mice were analyzed each week. Error bars represent the mean ± SD at each timepoint.

5.3.3 ES/TRAIL functionalized leukocytes reduce the number of circulating tumor cells in a prostate orthotopic tumor model

In a previous publication, we showed that ES/TRAIL functionalized leukocytes were able to kill over 90% of CTCs within 2 hrs of circulation time using COLO 205 human cancer cells [23]. In the current study, we seek to determine whether ES/TRAIL liposomes were successful in eliminating CTCs over a sustained period of time where there was already an established primary tumor. For this study we used a different cancer cell line and found that DU145 cells also undergo apoptosis when exposed to ES/TRAIL liposomes in blood (Supplementary Fig. 2). Blood was collected from all mice at the end of the *in vivo* study to quantify number of CTCs. Quantitative comparison of the CTC count in buffer-treated mice (~1,600 CTCs/mL blood) vs. ES/TRAIL liposome-treated mice (~100 CTCs/mL blood) shows a difference of about 94% (Fig. 4A). Representative fluorescent images reveal dramatic decrease in collected CTCs from ES/TRAIL liposome-treated mice (Fig. 4B).

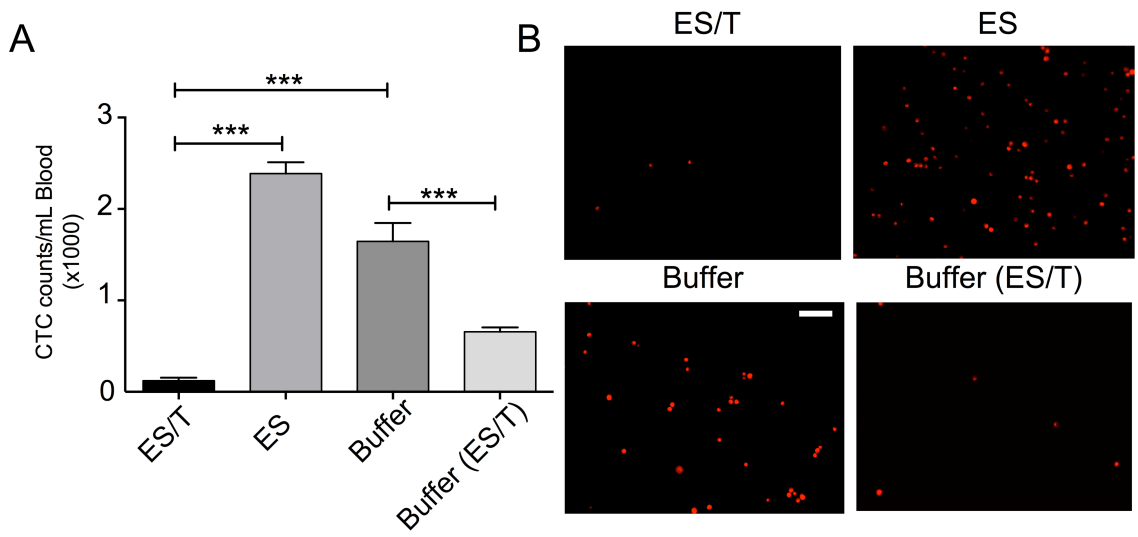

Figure 5.4 ES/TRAIL liposome treatment is effective in significantly reducing the number of circulating tumor cells in blood. (A) Average number of CTCs in the peripheral circulation post treatment. n=3 mice for each group. Bars represent mean ± SD for each group. (B) Representative fluorescent micrographs showing mCherry positive DU145 cells isolated from whole blood of animals from different treatment groups at the end of the study. Scale bar = 100μm. n= 6, 6, 6, and 3 for treatment groups ES/T, ES, Buffer, Buffer(ES/T), respectively. Error bars represent the mean ± SD in each group. ***p<0.0001

To determine the effect of ES/TRAIL liposomes on untreated blood with high tumor burden, 3 animals from the Buffer-treatment group were treated with a single dose of ES/TRAIL (indicated as Buffer (ES/T)). Remarkably, this single dose resulted in a greater than 50% reduction in CTC count (Fig. 4A). Furthermore, the dramatic effect of a single late-stage dose of ES/TRAIL suggests that CTC targeting could yield therapeutic benefit to patients even at later stages associated with high CTC count. Taken together with the absence of metastatic tumors observed in ES/TRAIL liposome-treated mice (Figs. 5 and Supplementary Fig. 1), this indicates that CTC targeting need not be 100% effective in order to achieve the clinically significant outcome of metastasis prevention. That is, by tipping the scales and reducing the metastatic load in the peripheral circulation to a fraction of its untreated numbers, the inherent inefficiency of the metastatic process could take over to benefit the patient. Likely, these remaining CTCs undergo anoikis and immune clearance and lack sufficient numbers to successfully colonize distant organs.

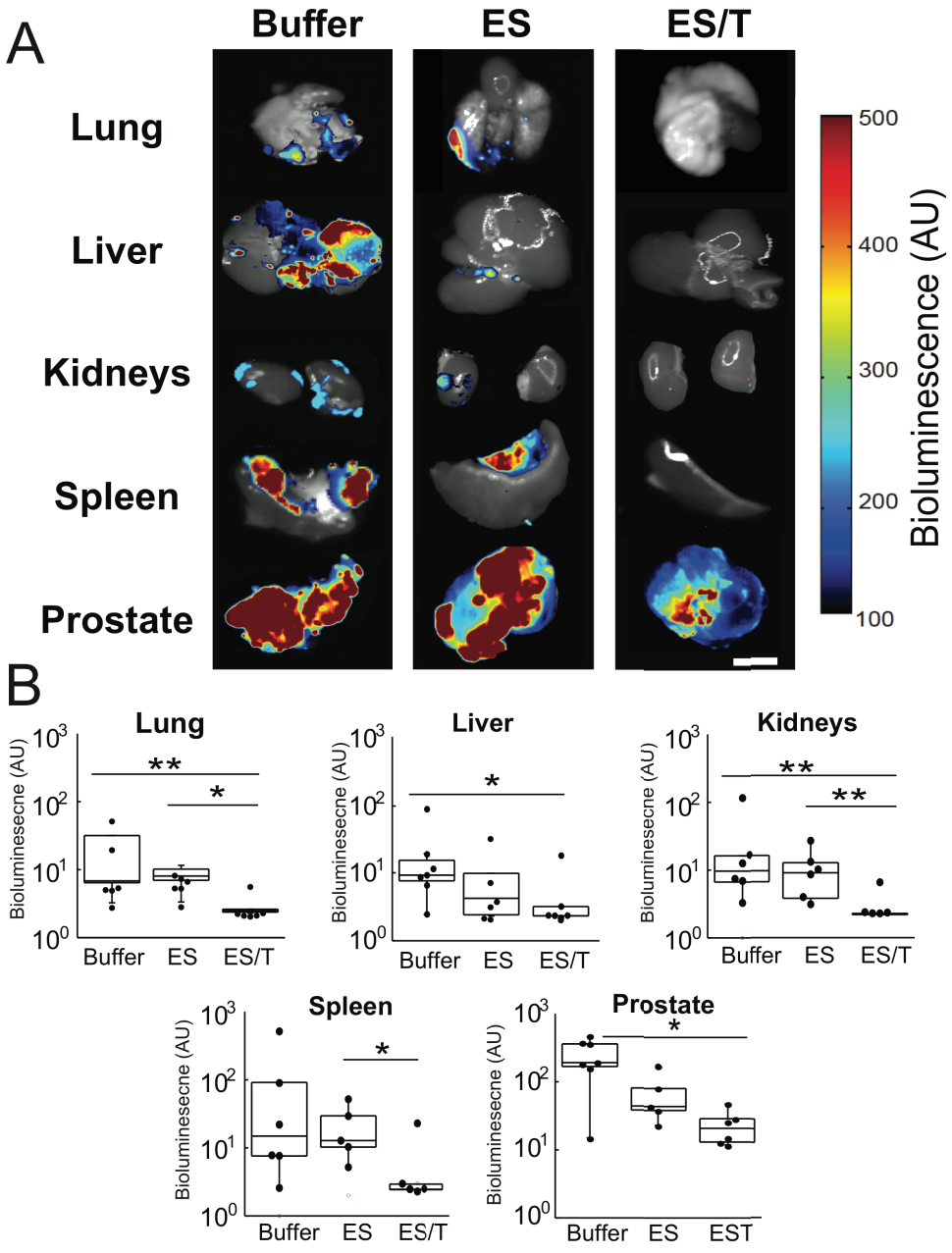

Figure 5.5 *Ex vivo* BLI analysis reveals that ES/TRAIL liposomes block widespread metastasis. (A) Representative BLI images reveal the spread of DU145-Luc cells to lung, liver, kidney and spleen across Buffer, ES, and ES/T treatment groups (left-to-right). Scale bar=1cm. (B) Bioluminescent signal from each organ was quantified for each treatment groups: Buffer (n=8), ES-liposomes (n=6), and ES/T (n=6). Data are plotted on a log scale. Individual data points represent total organ signal from an individual animal. Superimposed box plots bound the 25th to 75th percentage of all data points and the whiskers extend 1.5 times the interquartile range beyond boxes. *P<0.05, **P<0.01 (one-way ANOVA with Tukey posttest).

5.3.4 Ex-vivo organ analysis reveals reduction in metastasis in ES-TRAIL treated animals.

To determine whether ES-TRAIL was successful in reducing metastases, we assayed growth of tumors in distant organs. Organs removed for ex vivo BLI analysis revealed widespread proliferation of luciferase-expressing DU145 cancer cells in the lungs and liver, kidneys and spleen of the buffer-treated and ES liposome treated control mice (Fig. 5A) with virtually no signal above background in ES/TRAIL liposome treated mice (Fig. 5B). All images were taken at the same exposure. Each image is a composite of the black and white camera photo and bioluminescence signal. Difference in organ coloration is due to natural organ pigmentation in addition to variations in the presence of blood at the time of organ harvesting.

While the present study was principally focused on suppressing the development of bloodborne metastasis, a significant decrease in primary tumor size was also observed (Supplementary Fig. 1), together with a reduction in the presence of abdominal visceral metastases observed at the organ boundaries in untreated mice. This suggests that TRAIL-coated leukocytes, such as lymphocytes, enter into the visceral fluid of the peritoneal cavity and the primary tumor. The presence of lymphocytes is consistent with the well-documented leaky phenotype associated with the NOD.CB17-*Prkdc*^{scid}/J mouse line and is confirmed with our previous characterization of ES liposome binding to nearly all leukocyte subtypes [23]. Hence, decorating leukocytes with ES/TRAIL liposomes can provide the additional benefit of

drug delivery to tumors by attaching drug to cell populations that will intrinsically aggregate in the region of disease.

Histology was performed on all organs and interpreted by an independent veterinary pathologist, with results found to be consistent with the BLI analysis (Supplementary Fig. 3). Specifically, metastatic prostate carcinoma was found in the lung, diaphragm, liver and peri-adipose tissue of the kidneys and spleen in buffer and ES liposome treated animals, with some minimal evidence of scattered neoplastic cells in the lungs and liver of ES/TRAIL treated animals.

5.3.5 Toxicity studies indicate little negative effects with ES-TRAIL liposome treatment

The dosage of TRAIL used in the ES/TRAIL liposome formulation represents ~1.0% of the concentrations that were well tolerated in previous animal and human trials with soluble TRAIL protein [24,25], and so consistent with our prior study we did not expect to see evidence of toxicity [23]. We examined for common signs of TRAIL toxicity observed in previous rodent trials featuring extremely high doses of TRAIL [26,27]. Indeed, mice treated with 15 consecutive doses of ES/TRAIL liposomes showed no evidence of: (Fig. 6A) elevated liver enzymes in the serum; (Fig. 6B) significant difference in hematocrit relative to untreated mice; (Fig. 6C) loss of appetite or body weight or behavioral distress compared to untreated mice; (Fig. 6D); or enlarged kidney mass (Fig. 6E). It should be noted that two mice in the treatment group died within hours of liposome injection in week 5, which we attribute to

imperfect liposome sterilization since local retro-orbital inflammation was immediately evident and no characteristic signs of TRAIL toxicity were noted in these animals. In a previous pilot study, 100% of liposome-treated animals experienced such acute sepsis before our liposome sterilization procedures were improved to include an autoclaving step prior to protein conjugation. Future work with these materials should utilize current Good Manufacturing Processes that are not currently available to our laboratory.

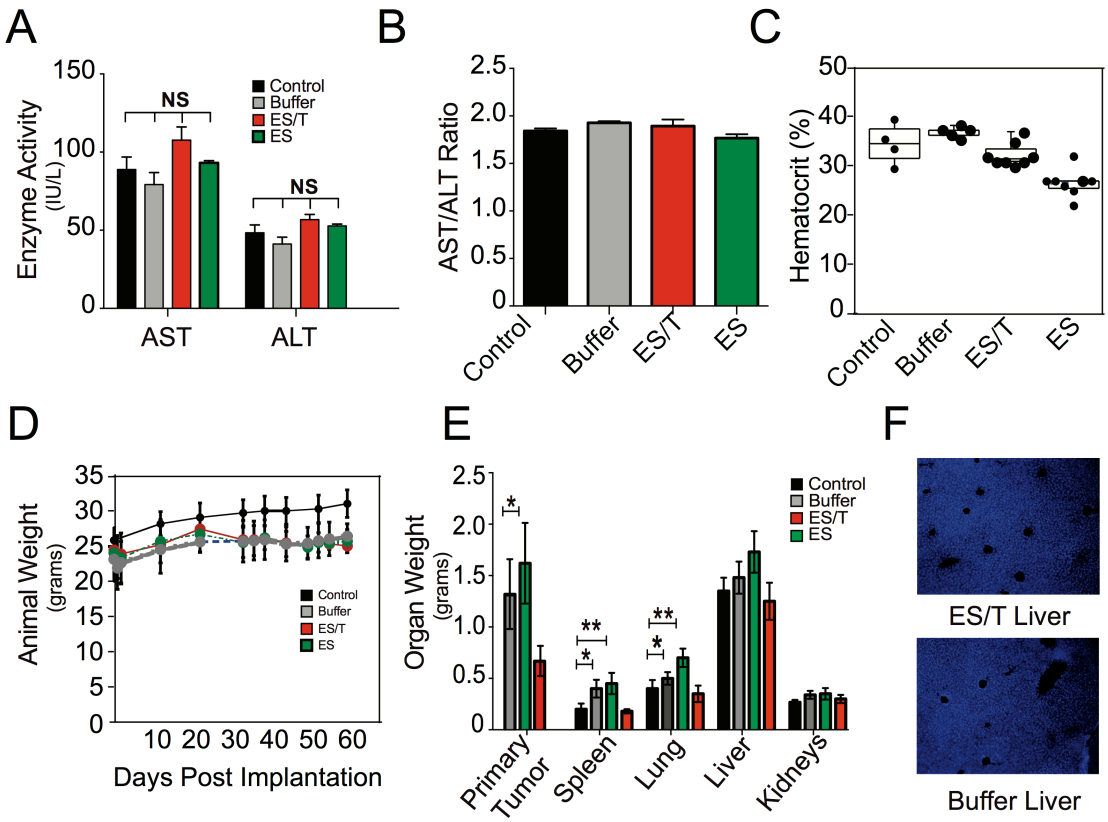

Figure 5.6 ES/TRAIL treatment does not induce toxicity. (A) Serum levels of aspartate aminotransferase (AST) and alanine aminotransferase (ALT) liver enzymes in mice from different treatment groups and aged matched controls at the end of the study. Bars represent mean ± SD for enzyme levels from three mice in each treatment group. (B) AST/ALT ratio for mice from different treatment groups and aged matched controls. AST/ALT >2 indicates liver toxicity. (C) Systemic hematocrit of mouse blood. Each dot represents the hematocrit measurement from an individual animal. Blood was drawn prior to euthanasia. Control group (Control) represents age-matched and strain-matched animals that received no tumor or drug. (D) Weight of animals throughout the experiment. Each dot represents the average weight (grams) of each animal. Control group represents age-matched and strain-matched animals that received no tumor or drug. (E) Weight of excised organs post-mortem. (F) TUNEL staining of liver from ES/T liposome and Buffer treated animals. Error bars represent mean ± SD of each treatment group. NS= non-significant difference. Comparisons made using one way-ANOVA. *$p<0.01$, **$p<0.001$.

5.4 Discussion

In this paper, we present an innovative scheme for TRAIL presentation to treat metastatic disease by specifically targeting circulating tumor cells. Past preclinical studies and clinical trials have focused on delivery of TRAIL variants to treat solid tumors, rather than metastatic cells within the bloodstream [28,29]. In fact, CTCs are mostly valued as predictors of disease progression rather than a bottleneck of metastasis that are available for targeting. Our study explicitly demonstrates that directly eliminating CTCs can reduce metastasis disease in secondary organs.

The therapeutic effect is due to the liposomal-bound TRAIL presentation on the surface of leukocytes and amplified binding opportunities between TRAIL and CTCs mediated by margination in the bloodstream. TRAIL is a membrane bound protein expressed on the surface of natural killer cells. Liposomal carriers increase therapeutic efficacy by presenting TRAIL in its natural, membrane-bound state. No further cleavage or activation of TRAIL is necessary for this formulation. We have also shown that ES/TRAIL liposomes are stable in whole blood isolated from healthy volunteers. In our previous work we established that ES/TRAIL liposomes can effectively target cancer cells spiked into whole blood collected from healthy volunteers under physiologically relevant shear stress conditions, recapitulated in a cone-and-plate viscometer [23]. The ES/TRAIL liposomes were effective under different hematocrit levels, indicating their stability in whole blood.

Past and present works support these findings that the therapeutic potential of TRAIL is increased even in TRAIL resistant cancer cell lines—without the use of sensitization agents—when presented on lipid bilayers [30]. Furthermore, the fluid dynamics of blood flow cause an effect called margination that results in increased binding/contact opportunities between ES/TRAIL coated leukocytes and CTCs. In the fluid shear stress microenvironment of the blood circulation, larger, less deformable objects are deflected away from the center and towards the vascular wall. Both CTCs and leukocytes are both relatively large cells and bind to ES ligands to roll along the vascular endothelium. It is in this environment that these cells are able to undergo repeated collisions and TRAIL that is bound to leukocytes has more opportunities to bind to CTCs. It should also be noted that TRAIL liposomes tethered to the surface of circulating leukocytes exhibited a circulation half-life (Fig. 1) significantly longer than any previously described nanoparticle formulations of TRAIL [31-33]. Nanomedicine-based therapeutic approaches such as the one demonstrated here may hold the key to exploiting the potency of TRAIL within the circulation.

In addition, many cell-based therapies are rising in popularity due to their natural ability to migrate toward and penetrate inflamed regions that are often difficult to achieve with drug delivery mechanisms. The mechanism presented here is unique because it does not require any *ex vivo*-based manipulations of immune cells for enhanced therapeutic effect. In this way, one is able to avoid donor harvesting, specific activation and production challenges associated with adoptive T cell therapies and cell-mediated drug delivery, which carries drug nanoparticles internally. Since

many other common cancers such as those derived from breast, lung, colon and skin are known to metastasize through the bloodstream [34] and given the dramatic decrease in the number of CTCs after only one dose, ES/TRAIL liposomes could be administered clinically as a preventative measure for newly diagnosed patients. Most cell types exhibit some level of apoptosis response to the TRAIL ligand [35], nonetheless, should a specific tumor prove to be completely resistant to TRAIL therapy, scores of studies have been published over the past 15 years that report new chemical agents (chemotherapeutics, inhibitors, natural products) that are able to sensitize cancer cells to TRAIL-mediated apoptosis [36].

Future work should focus on testing the efficacy of ES/TRAIL liposomes in other models of bloodborne metastatic cancer, and the *ex vivo* testing of patient-derived CTCs under physiologic blood flow conditions. While E-Selectin is a broad target for leukocytes, further specificity can be gained by using ligands specific for leukocyte subpopulations such as NK killer cells, B-cells and T-cells that are current promising targets in cancer immunotherapy. Finally, it should be noted that while our focus has been on cancer metastasis, this drug delivery mechanism could be applied to other diseases where there is substantial leukocyte infiltration such as neurodegenerative diseases.

5.5 Supplementary Figures

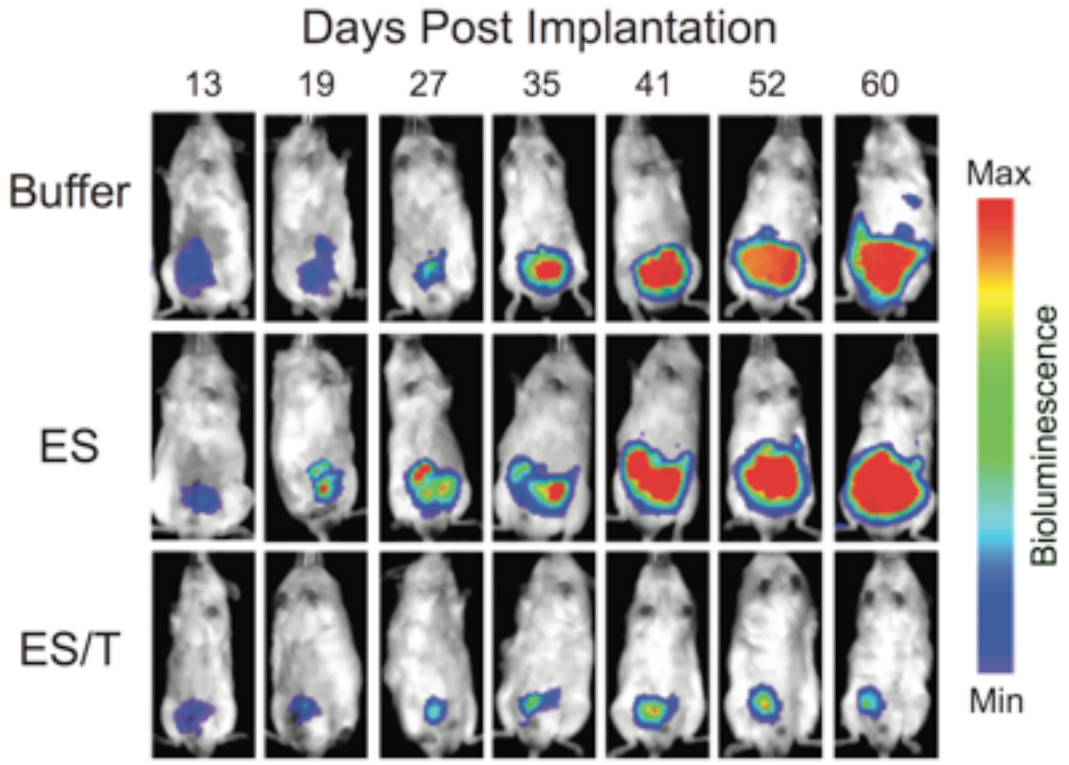

Supplementary Figure 5.1 Representative whole-body bioluminescence images from three treatment groups.
Representative images from Buffer (row 1), ES (row 2), and ES/TRAIL (row 3) from 13 days through 60 days past tumor implantation. Images reveal stagnant primary tumor growth of ES/TRAIL treated animals.

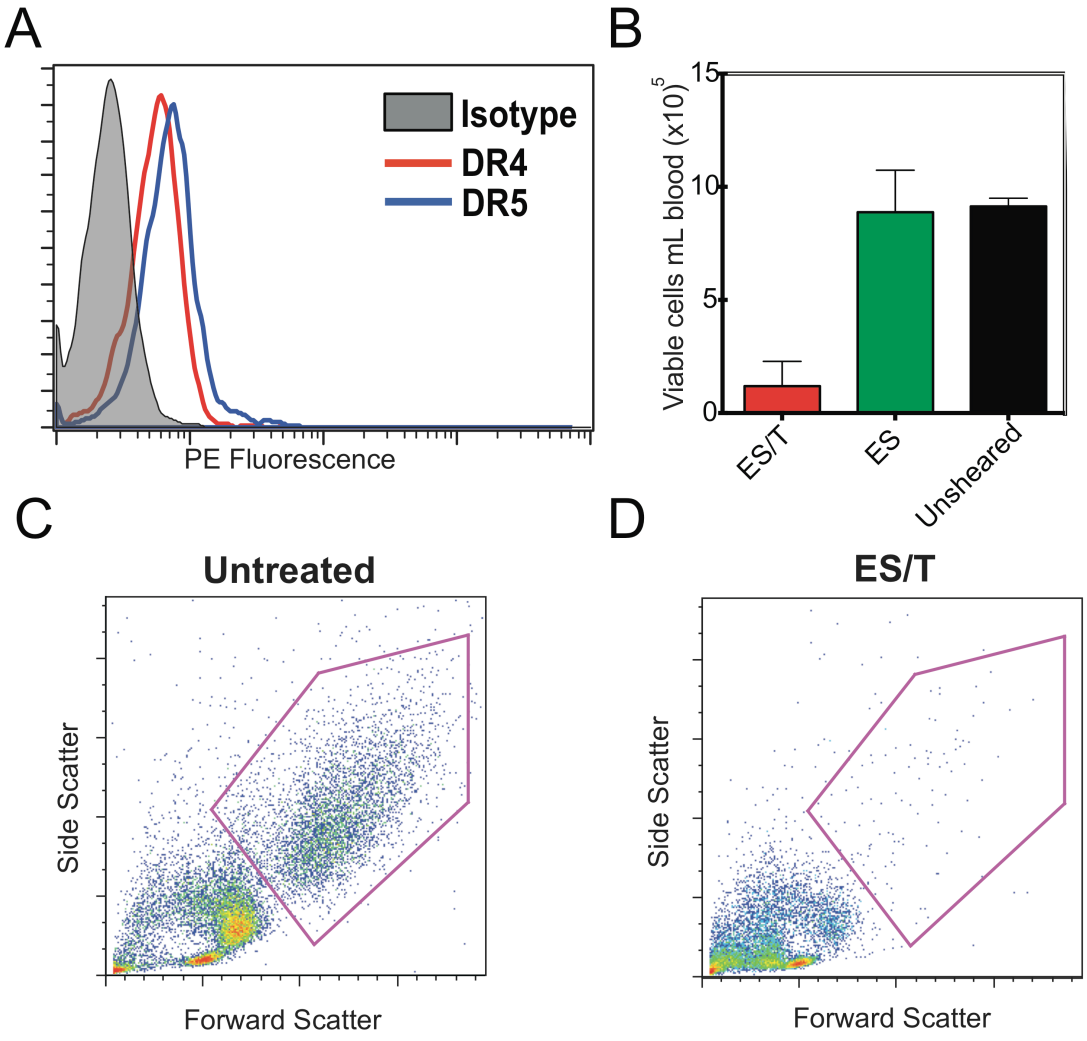

Supplementary Figure 5.2 DU145 cells express death receptors and undergo apoptosis when sheared with ES/TRAIL liposomes in blood. (A) Flow cytometric analysis of DU145 cells for death receptor (DR4 and DR5) expression. (B) Number of viable DU145 cells per volume of blood after treatment with ES/TRAIL or ES liposomes in blood under shear flow. n=3 for all samples. Bars represent mean +/- SD in each group. (C) and (D) Flow cytometry of DU145 cells without and with ES/TRAIL treatment in a cone-and-plate viscometer at 188 s^{-1} for 2h.

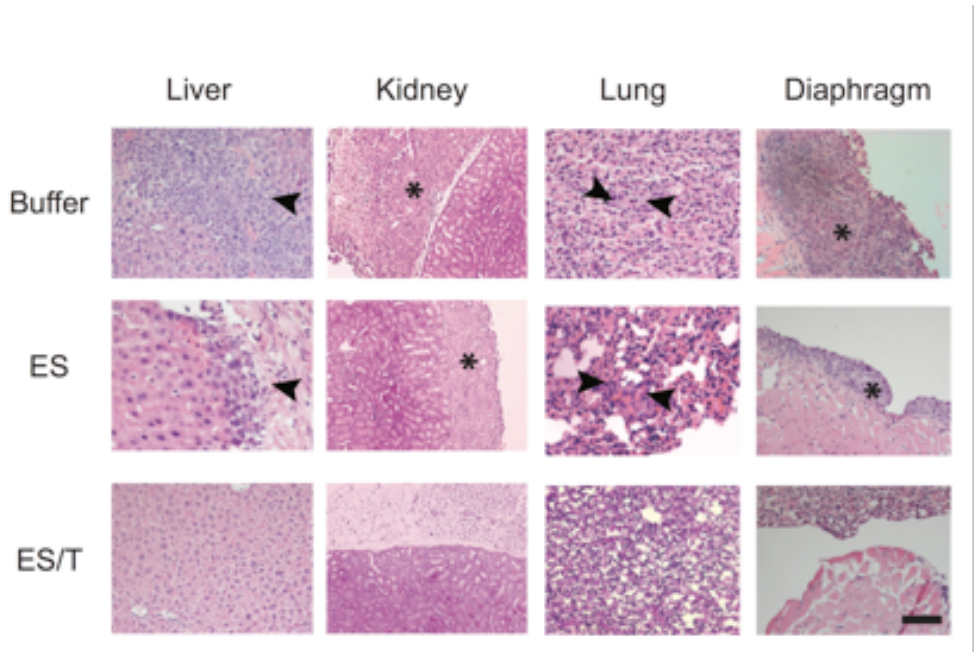

Supplementary Figure 5.3 Hematoxylin & eosin stained sections from various organs in each treatment group. Black arrows point to regions of neoplastic colonization within the organ parenchyma. The diaphragm in ES/T liposome treated animals were found to be free of tumor burden, in contrast to ES liposome and Buffer treated animals with widespread tumor growth as indicated by asterisks. A similar tumor burden pattern was observed in the peri-adipose tissue surrounding the kidneys (see asterisks). (Scale bar = 200μm)

5.6 References

1. Torre LA, Bray F, Siegel RL, Ferlay J. Global cancer statistics, 2012. CA Cancer J Clin. 2015;65:87–108.

2. Crehange G, Roach MI, Martin E, Cormier L, Peiffert D, Cochet A, et al. Salvage reirradiation for locoregional failure after radiation therapy for prostate cancer: Who, when, where and how? Cancer Radiotherapie. 2014 Oct;18(5-6):524–34.

3. Wilt TJ, Ahmed HU. Prostate cancer screening and the management of clinically localized disease. BMJ. 2013;346:f325.

4. Delacruz A. Using circulating tumor cells as a prognostic indicator in metastatic castration-resistant prostate cancer. Clin J Oncol Nurs. 2012 Apr;16(2):E44–7.

5. Ma X, Xiao Z, Li X, Wang F, Zhang J, Zhou R, et al. Prognostic role of circulating tumor cells and disseminated tumor cells in patients with prostate cancer: a systematic review and meta-analysis. Tumour Biol. 2014 Jun;35(6):5551–60.

6. Grosse-Wilde A, Kemp CJ. Metastasis Suppressor Function of Tumor Necrosis Factor-Related Apoptosis-Inducing Ligand-R in Mice: Implications for TRAIL-Based Therapy in Humans? Cancer Research. 2008 Aug 1;68(15):6035–7.

7. Goldberg GS, Jin Z, Ichikawa H, Naito A, Ohki M, El-Deiry WS, et al. Global effects of anchorage on gene expression during mammary carcinoma cell growth reveal role of tumor necrosis factor-related apoptosis-inducing ligand in anoikis. Cancer Research. 2001 Feb 15;61(4):1334–7.

8. Lane D, Cartier A, Rancourt C, Piché A. Cell detachment modulates TRAIL resistance in ovarian cancer cells by downregulating the phosphatidylinositol 3-kinase/Akt pathway. Int J Gynecol Cancer. 2008 Jul;18(4):670–6.

9. Phipps LE, Hino S, Muschel RJ. Targeting Cell Spreading: A Method of Sensitizing Metastatic Tumor Cells to TRAIL-Induced Apoptosis. Molecular Cancer Research. 2011 Mar 15;9(3):249–58.

10. Mitchell MJ, King MR. Fluid shear stress sensitizes cancer cells to receptor-mediated apoptosis via trimeric death receptors. New J Phys. 2013 Jan 1;15(1):015008.

11. Wallace TJ, Torre T, Grob M, Yu J, Avital I, Bruecher B, et al. Current Approaches, Challenges and Future Directions for Monitoring Treatment Response in Prostate Cancer. Journal of Cancer. 2014;5(1):3–24.

12. Fernández-García EM, Vera-Badillo FE, Perez-Valderrama B, Matos-Pita AS,

Duran I. Immunotherapy in prostate cancer: review of the current evidence. Clin Transl Oncol. 2015 May;17(5):339–57.

13. Mitchell MJ, King MR. Leukocytes as carriers for targeted cancer drug delivery. Expert Opinion on Drug Delivery. Informa UK, Ltd; 2015;12(3):000–0.

14. Rembrink K, Romijn JC, vanderKwast TH, Rubben H, Schroder FH. Orthotopic implantation of human prostate cancer cell lines: A clinically relevant animal model for metastatic prostate cancer. Prostate. 1997;31(3):168–74.

15. Bastide C, Bagnis C, Mannoni P, Hassoun J, Bladou F. A Nod Scid mouse model to study human prostate cancer. Prostate Cancer Prostatic Dis. 2002;5(4):311–5.

16. Scatena CD, Hepner MA, Oei YA, Dusich JM, Yu S-F, Purchio T, et al. Imaging of bioluminescent LNCaP-luc-M6 Tumors: A new animal model for the study of metastatic human prostate cancer. Prostate. 2004 May 15;59(3):292–303.

17. Waters DJ, Janovitz EB, Chan TCK. Spontaneous metastasis of PC-3 cells in athymic mice after implantation in orthotopic or ectopic microenvironments. Prostate. 1995 May;26(5):227–34.

18. Chaturvedi PR, Patel NM, Lodhi SA. Effect of terminal heat sterilization on the stability of phospholipid-stabilized submicron emulsions. Acta Pharm Nord. 1992;4(1):51–5.

19. Honary S, Zahir F. Effect of Zeta Potential on the Properties of Nano-Drug Delivery Systems - A Review (Part 1). Trop J Pharm Res. 2013 May 9;12(2).

20. Blenke EO, Klaasse G, Merten H, Plückthun A, Mastrobattista E, Martin NI. Journal of Controlled Release. J Control Release. Elsevier B.V; 2015 Mar 28;202(C):14–20.

21. Gabelloni ML, Trevani AS, Sabatté J, Geffner J. Mechanisms regulating neutrophil survival and cell death. Semin Immunopathol. 2013 Feb 1;35(4):423–37.

22. Mantovani A, Allavena P, Sica A, Balkwill F. Cancer-related inflammation. Nature. 2008 Jul 24;454(7203):436–44.

23. Mitchell MJ, Wayne E, Rana K, Schaffer CB, King MR. TRAIL-coated leukocytes that kill cancer cells in the circulation. Proceedings of the National Academy of Sciences. 2014 Jan 21;111(3):930–5.

24. Ashkenazi A, Holland P, Eckhardt SG. Ligand-Based Targeting of Apoptosis in Cancer: The Potential of Recombinant Human Apoptosis Ligand 2/Tumor Necrosis Factor-Related Apoptosis-Inducing Ligand (rhApo2L/TRAIL). Journal of Clinical Oncology. 2008 Jul 20;26(21):3621–30.

25. Herbst RS, Eckhardt SG, Kurzrock R, Ebbinghaus S, O'Dwyer PJ, Gordon MS, et al. Phase I Dose-Escalation Study of Recombinant Human Apo2L/TRAIL, a Dual Proapoptotic Receptor Agonist, in Patients With Advanced Cancer. Journal of Clinical Oncology. 2010 Jun 8;28(17):2839–46.

26. Zhang D, Hu X, Qian L, Chen SH, Zhou H. Microglial MAC1 receptor and PI3K are essential in mediating b-amyloid peptide-induced microglial activation and subsequent neurotoxicity. Journal of Neuroinflammation. 2011;8(3):1–14.

27. Zou YX, Zhang XD, Mao Y, Lu GC, Huang M, Yuan BJ. Acute toxicity of a single dose DATR, recombinant soluble human TRAIL mutant, in rodents and crab-eating macaques. Hum Exp Toxicol. 2010 Aug;29(8):645–52.

28. Tolcher AW, Mita M, Meropol NJ, Mehren von M, Patnaik A, Padavic K, et al. Phase I pharmacokinetic and biologic correlative study of mapatumumab, a fully human monoclonal antibody with agonist activity to tumor necrosis factor-related apoptosis-inducing ligand receptor-1. Journal of Clinical Oncology. 2007 Apr 10;25(11):1390–5.

29. Zhang H-Y, Man J-H, Liang B, Zhou T, Wang C-H, Li T, et al. Tumor-targeted delivery of biologically active TRAIL protein. Cancer Gene Therapy. Nature Publishing Group; 2010 Jan 15;17(5):334–43.

30. Nair PM, Flores H, Gogineni A, Marsters S, Lawrence DA, Kelley RF, et al. Enhancing the antitumor efficacy of a cell-surface death ligand by covalent membrane display. Proceedings of the National Academy of Sciences. 2015 Apr 20;:201418962.

31. Seifert O, Pollak N, Nusser A, Steiniger F, Rüger R, Pfizenmaier K, et al. Immuno-LipoTRAIL: Targeted delivery of TRAIL-functionalized liposomal nanoparticles. Bioconjug Chem. 2014 May 21;25(5):879–87.

32. Lim SM, Kim TH, Jiang HH, Park CW, Lee S, Chen X, et al. Improved biological half-life and anti-tumor activity of TNF-related apoptosis-inducing ligand (TRAIL) using PEG-exposed nanoparticles. Biomaterials. 2011 May;32(13):3538–46.

33. Chae SY, Kim TH, Park K, Jin CH, Son S, Lee S, et al. Improved Antitumor Activity and Tumor Targeting of NH2-Terminal-Specific PEGylated Tumor Necrosis Factor-Related Apoptosis-Inducing Ligand. Molecular Cancer Therapeutics. 2010 Jun 9;9(6):1719–29.

34. MacDonald IC, Groom AC, Chambers AF. Cancer spread and micrometastasis development: quantitative approaches forin vivo models. Bioessays. 2002 Sep 7;24(10):885–93.

35. Stuckey DW, Shah K. TRAIL on trial: preclinical advances in cancer therapy. Trends Mol Med. 2013 Nov;19(11):685–94.

36. Ashkenazi A, Herbst RS. To kill a tumor cell: the potential of proapoptotic receptor agonists. J Clin Invest. 2008 Jun 2;118(6):1979–90.

CHAPTER 6

ROLE OF MICROGLIA IN THE EARLY STEPS OF BRAIN METASTASIS

Brain metastases are a devastating event with poor prognosis, often occurring in the final stages of disease progression. Nearly 20% of all cancer patients will develop a brain metastasis and that number is increasing because of longer overall survival of patients. The majority of brain metastases originate from lung (40%, 50%), melanoma (10%), and from unknown primary origin (10%, 14%) and breast (15%, 30%), in men and women, respectively (1-3). Treatment options for brain metastasis include tumor resection and radiotherapy. Prognosis is poor and typical survival after treatment is 3-6 months (4).

Despite the success of current therapies in reducing tumor growth, there is inevitably a small population of tumor cells that evade original tumor therapy causing eventually disease recurrence. These surviving cells gain *de novo* protection through interaction with the microenvironment and can eventually develop *acquired* drug resistance against existing therapies. Furthermore, there is evidence to support that highly metastatic cancer cells are most differentiated by their ability to interact with the host microenvironment(5, 6). In a chick embryo study by Morris et al., the extravasation rates between cancer cell lines of varying metastatic potential were found to be equivalent (95% of all cells extravasated within 3 days of injection), however, the ability of cells to migrate and proliferate post extravasation was significantly different (5). In an in vivo mouse model, cholesterol emboli were able to extravasate into the brain parenchyma within 3 days suggesting that there are passive mechanisms of vascular recanalization that support extravasation of anything occluding vessels, whether cancer cell or other emboli (7, 8). Thus understanding the role of the tumor

microenvironment has never been more vital for treating cancer metastasis. The host microenvironment is the final frontier of cancer metastasis. In particular, the inflammatory response of the brain environment is a potential target for therapy and has been shown to be involved in primary brain tumor formation and metastasis development (9-11). In this chapter, I will discuss the role of microglia in maintaining the brain environment, review previous animal models for studying microglia involvement in brain metastasis, and finally summarize the preliminary results of the interaction between circulating tumor cells and microglia during extravasation, dormancy, and/or proliferation in the brain microenvironment.

The role of microglia in the brain microenvironment

The brain is a tightly regulated environment. The blood brain barrier prevents passage of small molecules and blocks transport of circulating immune cells into the brain parenchyma. Because of this lack of outside support, the brain has a network of specialized internal cells that protect the brain against possible injury including astroyctes, microglia, pericytes, perivascular macrophages, and oligodendrocytes. Microglia[1] are but one of those cell populations and are activated in many neurodegenerative diseases such as multiple sclerosis, Parkinson's disease, stroke, gliomas. What role they play in brain metastasis remains poorly understood.

Microglia are the specialized innate immune cells of the brain. They provide continuous surveillance of brain and serve to protect the brain against foreign

[1] Bloodborne macrophages, often abbreviated as mo-MΦ , are also play some role in neurodegenerative diseases (Figure 6.1), however, the main focus of this thesis chapter is on brain resident microglia.

pathogens and injury as well as to mediate repair. Upon sensing a brain injury/insult, microglia undergo rapid activation that manifests via migration, morphological change, and increased phagocytosis and secretion activity **(Figure 6.1)**. Microglia are the most common glial cell in the brain and make up at least 10%-12% of the total brain cell population in mice(12, 13). While microglia are the most common, they are also the most unique cell population of the brain. Unlike neurons and astrocytes, microglia are territorial and do not form permanent contacts with other microglia (14, 15). Microglia have extended processes that do not overlap and their regional density corresponds inversely with the density of other cell populations in the brain (i.e. lower microglia density in regions with high density of neural cell bodies). This strategy seems to benefit the brain; in this configuration microglia are able to scan the entire brain environment at least once every few hours (13, 16). A 2005 time-lapse *in vivo* study by Nimmerjahn et al. masterfully demonstrated the rapid scanning activity of microglia in their "resting state", finding that microglia extensions and retractions occur at up to 4.1 μm/min (13).

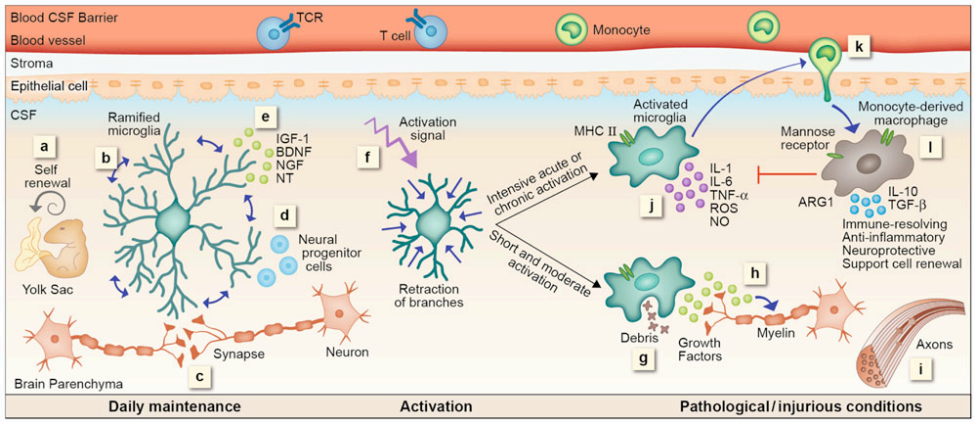

Figure 6.1 Microglial and mo-MΦ functions – cascade of events. (a) Resident microglia originate from yolk sac macrophages that repopulate CNS parenchyma during early development and are self-renewed locally, independent from bone marrow-derived monocytes, by proliferation of primitive progenitors. (b) In the steady state microglia are constantly scanning their environment through their highly motile processes. These cells facilitate the maintenance of synapses (c) and neurogenesis (d), as well as secrete growth factors essential for normal CNS performance (e). Upon recognition of a danger signal, microglia retract their branches, become round and ameboid, and convert into an activated mode (f). A short or moderate signal directs microglia toward a neuroprotective phenotype; these cells clear debris by phagocytosis (g), secrete growth factors associated with remyelination (h) and support regeneration (i). Intensive acute or chronic activation renders microglia neurotoxic; under such conditions microglia fail to acquire a neuroprotective phenotype. Instead, these cells produce reactive oxygen species (ROS), nitric oxide (NO), proteases, and pro-inflammatory cytokines such as IL-1, IL-6, and TNF-α, all of which endanger neuronal activity (j). Microglial malfunction results in the recruitment of mo-MΦ to the damage site (k). mo-MΦ secrete anti-inflammatory cytokines such as IL-10 and TGF-β, express factors associated with immune resolution such as manose receptor and arginase 1 (ARG1), and promote neuroprotection and cell renewal (l), all of which are functions that cannot be provided, under these conditions, by the resident microglia. Adapted and expanded from London et al. (2013).

Microglia are extremely versatile cells. Microglia exhibit different functional capabilities; gene array and real-time PCR studies suggests there are subset populations of microglia that form the reactive phenotypes that characterize microglial activation(17-19). Scheffel et al., activated microglia via LPS stimulation and found MHCI, TNFα, COX, and CCL3 induction as established in previous publications, however flow cytometer analysis reveals the induction is coming from a small subset of microglia (20). Immunohistochemical staining showed that the activated cells appears to be distributed arbitrarily and did not correlate to a particular morphology. LPS injection into different brain regions exhibited different levels of microglia activation, alluding to a regional level of microglia response (21). Microglia differ in their ability to recognize and respond to pathogen and possess differing abilities of cytokine secretion and phagocytosis **(Figure 6.2)**. Exploring this topic of heterogeneity could be linked to heterogeneous response of microglia to invading tumor cells that has been found in past studies.

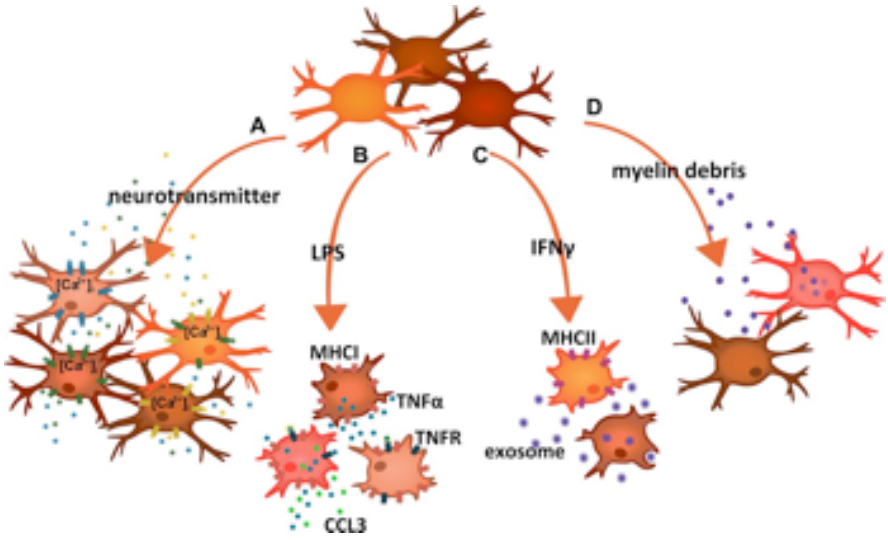

FIGURE 6.2 Schematic summary of examples indicating microglial response heterogeneity. (A) Stimulation of microglia cells with neurotransmitters and neurohormones triggering calcium signals revealed that only small fractions responded to each compound. Combined stimulation and population analysis thereby suggested an enormous variety in terms of functional receptor expression. **(B)** Exposure to LPS induced a panpopulational expression of major histocompatibility complex I (MHCI) molecules, indicating that all microglia expressed TLR4. In contrast, only subsets also produced TNFα and/or CCL3. **(C)** Treatment of microglia with IFNγ caused the expression of major histocompatibility complex II (MHCII) in some but not all cells. On the other hand, MHCII-expressing microglia did not clear myelin-laden exosomes, a function that rather associated with MHCII-negative cells. **(D)** Exposure of cells to myelin debris resulted in the phagocytic uptake of the material in a subset of microglia. Adapted and expanded from Scheffel et al. (2012).

6.1 Microglial Activation in Cancer

Microglia have a complex, far from uniform response to brain metastases, exhibiting both tumor supportive and tumor destructive properties (22-26). Lorger et al, injected various human cancer cell lines into immune-compromised and immune-competent mice and showed that microglia presented amoeboid morphology around some cancer tumor cells clusters but ramified, seemingly non-activated morphology around others (22). Further this difference in morphology was present at early stages as well as near tumor growths 50 days post tumor cell injection. Because of the heterogeneous response the role of microglia activation in tumor development remained unclear. Using organotypic brain slice models which are discussed later in the chapter, Pukrop et al, demonstrated the microglia can assist invading cells by act as guiding rails to enable invasion of surrounding parenchyma and that there is less invasion when microglia or inactivated (27). Results have also shown microglia can exhibit anti-tumor effects. Microglia possess the ability to lyse human cancer cells via release of nitric oxide (28). LPS activated microglia have been shown to have cytotoxicity activity to lung cancer cell in vitro (29). Unfortunately, most of the studies demonstrating tumor destructive behaviors by microglia are *in vitro*. Using *in vivo* studies, microglia appear to not be activated in this manner and both genetic and IHC analysis show that brain metastasis associated microglia have an immune-suppressive phenotype that supports tumor growth (26, 30).

However, there is an inherent flaw in this reasoning—successful metastases will undoubtedly be surrounding by tumor-supportive microglia whereas non-

successful metastatic events (and thus potential tumor-destructive microglia) will go unobserved and unevaluated. In order to unmask the role of microglia in brain metastases, there needs to be tracking of all metastatic events. The heterogeneous response to brain metastasis may be related to the heterogeneous distribution of phenotype of microglia themselves. The manner in which microglia respond to circulating tumor cells may be depend on location of arrest and extravasation as well as the intercellular signaling between CTCs and the brain microenvironment. In order to address this hypothesis, there needs to be an effective in vivo animal approach that can not only track the interaction of CTCs and microglia upon initial arrest but can quantify whether or not each individual metastatic event leads to a successful metastatic tumor.

6.2 Animal Models to study microglia activation

Tracking single tumor cells during stages of metastasis is a very important question that scientists have tried to tackle for decades. Primary tumors are very heterogeneous, so understanding what obstacles CTCs encounter and discerning which mechanisms enable successful cells to complete metastasis can yield more information about how to treat tumors. The ability to track tumor cells has been heavily coupled to the advancement of technology in imaging, which has been outlined in (**Table 1**). Early studies were geared towards naturally amenable models such as using optically transparent models, or highly vascularized animal models such as chick embryos and zebrafish. However, while these models offer great information about intravasation,

extravasation, and angiogenesis, they do not recapitulate other stages in metastasis very well. Below is a description of the models used to understand metastasis.

Organotypic models are a co-culture of thick brain slices with tumor pieces to capture invasion and interaction of cancer cells with the brain host cells (11, 31-33). They are reproducible systems that can be fluorescently labeled for imaging purposes and pharmacologically modified. These co-cultures exclude circulation, which can be advantageous when seeking to isolate the role of resident brain cell populations. The culture can practically be sustained for up to 2 weeks, making it unfavorable for visualizing longer-term tumor progression.

Histology studies using *in situ* mouse models have been also been used to track tumor cells (9, 22, 34, 35). The benefit of *in situ* analysis is that you can label a nearly unlimited number of cell populations or soluble factors that are not feasible *in vivo*. Lorger et al, injected various cancer cells into mice and identified astrocytes and microglia as the most reactive cells population to invading tumor cells (22). The most obvious limitation is that you are not able to investigate the fate of observed cells.

Intra-vital window implants in mice have facilitated visualization of nearly all stages of metastasis (36, 37). Many models have emerged for visualizing metastasis including in the brain (7, 36, 37), liver (38) and skin flap (39, 40). In the case of studying proliferation or invasion, organ windows are extremely strategic because you can choose the tumor origin. However for intravenously injected CTCs or models that spontaneously shed CTCs from a primary tumor, tracking cells dynamics is much more challenging. CTC arrest in vasculature is stochastic, making this model not as reproducible and streamlined. In addition, this method is very laborious and surgery

intensive, and requires specialized optical techniques. Overall, this is the model that offers the most accurate, most unaltered opportunity to visualize single CTC metastasis into a secondary organ. 2PEF has greatly enabled this progress in single cell visualization within an intact, living organism. In 2009, Kienast et al., was able to track cancer cell arrest, extravasation, migration, regression and/ or proliferation (36). Furthermore, Kienast et al. used this model to demonstrate that of the 150-200 cancer cells tracked only roughly 2% of those formed successful metastasis. This is the model used for studying CTC interaction with microglia cells in the brain.

Model	Advantages	Disadvantages	Reference
Artificial or Spontaneous CTCs Models	• High resolution • Mimic circulation of tumor cells	• Stochastic CTC arrest. Rely of probability of seeing cell • Technically complex	(7, 8, 36)
Orthotopic Window	• User decides location of tumor origin and imaging window placement	• Difficult to visualize later stages of metastasis	(6, 41)
Organotypic	• Isolate parenchymal microglia from bloodborne /peripheral macrophages • Allow selective environment changes (i.e. testing of pharmacological agents or cell populations)	• Limited *ex vivo* culture window, only viable for ~2weeks • In vitro, missing early steps of metastasis	(11, 27, 31-33, 42, 43)
Zebrafish	• Optically transparent • Uniformly patterned vasculature facilitates CTC detection • Supports human cancer cells • Non-invasive • Amenable for genetic and pharmacological alterations	• Non-mammalian model	(44-48)
Chick	• Highly vascularized (ideal for extravasation studies) • Ideal thickness for optical imaging	Non-mammalian model	(5, 6, 49, 50)

Table 6.1 Models of CTC Metastasis

The role of the host microenvironment and in particular, the role of microglia in metastasis remains elusive due to the lack of evidence *in vivo* showing the progression of a tumor cell to a successful metastatic growth, or to a failure to establish a new tumor. In the brain there are *in vivo* studies have shown the importance of vessel co-option in CTC metastasis in an in vivo mouse model (36). In this remainder of this chapter, I discuss the relevance of microglia activation in neurodegenerative disease and how my preliminary results of cancer metastasis fit into the paradigm. This chapter will serve as a guide for future attempts to study microglia involvement in cancer metastasis. I conclude with some comments on the model and future directions.

6.3 Microglia respond to occlusions via morphological transformation

Microglia undergo a fast morphological transformation, altering their shape from a ramified, resting state to a shape with a larger soma, thicker, short, or more directed processes, and in the final stage to a fully amoeboid phagocytic state (**Figure 6.1**). Remarkably, these morphological transformations can occur within mere minutes, depending on the injury. Attempts have been made to quantify microglia morphology in order to develop classifications or stages within the microglia's transition from fully ramified to fully amoeboid. Area, perimeter, roundness, convex perimeter, number, thickness, and length of processes are few of the morphological parameters that have been analyzed (12, 33, 51-53). In addition, the dynamic behavior of microglia such as process extension, retractions have been characterized extensively

(13). Such methods to quantify microglia morphology may add more cohesiveness and validity to the literature by means of reducing the vagueness of describing microglia activation.

In vivo imaging of invading circulating tumor cells reveal that microglia respond quickly to circulating tumor cell arrest via morphological changes. In particular, the soma, the main body of the microglia, increase in size over time **(Figure 6.3)**. Microglia monitored over time in non-CTC injected animals show stable levels of microglia size, indicating that change in size may be due to CTC arrest. When measuring individual microglia size changes over time **(Figure 6.3 C),** we found that not all microglia are increasing in size, or at the same rate. This is an interesting finding because it yields more evidence to the idea that microglia are not identical.

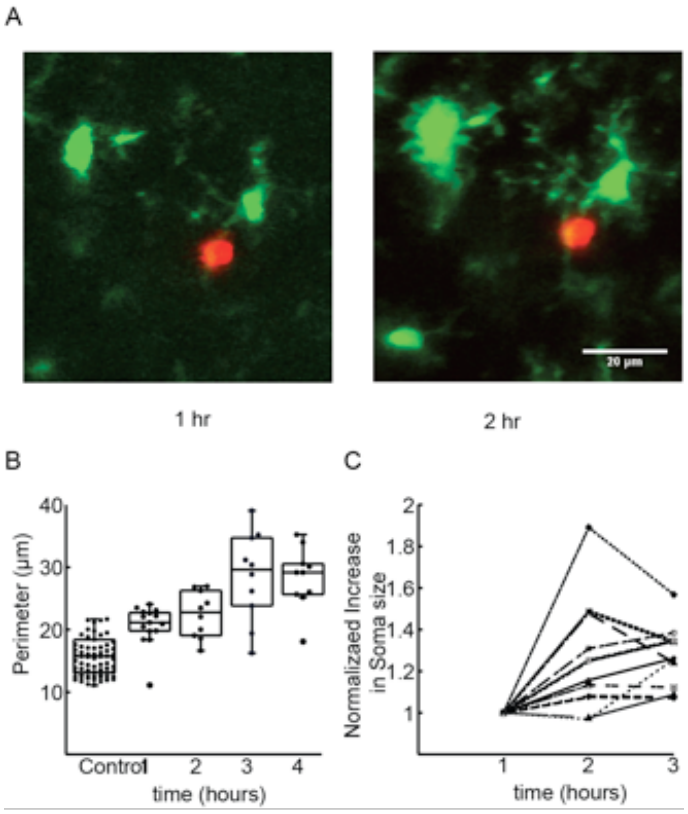

Figure 6.3 Microglia Size Increases Over Time. A) 2PEF images of microglia (green) soma size increase within an hour after CTC (red) injection. B) Quantification of soma size increase over time. C) Lines represent trajectory of individual microglia size change. The microglia represented here were all within a 150µm radius.

Microglia near the CTC increased in size over time. We also found that this increase in size was dependent on the initial distance of the microglia to the invading CTC. A plot of microglia size vs. distance from the CTC **(Figure 6.4)** shows that the largest microglia are closest to the CTC and that microglia generally decrease in size with increasing distance. This would suggest that microglia may be responding to a chemical and/or physiological gradient induced by the CTC. This corroborates previous data that suggest microglia are the earliest responders to brain metastasis (23).

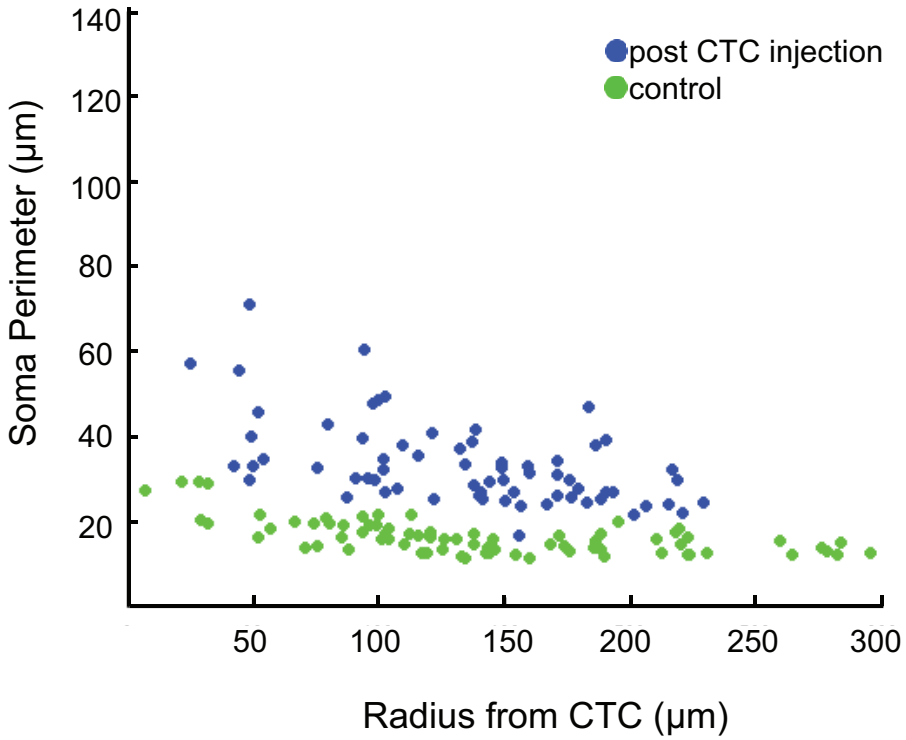

Figure 6.4 Microglia increase in size as a function of distance from Invading CTC A plot of microglia size versus radial distance from arrested CTC (blue). For comparison of microglial size, microglia size as function of distance from an arbitrary spot in a control animal were measured (green).

6.4 Microglia form phagocytic cups around circulating tumor cells

Perhaps the most iconic form of activation for a macrophage would be phagocytosis (17, 54-56). Microglia, being the macrophages of the brain, are known for clearing apoptotic neurons or debri as a natural process in brain development and during neurodegeneration (54, 57). However, microglia also perform this role (or fail to) in many neurodegenerative diseases.

In our in vivo model of metastasis, microglia are observed to phagocytose cell and/or cell debris. The phagocytosis event occurred on relatively short time scales, only 2 hours **(Figure 6.5).** Phagocytosis appears to occur via engulfment by a phagocytic cup, a structure that has been seen in other studies(58-61), where microglia extend their processes around a cell. The results herein are preliminary due to the small sample number, however, observations of phagocytosis has been rare but important in understanding mechanisms the brain uses to eradicate tumor cell populations. Interestingly, the same morphological and migration activities demonstrated in previous sections are also occurring in this phagocytic example. As the microglia "corner" the CTC, they exhibit increased soma sizes over time and visually appear to have fewer and/or thicker processes.

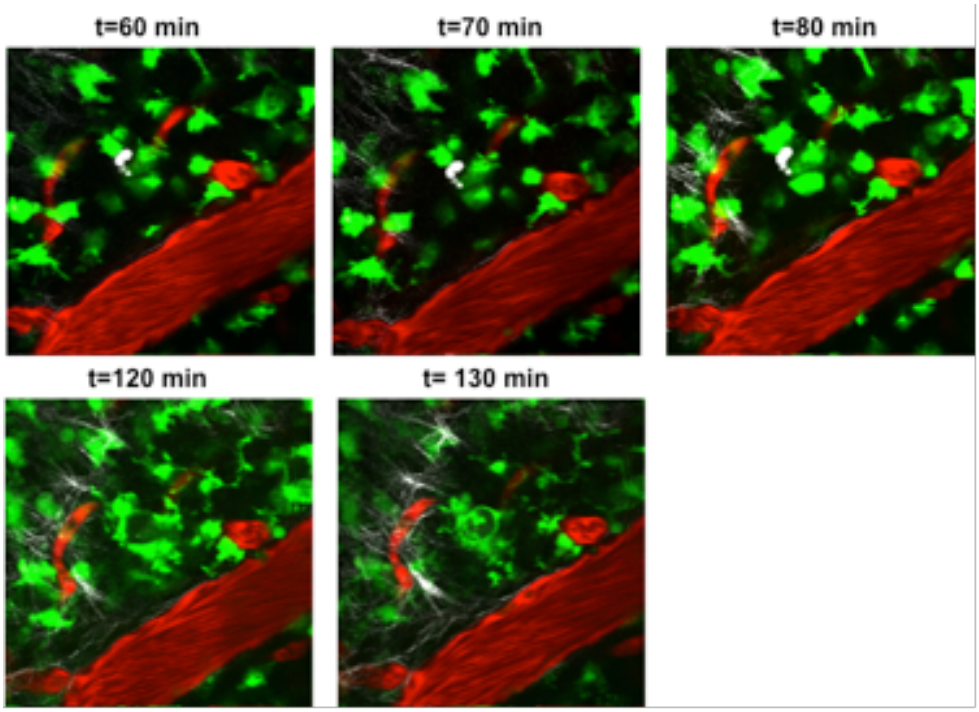

Figure 6.5 Microglia phagocytosis. Microglia (green) migrate toward an invading CTC (white) in the brain. Vessels (red). By 2hrs the CTC has disappeared leaving only the remnants of the phagocytic "cup" formation as shown at (t=130 min).

6.5 Comments on the Model

Imaging circulating tumor cell extravasation into the brain parenchyma is a powerful tool for understanding how metastasis occur. This model yields insight into the tumor-destructive behaviors of microglia that go unnoticed in other models. However, as mentioned previously, the random nature of CTC arrest in brain vasculature is one of the most challenging aspects of the study. Of the 150 documented attempts, including both in vivo and histology-based analysis of ICA injections of cancer cells; only around 5 resulted in positive identification of CTCs in the brain. Furthermore, for the animal studies performed *in vivo*, all mice died within 24 hours after the imaging sessions, limiting the ability to track dynamics of CTCs post vasculature arrest. It should also be noted that neither ICA injection of cancer cells alone or ICA injection of saline followed by imaging results in premature death. The combination of ICA cancer cell injections and subsequent imaging resulted in poor likelihood of animal survival. This unintended death is likely due to cancer cells lodging into other vital organs in a manner supported by the blood flow changes associated with prolonged isoflurane anesthesia.

There are several possible experimental design reasons for this low success rate. This study was designed to use an immune-competent mouse cancer model to account for the positive role of the immune system and enable use of syngeneic cancer cell lines. In this case, using C57Bl6 transgenic mice and C57Bl6 derived melanoma and prostate cell lines. The majority of publications that study brain metastasis have used immune-deficient mice and human cancer cell lines. The difference was thought

to be insignificant, however, the high failure rate suggests that there are more complex interactions involved than initially thought. For example, B16F10 melanoma cells have been shown to preferentially proliferate in the meninges and ventricles of the brain (35) and as such, these cells did not home to brain parenchymal tissue where they could be observed in intravital microscopy. Although the RM1 prostate cell line had no strong tropisms, detection of these cells were also difficult.

Experiments where micrometer-sized beads are injected into the ICA reveal that size restriction plays a big role in initial arrest in the brain vasculature. Obstructing brain blood flow by ICA injection of polystyrene beads is a classic model for testing the impact of size restriction on brain inflammation and changes in blood flow (62-64). Larger sized beads were more likely to remain in vasculature after 3 days than small sized beads **(Figure 6.6 and Figure 6.7)**. In addition, the number of beads injected affected the number retained in vasculature. Even with larger beads that have a higher probably of arresting in vasculature were found in low quantities when fewer beads were injected. While one can increase the number of cancer cells injected, this may also result in undesirable pathologies that hinder the ability to study the microenvironment of cancer metastasis such as stroke and pulmonary embolism. This was observed when injecting over 200,000 mouse or human cancer cells and when injecting over 5,000 fluorescent 25 μm beads. Mouse cancer cell lines can be smaller than human cell lines **(Figure 6.8)**. Given the data previously stated, objects smaller than 10μm in diameter are likely to clear the brain and lodge into other parts of the body. The smaller size of mouse cancer cells may be the most significant risk factor causing premature death in our in vivo mouse experiments. This yields important

information for the models of metastasis being chosen and how to choose cancer cell lines and animal models.

To highlight the stochastic nature of emboli retention in the brain, we further quantified the number of fluorescent beads that were found in a region likely to be visibly using 2PEF microscopy. The results mirrored those found overall but with even fewer beads found. In addition, while the fluorescent beads were useful for understanding retention patterns in the brain, the beads lodged by mechanical restriction and therefore lack the ability to actively interact with the environment as a cancer cells would. The added complexity that cancer cells were also lodge in regions because they prefer the environment further complicates the ICA injection model for imaging brain metastasis.

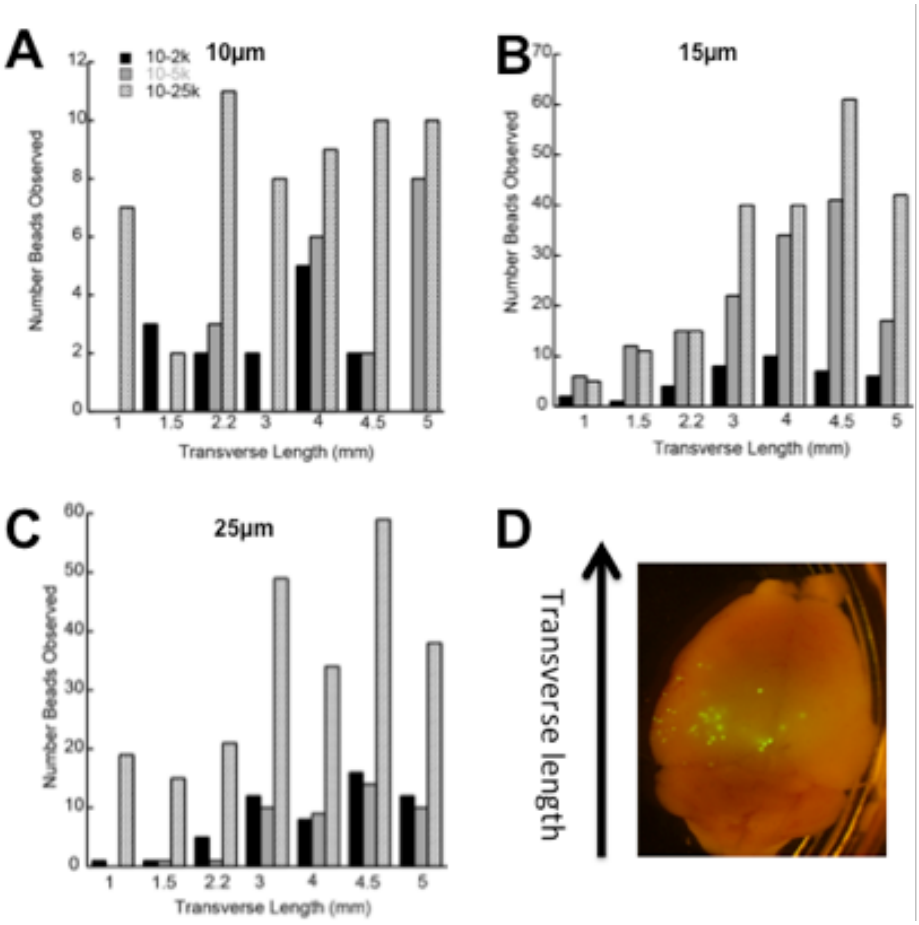

Figure 6.6 Effect of Emboli Size and Injection Amount on Retention in Brain Fluorescent beads of 10µm (A), 15µm (B), and 25µm (C) were injected via intra-carotid artery into the brain of C57Bl6 mice. After 3 days, brains were harvested for sectioning and quantitative analysis. (D) Macroscopic image of fluorescent beads lodged in an intact brain. Courtesy: Evan Bander.

A

	# Beads Within 1mm of Cortex surface	# Beads in Brain
10µm		
2.5K	3	10
5K	8	15
10K	--	50
15µm		
2.5K	24	60
5K	69	40
10K	81	230
25µm		
2.5K	--	40
5K	51	160
10K	41	240

B

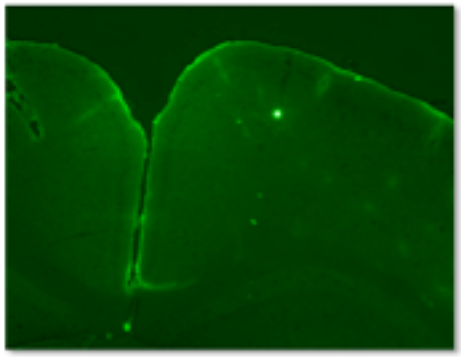

Figure 6.7 Distribution of beads near cortex surface. Quantification of total number of beads observed in brain vs number of beads found near cortex surface. (A), (B) Example of fluorescent bead depicted as being close to cortex surface.

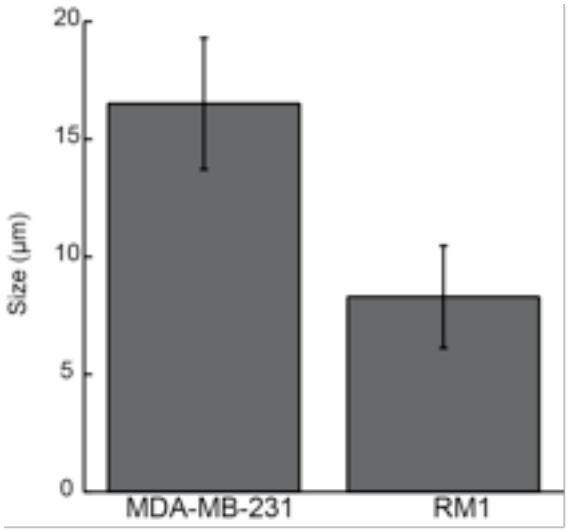

Figure 6.8 Measurement of Human and Mouse Cancer Cell Lines Diameter of human breast cancer cells (MDA-MB-231) and mouse prostate cancer cells (RM1).

6.6 Conclusions

Overall, tracking circulating tumor cell fate as it attempts to proliferate in a secondary organ can yield vital information for understanding why cancer therapies fail. 2PEF microscopy is the best method to observe these cell-cell interactions because of its superior resolution and ability to image deep into scattering tissue. Microglia are remarkable cells in the brain that within a short time scale sense and respond to invading cancer cells in a manner that if controllable can have wide sweeping outcomes for treatment of not only brain metastases but primary brain tumors and possibly other neurodegenerative diseases where microglia activation is involved.

Future work should explore using tracking CTCs in the metastatic environment over longer periods of time. Many of the difficulties with such a study are technical; work should be devoted towards streamlining the experimental processes of imaging a stochastic process. Ideas include, priming growth of tumors cells with tropism for regions of organs that are optically accessible, and developing imaging acquisition algorithms that allow for faster and automated data collection. Developing organ specific tumors, while still artificial has the benefit of allowing the operator to inject cells in less invasive manners such as tail vein or cardiac injection. In addition, future work should explore using a CTC model with emboli rather than single cell events. The advantage here is twofold: large objects are more likely to lodge in a region observable via 2PEF microscopy, and furthermore, embolus is a more relevant presentation of how CTCs travel in the bloodstream.

Finally, imaging is a vital tool to understand spatial and temporal dynamics, however there are features of the tumor microenvironment that cannot easily be fluorescently labeled such as cytokine signaling. Now that we have a sense of *how* microglia response, the cytokine secretion aspect of microglia activation should be investigated to understand what factors are causing microglia to respond.

6.7 References

1. Carbonell WS, Ansorge O, Sibson N, Muschel R (2009) The Vascular Basement Membrane as "Soil" in Brain Metastasis. *PLoS ONE* 4(6):e5857.

2. Hanibuchi M, Kim S-J, Fidler IJ, Nishioka Y (2014) The molecular biology of lung cancer brain metastasis: an overview of current comprehensions and future perspectives. *J Med Invest* 61(3-4):241–253.

3. Wen PY, Loeffler JS (2000) Brain metastases. *Curr Treat Options in Oncol* 1(5):447–457.

4. Honda Y, et al. (2015) Prolonged survival after diagnosis of brain metastasis from breast cancer: contributing factors and treatment implications. *Jpn J Clin Oncol* 45(8):713–718.

5. Morris VL, et al. (1994) Mammary carcinoma cell lines of high and low metastatic potential differ not in extravasation but in subsequent migration and growth. *Clin Exp Metastasis* 12(6):357–367.

6. Luzzi KJ, et al. (1998) Multistep nature of metastatic inefficiency: dormancy of solitary cells after successful extravasation and limited survival of early micrometastases. *The American Journal of Pathology* 153(3):865–873.

7. Lam CK, Yoo T, Hiner B, Liu Z, Grutzendler J (2010) Embolus extravasation is an alternative mechanism for cerebral microvascular recanalization. *Nature* 465(7297):478–482.

8. Grutzendler J, et al. (2014) Angiophagy prevents early embolus washout but recanalizes microvessels through embolus extravasation. *Science Translational Medicine* 6(226):226ra31.

9. Hamilton A, Sibson NR (2013) Molecular and Cellular Neuroscience. *Molecular and Cellular Neuroscience* 53(C):42–51.

10. Mantovani A, Allavena P, Sica A, Balkwill F (2008) Cancer-related inflammation. *Nature* 454(7203):436–444.

11. Chuang H-N, et al. (2013) Carcinoma cells misuse the host tissue damage response to invade the brain. *Glia* 61(8):1331–1346.

12. Lawson LJ, Perry VH, Dri P, Gordon S (1990) Heterogeneity in the distribution and morphology of microglia in the normal adult mouse brain. *Neuroscience* 39(1):151–170.

13. Nimmerjahn A (2005) Resting Microglial Cells Are Highly Dynamic Surveillants of Brain Parenchyma in Vivo. *Science* 308(5726):1314–1318.

14. Walker FR, et al. (2014) Brain, Behavior, and Immunity. *Brain Behavior and Immunity* 37(C):1–14.

15. Hume DA, Perry VH, Gordon S (1983) Immunohistochemical localization of a macrophage-specific antigen in developing mouse retina: phagocytosis of dying neurons and differentiation of microglial cells to form a regular array in the plexiform layers. *The Journal of Cell Biology*.

16. Davoust N, Vuaillat C, Androdias G, Nataf S (2008) From bone marrow to microglia: barriers and avenues. *Trends in Immunology* 29(5):227–234.

17. Gertig U, Hanisch U-K (2014) Microglial diversity by responses and responders. *Frontiers in Cellular Neuroscience* 8:101.

18. Hickman SE, et al. (2013) The microglial sensome revealed by direct RNA sequencing. *Nature Publishing Group* 16(12):1896–1905.

19. Gautier EL, et al. (2012) Gene-expression profiles and transcriptional regulatory pathways that underlie the identity and diversity of mouse tissue macrophages. *Nat Immunol* 13(11):1118–1128.

20. Scheffel J, et al. (2012) Toll-like receptor activation reveals developmental reorganization and unmasks responder subsets of microglia. *Glia* 60(12):1930–1943.

21. Kim W-G, et al. (2000) Regional Difference in Susceptibility to Lipopolysaccharide-Induced Neurotoxicity in the Rat Brain: Role of Microglia. *The Journal of …*.

22. Lorger M, Felding-Habermann B (2010) Capturing Changes in the Brain Microenvironment during Initial Steps of Breast Cancer Brain Metastasis. *The American Journal of Pathology* 176(6):2958–2971.

23. O'Brien ER, et al. (2014) Glial Activation in the Early Stages of Brain Metastasis: TSPO as a Diagnostic Biomarker. *Journal of Nuclear Medicine* 55(2):275–280.

24. Leal WG (2012) Microglial physiopathology: how to explain the dual role of microglia after acute neural disorders? - Gomes-Leal - 2012 - Brain and Behavior - Wiley Online Library. *Brain and behavior*.

25. Berghoff AS, Preusser M (2015) The inflammatory microenvironment in brain metastases: potential treatment target? *Chin Clin Oncol* 4(2):21.

26. Preusser M, et al. (2012) Brain metastases: pathobiology and emerging targeted therapies. *Acta Neuropathol* 123(2):205–222.

27. Pukrop T, et al. (2010) Microglia promote colonization of brain tissue by breast cancer cells in a Wnt-dependent way. *Glia*:n/a–n/a.

28. Brantley EC, et al. (2010) Nitric Oxide. *Translational Oncology* 3(6):380–388.

29. He B, Wang J (2006) Differential Reactions of Microglia to Brain Metastasis of Lung Cancer. *Molecular Medicine* 12(7-8):161–170.

30. Berghoff AS, Lassmann H, Preusser M, Höftberger R (2012) Characterization of the inflammatory response to solid cancer metastases in the human brain. *Clin Exp Metastasis* 30(1):69–81.

31. Jenei V, Nystrom ML, Thomas GJ (2011) Measuring invasion in an organotypic model. *Methods Mol Biol* 769:223–232.

32. Chuang H-N, et al. (2013) Coculture System with an Organotypic Brain Slice and 3D Spheroid of Carcinoma Cells. *JoVE* (80). doi:10.3791/50881.

33. Gabrusiewicz K, et al. (2011) Characteristics of the Alternative Phenotype of Microglia/Macrophages and its Modulation in Experimental Gliomas. *PLoS ONE* 6(8):e23902.

34. Lorger M, Lee H, Forsyth JS, Felding-Habermann B (2011) Comparison of in vitro and in vivo approaches to studying brain colonization by breast cancer cells. *J Neurooncol* 104(3):689–696.

35. Fidler IJ (2011) The role of the organ microenvironment in brain metastasis. *Seminars in Cancer Biology* 21(2):107–112.

36. Kienast Y, et al. (2009) technical reports. *Nature Medicine* 16(1):116–122.

37. Winkler F, et al. (2009) Imaging glioma cell invasion in vivoreveals mechanisms of dissemination and peritumoral angiogenesis. *Glia* 57(12):1306–1315.

38. Tanaka K, et al. (2014) In vivo optical imaging of cancer metastasis using multiphoton microscopy: a short review. *Am J Transl Res* 6(3):179–187.

39. Wyckoff JB, Jones JG, Condeelis JS, Segall JE (2000) A critical step in metastasis: in vivo analysis of intravasation at the primary tumor. *Cancer Research* 60(9):2504–2511.

40. Wang W, et al. (2002) Single cell behavior in metastatic primary mammary tumors correlated with gene expression patterns revealed by molecular profiling. *Cancer Research* 62(21):6278–6288.

41. Condeelis J, Segall JE (2003) Intravital imaging of cell movement in tumours. *Nat Rev Cancer* 3(12):921–930.

42. Zhai H, Heppner FL, Tsirka SE (2010) Microglia/macrophages promote glioma progression. *Glia* 59(3):472–485.

43. Valiente M, et al. (2014) Serpins Promote Cancer Cell Survival and Vascular Co-Option in Brain Metastasis. *Cell* 156(5):1002–1016.

44. Stoletov K, Montel V, Lester RD, Gonias SL, Klemke R (2007) High-resolution imaging of the dynamic tumor cell vascular interface in transparent zebrafish. *Proc Natl Acad Sci USA* 104(44):17406–17411.

45. Stoletov K, et al. (2010) Visualizing extravasation dynamics of metastatic tumor cells. *Journal of Cell Science* 123(13):2332–2341.

46. Teng Y, et al. (2013) Evaluating human cancer cell metastasis in zebrafish. *BMC Cancer* 13(1):1–1.

47. Marques IJ, et al. (2009) Metastatic behaviour of primary human tumours in a zebrafish xenotransplantation model. *BMC Cancer* 9(1):128.

48. Chen X, et al. (2015) Invasiveness and metastasis ofretinoblastoma in an orthotopiczebrafish tumor model. *Nature Publishing Group*:1–11.

49. Chambers AF, et al. (1995) Steps in tumor metastasis: new concepts from intravital videomicroscopy. *Cancer Metastasis Rev* 14(4):279–301.

50. MacDonald IC, Groom AC, Chambers AF (2002) Cancer spread and micrometastasis development: quantitative approaches forin vivo models. *Bioessays* 24(10):885–893.

51. Hinwood M, et al. (2013) Chronic Stress Induced Remodeling of the Prefrontal Cortex: Structural Re-Organization of Microglia and the Inhibitory Effect of Minocycline. *Cerebral Cortex* 23(8):1784–1797.

52. Kozlowski C, Weimer RM (2012) An Automated Method to Quantify Microglia Morphology and Application to Monitor Activation State Longitudinally In Vivo. *PLoS ONE* 7(2):e31814.

53. Plog BA, et al. (2014) ARTICLE IN PRESS. *Journal of Neuroscience Methods*:1–9.

54. Sokolowski JD, Mandell JW (2011) Phagocytic Clearance in Neurodegeneration. *The American Journal of Pathology* 178(4):1416–1428.

55. Gomez-Nicola D, Perry VH (2014) Microglial Dynamics and Role in the Healthy and Diseased Brain: A Paradigm of Functional Plasticity. *The Neuroscientist*. doi:10.1177/1073858414530512.

56. Pul R, Chittappen KP, Stangel M (2013) Quantification of Microglial Phagocytosis by a Flow Cytometer-Based Assay. *Methods in Molecular Biology*, Methods in Molecular Biology. (Humana Press, Totowa, NJ), pp 121–127.

57. Napoli I, Neumann H (2009) Microglial clearance function in health and disease. *Neuroscience*.

58. Flannagan RS, Harrison RE, Yip CM, Jaqaman K, Grinstein S (2010) Dynamic macrophage "probing" is required for the efficient capture of phagocytic targets. *The Journal of Cell Biology* 191(6):1205–1218.

59. Sharma L, et al. (2014) Assessment of Phagocytic Activity of Cultured Macrophages Using Fluorescence Microscopy and Flow Cytometry. *Cytokine …*, Methods in Molecular Biology. (Springer New York, New York, NY), pp 137–145.

60. Sawin DP, Banach L, Harry GJ (2009) Raft aggregation with specific receptor recruitment is required for microglial phagocytosis of Aβ42. *Glia*.

61. Stence N, Waite M, Dailey ME (2001) Dynamics of microglial activation: A confocal time-lapse analysis in hippocampal slices. *Glia* 33(3):256–266.

62. Miyake K, Takeo S, Kaijihara H (1993) Sustained decrease in brain regional blood flow after microsphere embolism in rats. *Stroke*.

63. Harris NG, Gauden V, Fraser PA, Williams SR (2002) MRI measurement of blood-brain barrier permeability following spontaneous reperfusion in the starch microsphere model of ischemia. *Magnetic resonance …*.

64. Han F, Shirasaki Y, Fukunaga K (2006) Microsphere embolism-induced endothelial nitric oxide synthase expression mediates disruption of the blood?brain barrier in rat brain. *J Neurochem* 99(1):97–106.

CHAPTER 7

CONCLUSION AND FUTURE DIRECTIONS

Cancer is a devastating and costly disease to treat and affects over 14.5 million Americans every year with an estimated 1,620 deaths per day [1]. The current cancer treatment paradigm uses therapeutics that limit tumor growth and because of this inherently cannot prevent metastasis because it only addresses the final stage of metastasis. While some therapies attempt to inhibit particular facets of metastasis development, they are often given after other treatment options have failed and the disease is much more resistant. It should then be no surprise that metastasis accounts for over 90% of cancer deaths. The future treatment of cancer must create more therapies that address prior stages of cancer metastasis and do so at an earlier time in patient treatment. Addressing circulating tumor cells (CTCs) is an ideal stage of metastasis to target because it is a population of convergence for the spread of cancer. Furthermore, tumors that are treated before distant metastasis has formed have over a remarkable 60% increase in overall survival prognosis in nearly all-epithelial cancers. Eliminating the CTCs population is both the secret and the solution to treating cancer metastasis.

Using advanced preclinical animal models of cancer metastasis, combined with bioluminescent and two-photon imaging modalities, the work in this dissertation addresses circulating tumor cells as a therapeutic target and the role of the innate immune system as a therapeutic carrier. Research to date on CTCs has primarily focused on their use as a diagnostic and prognostic indicator. In this thesis, we describe an approach to directly target and kill CTCs in the bloodstream that relies on coating leukocytes with liposomes that contain both cytotoxic and CTC targeting

elements. Circulating leukocytes decorated with TNF-related apoptosis inducing ligand (TRAIL) and E-selectin adhesion receptor selectively killed over 75% of CTCs within 3 hours in an acute animal model. Moreover, in a 9-week orthotopic prostate cancer model ES-TRAIL liposome therapy reduced number of CTCs by over 70% and reduced metastasis to other organs as compared to control groups. The use of leukocytes as a delivery vehicle for TRAIL increases the potency of TRAIL therapy while maintaining low toxicity. The potential for this study has widespread implications. Developing a target for CTCs apoptosis makes it a therapy that can be used to reduce metastasis across numerous cancers. Given the current drug market climate for making highly specific drugs that can benefit a narrow group of patients, having a "blockbuster" drug would not only have great success for patient overall survival, it would be good in the pharmaceutical market.

In 2000, the role of the immune system was not even included by Weinberg and Hanahan's seminal paper "Hallmarks of Cancer". In 2011 when the authors published Part II, the immune is not only given a larger section but it is listed as "Emerging Hallmark" [2]. This is a testament to the exponential advances in cancer immunology. Paired with the increase in interdisciplinary research collaborations, the field of cancer immunoengineering is ever expanding. In this particular vein, knowledge of cancer immunology is paired with drug delivery technology to expedite how cells in the immune system recognize and kill cancer cells. Some key examples of immunoengineering are CAR T and ACT cell therapy. Chimeric antigen receptor (CAR) T cell therapy modifies harvested T cells with extracellular ligands to enhance

T cell cytotoxic activity towards cancer cells. CAR T cell therapy has shown some efficacy in clinical trials, particularly in the treatment of gliomas [3, 4]. Another popular immunoengineering technique is Adoptive cell transfer (ACT) Cell therapy where donor-harvested cells are selectively passaged for tumor cytotoxicity before being introduced back to the recipient. This technique has widely been used in the treatment of Multiple Myeloma [5-7].

The ES/TRAIL functionalized leukocyte studies presented within this dissertation are a unique type of immunoengineering because the immune cells are used as passive carriers that do not require any ex vivo manipulation or activation. This makes the therapy all the more attractive as a cancer treatment. In addition, this formulation uses TRAIL in its most potent state: in the blood circulation. TRAIL has a long history, which encompasses the promise of a naturally occurring molecule that selectively kills cancer cells and unfortunately also includes disappointment from dozens of failed Phase III human clinical trials. The work presented here corroborates previously published data [8] demonstrating that TRAIL presented on liposomes are more effective than in its soluble form. Furthermore, TRAIL is more effective at killing isolated, non-adhered tumor cells rather than cells in solid tumors [9-11]. Goldberg et al., found that anchored cells exhibited reduced expression of TRAIL, thereby limiting its therapeutic potential [10]. Directing future TRAIL therapies toward circulating tumor cell populations has the potential to re-energize the use of TRAIL.

Pragmatically, future work should include more advanced characterization diagnostics. The next steps should be to determine the bio-distribution of ES/TRAIL liposomes throughout the mouse as well as the pharmacokinetics of such distribution. With what frequency and persistence do ES/TRAIL functionalized leukocytes traffic through the lymphatic system and other internal organs? In addition, a more thorough understanding of how dosage timing and concentration affect efficacy is needed. As an example, at what threshold concentration/percentage of ES/TRAIL functionalized leukocytes is the most cytotoxic activity induced? Finally, we should also investigate the long-term effects of ES/TRAIL administration on leukocyte health and behavior and blood composition. Understanding the long-term effect of drug treatment on leukocytes and the circulating tumor cell population as well as the primary tumor is vital. As mentioned previously, there a small population of CTCs remained. This population may be worth comparing to the primary tumor population to determine whether any genetic expression alterations occurred that helped these cells evade therapy.

If the assertion is correct that ES/TRAIL liposomes are able to functionalize the surface of leukocytes anywhere in the body, then this opens a pathway for passive but efficient drug delivery. While the primary focus of our studies was drug delivery within the blood circulation, one can imagine creating a library of drug bound liposomes chosen to target specific immune cell populations. Similar tactics are already emerging in the literature through the King Lab and in other laboratories.

The results of the ES/TRAIL therapy is undoubtedly a success story, however, it should be noted that although it demonstrated high efficacy, there remains the problem of whether the remaining cell population is sufficient to form a successful metastasis. This is true not only for the therapy at hand but for every therapy making its way through the preclinical and human clinical pipeline. Though metastasis is an inefficient process, it only takes a single cluster of CTCs to form a metastasis. The latter part of my thesis explores how CTCs interact with microglia, the innate immune cells of the brain, using an *in vivo* mouse model. Our findings are significant not only for treating brain metastasis but for understanding how to think about any therapy that may result in a minimal residual disease, a term used to signify the population of cells still vital following treatment [12]. The contribution of this study is 1) to set a platform for understanding how the fate of individual CTCs events of metastatic spread is directly linked to how CTCs are able to evade cancer therapies and 2) to examine the role of the host organ microenvironment in facilitating or rejecting CTC invasion. In this regard, 2PEF microscopy has been vital to capturing the intercellular interactions to comprise the metastatic cascade.

Future work should explore using tracking CTCs in the metastatic environment over longer periods of time. Many of the difficulties with such a study are technical; work should be devoted towards streamlining the experimental processes of imaging a stochastic process. Ideas include, priming growth of tumors cells with tropism for regions of organs that are optically accessible, and developing imaging acquisition algorithms that allow for faster and automated data collection. Developing organ

specific tumors, while still artificial has the benefit of allowing the operator to inject cells in less invasive manners such as tail vein or cardiac injection.

Additionally, the findings of our study attempt to link morphological changes in the microglia with the fate of CTC metastasis. Next steps should include investigating the genetic and molecular changes in microglia caused in response to an invading tumor cell. Microglia are known to possess an entire "sensome" of genes, which allow them to detect endogenous ligands and respond in either a neuro-protective or neuro-toxic manner [13-15]. Potential targets to investigate are markers for phagocytosis (CD36 [16, 17], CD14 [18], CD68 [19, 20]), proliferation (IL-34 [13], M-CSF [21, 22]), and cytokines known to be secreted by microglia (TGFβ1 [23], IL-1β [24, 25], TNF-α [26]). Where the methods in used in the study presented in this thesis solely used in vivo optical methods, the examination of molecular changes would be best done in organotypic co-culture since it is more easily modifiable to facilitate antibody labeling and flow cytometry analysis [27].

In conclusion, there is tremendous promise in immunoengineering and understanding the role of the host immune response to cancer metastasis. CTCs have more value than simply a cancer diagnostic. The synergy between nanomedicine and biomedical imaging has provided a powerful toolset for understanding how to create the next generation of cancer therapy.

References

1. Society AC (2015) Cancer Facts & Figures 2015. American Cancer Society 1–56.

2. Hanahan D, Weinberg RA (2011) Hallmarks of Cancer: The Next Generation. Cell 144:646–674. doi: 10.1016/j.cell.2011.02.013

3. Brown CE, Badie B, Barish ME, et al. (2015) Bioactivity and Safety of IL13Rα2-Redirected Chimeric Antigen Receptor CD8+ T cells in Patients with Recurrent Glioblastoma. Clin Cancer Res. doi: 10.1158/1078-0432.CCR-15-0428

4. Wang L, Jin N, Schmitt A, et al. (2015) T cell-based targeted immunotherapies for patients with multiple myeloma. Int J Cancer 136:1751–1768. doi: 10.1002/ijc.29190

5. June CH (2007) Adoptive T cell therapy for cancer in the clinic. J Clin Invest 117:1466–1476. doi: 10.1172/JCI32446

6. Barber A, Meehan KR, Sentman CL (2011) Treatment of multiple myeloma with adoptively transferred chimeric NKG2D receptor-expressing T cells. Gene Therapy 18:509–516. doi: 10.1038/gt.2010.174

7. Binsfeld M, Fostier K, Muller J, et al. (2014) Biochimica et Biophysica Acta. BBA - Reviews on Cancer 1846:392–404. doi: 10.1016/j.bbcan.2014.08.001

8. Nair PM, Flores H, Gogineni A, et al. (2015) Enhancing the antitumor efficacy of a cell-surface death ligand by covalent membrane display. Proceedings of the National Academy of Sciences 201418962. doi: 10.1073/pnas.1418962112

9. Grosse-Wilde A, Kemp CJ (2008) Metastasis Suppressor Function of Tumor Necrosis Factor-Related Apoptosis-Inducing Ligand-R in Mice: Implications for TRAIL-Based Therapy in Humans? Cancer Research 68:6035–6037. doi: 10.1158/0008-5472.CAN-08-0078

10. Goldberg GS, Jin Z, Ichikawa H, et al. (2001) Global effects of anchorage on gene expression during mammary carcinoma cell growth reveal role of tumor necrosis factor-related apoptosis-inducing ligand in anoikis. Cancer Research 61:1334–1337.

11. Lane D, Cartier A, Rancourt C, Piché A (2008) Cell detachment modulates TRAIL resistance in ovarian cancer cells by downregulating the phosphatidylinositol 3-kinase/Akt pathway. Int J Gynecol Cancer 18:670–676. doi: 10.1111/j.1525-1438.2007.01062.x

12. Meads MB, Gatenby RA, Dalton WS (2009) Environment-mediated drug

resistance: a major contributor to minimal residual disease. Nature Publishing Group 9:665–674. doi: 10.1038/nrc2714

13. Gomez-Nicola D, Perry VH (2014) Microglial Dynamics and Role in the Healthy and Diseased Brain: A Paradigm of Functional Plasticity. The Neuroscientist. doi: 10.1177/1073858414530512

14. Gautier EL, Shay T, Miller J, et al. (2012) Gene-expression profiles and transcriptional regulatory pathways that underlie the identity and diversity of mouse tissue macrophages. Nat Immunol 13:1118–1128. doi: 10.1038/ni.2419

15. Hickman SE, Kingery ND, Ohsumi TK, et al. (2013) The microglial sensome revealed by direct RNA sequencing. Nature Publishing Group 16:1896–1905. doi: 10.1038/nn.3554

16. Stolzing A (2004) Neuronal apoptotic bodies: phagocytosis and degradation by primary microglial cells. The FASEB Journal. doi: 10.1096/fj.03-0374fje

17. Fadok VA, Warner ML, Bratton DL, Henson PM (1998) CD36 is required for phagocytosis of apoptotic cells by human macrophages that use either a phosphatidylserine receptor or the vitronectin receptor (alpha v beta 3). J Immunol 161:6250–6257.

18. Liu Y, Walter S, Stagi M, et al. (2005) LPS receptor (CD14): a receptor for phagocytosis of Alzheimer's amyloid peptide. Brain

19. Fadok VA, Bratton DL, Frasch SC, et al. (1998) The role of phosphatidylserine in recognition of apoptotic cells by phagocytes. Cell Death Differ 5:551–562. doi: 10.1038/sj.cdd.4400404

20. Xu H, Chen M, Manivannan A, et al. (2008) Age-dependent accumulation of lipofuscin in perivascular and subretinal microglia in experimental mice. Aging Cell 7:58–68. doi: 10.1111/j.1474-9726.2007.00351.x

21. Davoust N, Vuaillat C, Androdias G, Nataf S (2008) From bone marrow to microglia: barriers and avenues. Trends in Immunology 29:227–234. doi: 10.1016/j.it.2008.01.010

22. Eggen BJL, Raj D, Hanisch UK, Boddeke HWGM (2013) Microglial Phenotype and Adaptation. Journal of Neuroimmune Pharmacology 8:807–823. doi: 10.1007/s11481-013-9490-4

23. Ladebya R, Wirenfeldta M, Garcia-Ovejerob D, et al. (2005) Microglial cell population dynamics in the injured adult central nervous system. Brain Research Reviews 48:196–206. doi: 10.1016/j.brainresrev.2004.12.009

24. Krykanides S, Olschowka JA, Williams JP, et al. (1999) TNFa and IL-1b

mediate intercellular adhesion molecule-1 induction via microglia–astrocyte interaction in CNS radiation injury. Journal of Neuroimmunology 95:95–106.

25. Abbott NJ, Rönnbäck L, Hansson E (2006) Astrocyte–endothelial interactions at the blood–brain barrier. Nat Rev Neurosci 7:41–53. doi: 10.1038/nrn1824

26. Bruce AJ, Boling W, Kindy MS, et al. (1996) Altered neuronal and microglial responses to excitotoxic and ischemic brain injury in mice lacking TNF receptors. Nature Medicine 2:788–794. doi: 10.1038/nm0796-788

27. Chuang H-N, Lohaus R, Hanisch U-K, et al. (2013) Coculture System with an Organotypic Brain Slice and 3D Spheroid of Carcinoma Cells. JoVE. doi: 10.3791/50881